

Electronic Thesis and Dissertation Repository

---

8-25-2020 1:45 PM

## Waste Hemp Fibers (HFs) Derived Porous Carbons: Preparation, Characterization, and Potential Applications

Manju Gurung, *The University of Western Ontario*

Supervisor: Paul A Charpentier, *The University of Western Ontario*

A thesis submitted in partial fulfillment of the requirements for the Master of Engineering Science degree in Chemical and Biochemical Engineering

© Manju Gurung 2020

Follow this and additional works at: <https://ir.lib.uwo.ca/etd>

 Part of the [Bioresource and Agricultural Engineering Commons](#), [Other Chemical Engineering Commons](#), and the [Transport Phenomena Commons](#)

---

### Recommended Citation

Gurung, Manju, "Waste Hemp Fibers (HFs) Derived Porous Carbons: Preparation, Characterization, and Potential Applications" (2020). *Electronic Thesis and Dissertation Repository*. 7455.  
<https://ir.lib.uwo.ca/etd/7455>

This Dissertation/Thesis is brought to you for free and open access by Scholarship@Western. It has been accepted for inclusion in Electronic Thesis and Dissertation Repository by an authorized administrator of Scholarship@Western. For more information, please contact [wlsadmin@uwo.ca](mailto:wlsadmin@uwo.ca).

## **Abstract**

The main objective of the present research was to develop environmentally friendly and cost-effective porous carbon materials of improved properties from waste hemp fibers. Two different types/categories of porous carbons were prepared from hemp fibers. In one type, porous carbon materials were developed by a simple one-step method of carbonization and activation. The other type of carbon materials developed in this study were nitrogen-containing activated carbons, which were developed by introduction of nitrogen-containing functional groups on the surface of hemp fibers followed by activation and carbonization. The pore structure/distribution and surface chemistry of the prepared carbons were investigated through the analysis of BET (Brunauer-Emmett-Teller) surface area, pore size and pore volume, X-ray diffraction (XRD), scanning electron microscopy (SEM) images, high resolution transmission electron microscopy (HRTEM) images, Fourier transform-infrared (FT-IR) spectra, and Raman scattering. The carbons developed in this study were mostly mesoporous, and the BET surface area and pore volume of the carbon prepared under optimal conditions were significantly higher than those of commercially available carbon products such as granular and powder activated carbons. The potential of hemp fiber-derived carbons as adsorbents for removal of model naphthenic acids from contaminated aqueous solutions was studied, and the removal efficacy of the prepared carbons was evaluated against that of commercial granular activated carbon. The carbons prepared in this study demonstrated substantially higher efficiency than the commercial carbons for removal of model naphthenic acids from aqueous streams.

## ***Keywords***

Renewable resource, Hemp fibers, Mesoporous carbon, Activated carbon, Granular activated carbon (GAC), Physical activation, chemical activation, Activating agent, Nitrogen-functionalized porous carbon, N-Aminoguanidine, Naphthenic acids, 2-Naphthoic acid, Benzoic acid, Oil sand process-affected water (OSPW), Adsorptive removal, Batch adsorption.

## Acknowledgments

This dissertation would not have been possible without the guidance and the help of several individuals who, in one way or the other, contributed and extended their valuable assistance during the course of my study.

First and foremost, I would like to express my deepest gratitude to Prof. Paul Charpentier for providing me the opportunity to carry on master's studies and conduct research under his guidance and supervision in his laboratory of Chemical Engineering at Western University. His excellent guidance, constructive feedback, insightful comments and suggestions, and continuous support made it possible to complete this dissertation successfully. I deem it as my privilege to work under his guidance. I am, and will remain ever grateful to him for this opportunity. Thank you, Dr. Paul!

The financial support provided by the Department of Chemical and Biochemical Engineering, University of Western Ontario, and industry partner through Mitacs Accelerate grant are gratefully acknowledged. The industry partner chose not to disclose their name, and thus remains anonymous throughout the thesis.

I am indebted to the members of Paul's group for their love, support, and more importantly for providing me the pleasant and fun filled working/learning atmosphere. I am very grateful to Dr. William Z. Xu and Dr. Abdul Mumin for their contribution to this research project (chapter 5). Thank you, Drs. Xu and Mumin. I will always remember all of your support and help in all situations, and the great times we have shared.

And last, but by certainly no means the least, I would like to give my special thanks to my husband Dr. Birendra Babu Adhikari whose understanding, love, unconditional support, generous care and prolific suggestions enabled me to complete this work. I am more than thankful to my kids Bimu and Krish who were deprived of my affection during my study period. I am highly indebted to you all.

Finally, I thank all those who have helped me directly or indirectly in the successful completion of my thesis. Anyone missed in this acknowledgement are also thanked.

## Abbreviations

HF <sub>s</sub>	Hemp fibers
HFC <sub>s</sub>	Hemp fibers-derived carbon
AC	Activated carbon
PC	Petroleum coke
GAC	Granulated activated carbon
N-HF <sub>s</sub>	N-aminoguanidine modified hemp fibers
N-HFC	Nitrogen-doped hemp fiber-derived activated carbon
FT-IR	Fourier transform infrared
SEM	Scanning electron microscopy
HRTEM	High resolution transmission electron microscopy
BET	Brunauer-Emmett-Teller
BJH	Barrett-Joyner-Halenda
XRD	X-ray diffraction
ICP-MS	Inductively coupled plasma-mass-spectrometry
NAs	Naphthenic acids
OSPW	Oil sands process-affected water
Uv-vis	Ultraviolet-visible spectroscopy
HTC	Hydrothermal carbon

SEM-EDX	Scanning electron microscopy with energy-dispersive X-ray spectroscopy
GPC	gel permeation chromatography

## List of Symbols

$M$	mol/litre
$I_D/I_G$	Intensity ratio
$D$	Molecular weight and dispersity
$C_i$	Initial concentration
$C_e$	Equilibrium concentration
$C_t$	Remaining concentration at any time (t)
$W$	Weight of the adsorbent (g)
$V$	Volume of the solution (mL)
$k_1$	Pseudo-first-order rate constants
$k_2$	Pseudo-second-order rate constants

# Table of Contents

Abstract.....	ii
Acknowledgments.....	iii
Abbreviations.....	iv
List of Symbols.....	v
Table of Contents.....	vi
List of Tables .....	xii
List of Figures.....	xiv
List of Appendices.....	xviii
Chapter 1. Review of literature.....	1
1.1. Carbon and it's allotropic forms.....	2
1.2. Biomass: attractive precursor for carbon production.....	2
1.3. Carbon production process.....	3
1.4. Activation of carbon.....	3
1.4.1. Physical activation.....	4
1.4.2. Chemical activation.....	6
1.5. Functionalization of porous carbon.....	9
1.6. Applications of porous activated carbon.....	9
1.7. Hemp fibers as a potential precursor for carbon production.....	9
1.8. Oil sands process-affected water (OSPW).....	11
1.8.1. Oil sands naphthenic acids .....	12
1.8.2. Toxicity of naphthenic acids.....	13
1.8.3. Model naphthenic acid compounds.....	13

1.9. Removal of NAs by adsorption on activated carbon.....	15
2.0. Statement of problems, research interest, and thesis outline.....	17
2.1. References.....	19
Chapter 2. One Step Preparation of Highly Porous Carbon derived from Biowaste Hemp Fibers: Process Optimization.....	30
2.1. Introduction.....	31
2.2. Experimental.....	33
2.2.1. Materials and chemicals.....	33
2.2.2. Methods.....	34
2.2.2.1. Preparation of hemp derived porous carbon materials (HFCs).....	34
2.2.2.2. Optimization of parameters for preparation of porous HFCs.....	34
2.2.2.3. Yield of porous carbon and burn-off.....	35
2.2.2.4. Characterization of HFs and obtained HFCs.....	35
2.3. Results and discussion.....	36
2.3.1. Evaluation of optimal parameters for preparation of HFCs.....	36
2.3.1.1. Effect of carbonization temperature.....	36
2.3.1.2. Effect of ZnCl <sub>2</sub> : HFs ratio.....	38
2.3.1.3. Carbon yield and burn-off.....	41
2.3.1.4. Effect of other activating agents.....	41
2.3.1.5. Comparative evaluations.....	43
2.3.2. Activation mechanism.....	45
2.3.2.1. ZnCl <sub>2</sub> activation.....	45

2.3.2.2. Activation with alkali metal carbonates and hydroxides.....	45
2.3.3. N <sub>2</sub> adsorption-desorption isotherms.....	47
2.3.4. FT-IR Spectra.....	48
2.3.5. SEM analysis.....	50
2.3.6. XRD analysis.....	51
2.3.7. Raman spectra.....	52
2.3.8. High resolution transmission electron microscopy (HRTEM) image.....	53
2.4. Conclusions.....	54
2.5. Acknowledgements.....	55
2.6. References.....	55
Chapter 3. Preparation of Nitrogen-doped Hemp Fibers-Based Mesoporous Carbon.....	61
3.1. Introduction.....	62
3.2. Experimental.....	64
3.2.1. Materials and chemicals.....	64
3.2.2. Methods.....	64
3.2.2.1. Preparation of N-HFCs.....	64
3.3.2.2. Surface characterization.....	67
3.3. Results and discussion.....	67
3.3.1. Elemental composition analysis.....	67
3.3.2. Nitrogen adsorption-desorption isotherms.....	68
3.3.3. Comparative evaluation.....	70
3.3.4. X-ray diffraction analysis.....	71

3.3.5. Spectroscopic analysis.....	72
3.4. Conclusions.....	74
3.5. References.....	74
Chapter 4. Utilization of Hemp Fibers-Based Carbon for Adsorptive Removal of Model Naphthenic Acids (NAs) from Aqueous Solution.....	
4.1. Introduction.....	82
4.2. Experimental.....	82
4.2.1. Materials and chemicals.....	82
4.2.2. Methods.....	82
4.2.2.1. Preparation of hemp fibers-derived mesoporous carbons.....	82
4.2.2.2. Batch adsorption experiments.....	83
4.2.2.3. Control experiment.....	84
4.3. Results and discussions.....	85
4.3.1. Effect of adsorbent dose on adsorption of model NAs.....	85
4.3.2. Adsorption efficiency in various initial concentrations of adsorbate.....	86
4.3.3. Adsorption isotherm.....	87
4.3.4. Adsorption kinetics.....	88
4.3.5. Effect of solution pH on adsorption of model NAs.....	96
4.3.6. Comparison of adsorption performance.....	97
4.3.7. Proposed adsorption mechanism.....	98
4.4. Conclusions.....	99
4.5. References.....	100
Chapter 5. Collaboration with Industry Partner: Characterization of Supplied Hydrothermal Carbon (HTC) and Production of Activated Carbon from HTC.....	
	104

5.1. Introduction.....	105
5.1.1. Project goals and deliveries.....	106
5.2. Morphology and structural characterization.....	107
5.2.1. Surface characterization of parent HTC materials.....	107
5.2.1.1. N <sub>2</sub> adsorption-desorption isotherm and BET surface area.....	107
5.2.1.2. XRD analysis.....	109
5.3. Carbonization of HTC samples.....	110
5.3.1. Method of carbonization.....	110
5.3.1.1. Effect of carbonization temperature on carbon yield.....	110
5.3.2. Raman spectra.....	111
5.3.3. N <sub>2</sub> adsorption-desorption isotherm.....	114
5.4. Analysis of crystalline silica.....	115
5.4.1. Ash preparation.....	115
5.4.2. Ash characterization.....	116
5.4.2.1. SEM-EDX of HTC ashes.....	116
5.4.2.2. ICP-MS analysis.....	118
5.5. Extraction of soluble fractions from HTC samples.....	119
5.5.1. Extraction methods.....	119
5.5.2. Extraction procedure.....	120
5.5.3. Extraction of HTC sample S17.....	120
5.5.4. Extraction of HTC sample S97.....	122
5.5.5. Extraction of HTC sample S2015.....	124
5.6. Summary of Soxhlet extraction.....	124
5.7. Gel permeation chromatography (GPC) of THF extract samples.....	125

5.7.1. Sample preparation.....	125
5.8. Molecular weight distriburion analysis.....	127
5.9. Conclusions.....	128
6.0. References.....	128
Chapter 6. Overall conclusions and future directives.....	131
6.1. Overall conclusions.....	131
6.2. Future directives.....	133
Appendices 5.1. Molecular weight distribution curves for parent feed materails obtained by GPC.....	135

## List of Tables

Table 1.1. List of model compounds identified in the literature survey.....	14
Table 2.1. Effect of mass ratio of activator: substrate ( $ZnCl_2$ :HFs) on surface areas of porous carbons produced.....	39
Table 2.2. Effect of temperature and mass ratio of activator: substrate on carbon yield (%) and burn off (%) in preparation of porous activated carbon from HFs using $ZnCl_2$ activating agents.....	42
Table 2.3. BET surface area, average pore diameter and pore volume of HFCs prepared by using different activators.....	42
Table 2.4. Comparison of surface area of HFC with similar nanoporous carbon materials derived from other biomass-based wastes by chemical activation method with $ZnCl_2$ activating agent.....	43
Table 2.5. Comparison of characteristics of HFC of this study with that of commercial activated carbons.....	44
Table 3.1. Elemental composition of HFs without chemical modification, and N-HFCs obtained by carbonization of N-HFs at different ratio of $ZnCl_2$ activator.....	67
Table 3.2. Surface characteristics of pretreated HFs as well as N-HFC materials.....	70
Table 3.3. Comparison of surface area and N-content of N-HFC-2 with N-enriched porous carbons prepared from various precursors.....	70
Table 4.1. Evaluated pseudo-first-order and pseudo-second-order rate constants and correlation coefficient for the adsorption of 2-naphthoic acid and benzoic acid on HFC.....	93
Table 4.2. Evaluated pseudo-first-order and pseudo-second-order rate constants and correlation coefficient for the adsorption of 2-naphthoic acid and benzoic acid on N-HFC.....	93

Table 4.3. Comparative studies of hemp-derived materials with various kinds of other adsorbents for model NAs reported in the literature.....	94
Table 5.1. Summary of BET surface area, total pore volume and pore size of the sample.....	108
Table 5.2. Yield (%) of carbon as a result of carbonization of HTC at different temperatures.....	111
Table 5.3. Summary of calcination results.....	116
Table 5.4. Elemental analysis by SEM-EDX.....	117
Table 5.5. Extraction of S17 with different solvents.....	121
Table 5.6. Extraction of S97 with different solvents.....	122
Table 5.7. Extraction of S2015 with different solvents.....	124
Table 5.8. Average concentration (mg/mL) and w% of THF extract of the samples subjected to GPC analysis.....	126
Table 5.9. Molecular weight parameters and polydispersity of THF extract of different parent materials using PAS columns.....	127

## List of Figures

Figure 1.1. Structure of some allotropes.....	2
Figure 1.2. Schematic process of production of highly porous carbon from biomass.....	3
Figure 1.3. Schematic diagram of the experimental set up used for carbonization and activation.....	7
Figure 1.4. Chemical structure of a representative naphthenic acid.....	12
Figure 2.1. Effect of carbonization temperature on surface area (a), pore volume (b) and pore size (c) of hemp derived porous carbons HFCs.....	38
Figure 2.2. The pore size distribution of HFCs determined by the BJH method.....	40
Figure 2.3. Nitrogen adsorption-desorption isotherms at 77 K for ZnCl <sub>2</sub> activated porous carbons prepared at variable mass ratio of activator: substrate (carbonization temperature = 500°C) and that of commercial granular activated carbon (commercial GAC).....	48
Figure 2.4. Comparison of FT-IR spectra of the pretreated HFs, HFCs and commercial GAC.....	50
Figure 2.5. SEM images of pretreated HFs (a), HFC-0-500 (b), HFC-2-500 (c) and commercial GAC (d).....	51
Figure 2.6. XRD patterns of HFs, HFCs and commercial GAC.....	52
Figure 2.7. Raman spectra of HFC-0-500 (a) and HFC-2-500 (b).....	53
Figure 2.8. HRTEM image of HFC-2-500.....	54
Figure 3.1. Nitrogen adsorption-desorption isotherms at 77 K (a), and (b) pore size distribution (b) of N-HFCs.....	69
Figure 3.2. XRD analysis of N-HFC samples.....	72

Figure 3.3. SEM image (a), Raman spectra (b), and high-resolution TEM spectrum (c) of N-HFC-2.....	73
Figure 4.1. Effect of adsorbent dose for removal of 2-naphthoic acid and benzoic acid from aqueous solution at pH 4.4 with (a) HFC and (b) N-HFC.....	86
Figure 4.2. Adsorption efficiency of (a) HFC and (b) N-HFC with varying initial concentrations of model NAs.....	87
Figure 4.3. Adsorption of 2-naphthoic acid and benzoic acid as a function of contact time on HFC (a and b) and N-HFC (c and d).....	88
Figure 4.4. Adsorption isotherm of (a) HFC and (b) N-HFC with varying initial concentrations of model NAs.....	90
Figure 4.5. Fitting of kinetic data of adsorption of 2-naphthoic acid and benzoic acid on HFC according to (a) pseudo-first-order kinetic model and (b) pseudo-second-order kinetic model.....	92
Figure 4.6. Fitting of kinetic data of adsorption of 2-naphthoic acid and benzoic acid on N-HFC according to (a) pseudo-first-order kinetic model and (b) pseudo-second-order kinetic model.....	92
Figure 4.7. Adsorption of model NAs at pH 8.5 on HF-derived carbon adsorbents. Adsorption of (a) 2-naphthoic acid and (b) benzoic acid on HFC and N-HFC.....	97
Figure 4.8. Comparison of adsorption performance of hemp-derived carbon materials and commercial activated carbon for adsorption of (a) 2-naphthoic acid, and (b) benzoic acid.....	98
Figure 5.1. Nitrogen adsorption-desorption isotherms of (a) S17, (b) S97, and (c) S2015.....	109
Figure 5.2. XRD analysis of S17, S97 and S2015.....	110
Figure 5.3. Raman spectra of HTC samples S17 and S97 (a), and the carbons prepared from the feed materials at different carbonization temperatures.....	113

Figure 5.4. Comparison of BET surface area of HTC samples and respective carbons prepared by carbonization at 1000 °C. The data obtained by BET analysis were also treated with Rouquerol transform software.....115

Figure 5.5. Photographs of the residues of burnt HTC samples.....116

Figure 5.6. ICP-MS analysis of ashes of S17 and S97.....119

Figure 5.7. Photographs of Soxhlet extraction of non-sieved S17 with THF.....121

Figure 5.8. Photographs of Soxhlet extraction of non-sieved S97 with THF.....123

Figure 5.9. Photographs of Soxhlet extraction of non-sieved S2015 with THF.....124

## List of Scheme

Scheme 3.1. Preparation route of N-aminoguanidine modified HFs (N-HFs).....	65
---	----

## List of Appendices

Appendix 5.1. Molecular weight distribution curves for parent feed materials obtained by GPC.....	135
---	-----

# Chapter 1

## 1 Review of Literature

### 1.1. Carbon and its allotropic forms

Some remarkable properties of carbon such as electrical and thermal conductivity, chemical stability, high porosity, and tunable surface chemistry have made carbon-based materials widely applicable in various fields of science and technology [1]. Being one of the most abundant crustal elements, carbon is viewed as a sustainable resource for the materials and engineering sector. It is one of the most well-known elements, and has been studied since ancient times. In the periodic table, carbon element occupies quite a unique position – it has an atomic number of six with four outer electrons, and is able to form multi-bonding due to its existence in  $sp^1$ ,  $sp^2$  and  $sp^3$  hybridizations. This unique property of carbon has made it an element of immense versatility enabling it to combine with hydrogen, oxygen, nitrogen, and other elements to form millions of compounds.

From a structural point of view, carbon atoms combine in different ways resulting into the formation of a variety of structures (some examples are shown in Figure 1.1) that exhibit specific properties which are intrinsically connected to their structure. These different structural forms of carbon are called allotropes of carbon. Conventionally known forms of carbon are amorphous carbon [2,3], graphite [4-6], diamond [7,8], and graphene [9-11]. Recent developments have resulted in other forms of carbon such as fullerenes [12,13], carbon nanotubes [14,15], nanosheets [10] and, nanowires [16]. Diamond, in which each carbon atom is covalently bonded with four neighboring carbon atoms, has the regular lattice arrangement of carbon atoms in tetrahedral fashion, and is the highly ordered crystalline form of carbon. Graphene is a two-dimensional form of crystalline carbon in which each carbon is bonded with three neighboring carbon atoms resulting in hexagonal lattice whereas graphite is a three-dimensional crystal structure of weakly bonded graphene layers. Graphene can be regarded as the parent form of all graphitic carbons including graphite, nanotubes, and fullerene. Thus, the structures in all

known carbon forms can be considered as a continuous decrease in the degree of orderness from the most highly ordered tetrahedral arrangement of carbons in diamond to three-dimensional hexagonal graphite to the most disordered porous carbon.

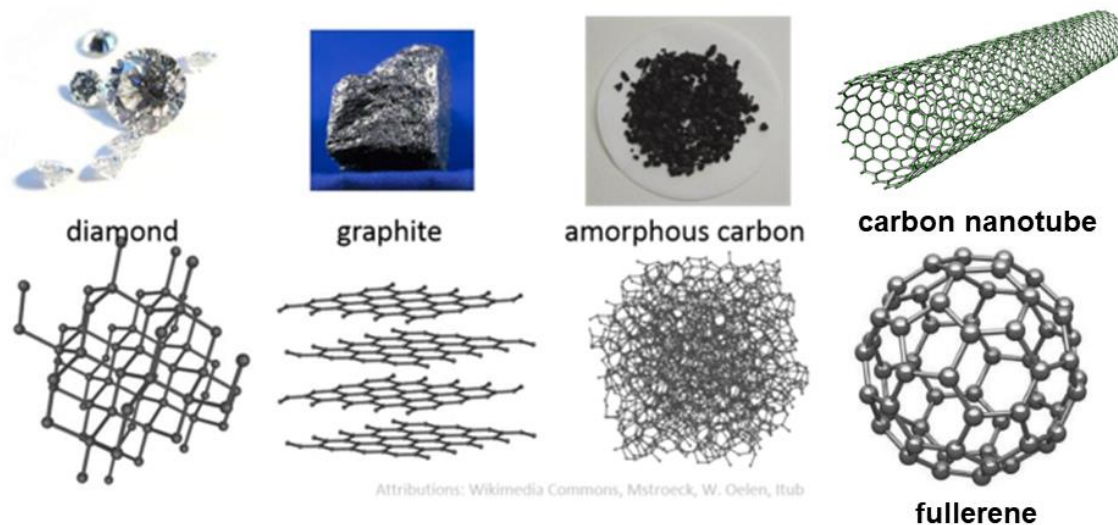


**Figure 1.1. Structure of some allotropes of carbon.**

## 1.2. Biomass: attractive precursor for carbon production

Any carbonaceous material with low content of inorganic compounds/salts can be used as a raw material for carbon preparation. Most of the carbon materials are prepared from fossil raw materials, which are non-renewable and depleting. In addition, obtaining carbon from fossil-based sources is not environmentally friendly. Consequently, in recent years, interest has shifted to biomass-based carbonaceous materials such as forestry or agricultural by-products for production of porous carbon. Biomass properties such as i) abundancy of carbon as one of the major constituent elements, ii) suitability to cope up with the issues of sustainability and availability, and iii) natural porous structure have made this waste stream (biomass) a promising carbon precursor (17,18). The use of bio-waste in carbon preparation potentially offers a considerable contribution to bio-based circular economy (which is recently highly sought after) and provides a sustainable alternative to existing commercially available coal-based carbons (19, 20). In addition, use of bio-waste for production of chemicals/reagents/materials as opposed to obtaining the same from fossil-based resources helps combat with ever increasing environmental

issues. This urges the need for developing sustainable technology platform for innovative utilization of bio-waste for the development of carbon alongside other useful products/chemicals/reagents.

### 1.3. Carbon production process

Production of porous carbon from carbonaceous materials involves the pyrolysis of raw carbonaceous materials in an inert gas environment to produce a richer carbon material, and the process usually takes place in two phases: carbonization and activation as shown in Figure 1.2 [21]. Carbonization involves the thermal degradation of the carbonaceous material and removal of volatile compounds (such as compounds of oxygen, hydrogen, nitrogen and sulphur species) from the raw materials. The primary purpose of activation is to enlarge the diameter of the fine pores and also to create new pores [22]. Chemical and physical/thermal activation are the common ways of modifying the pore size and/or pore distribution of carbons prepared from biomass.

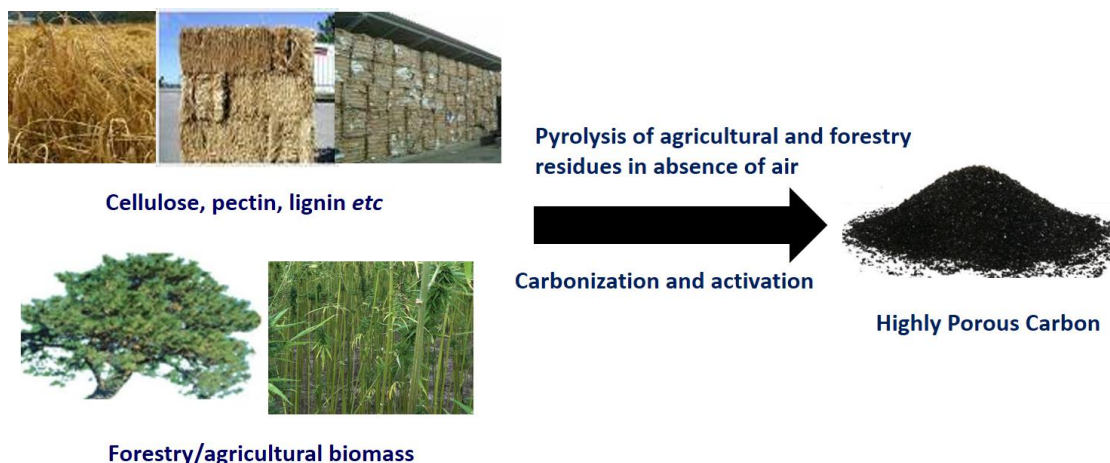


**Figure 1.2. Schematic process of production of highly porous carbon from biomass.**

### 1.4. Activation of Carbon

The porosities of carbon, as initially developed by carbonization, are not sufficiently developed for most applications, and porosity amelioration is a prerequisite step to

enhance the applicability of prepared carbon. This is done in a number of ways involving creation of further porosity, widening of existing pores/porosity, modifications on the surfaces for porosity development, and increasing surface area. There are two methods – physical activation and chemical activation – to activate carbon.

### 1.4.1. Physical activation

Physical activation consists of two steps: carbonization of carbon precursors at high temperature in an inert atmosphere to remove most of the non-carbon elements such as H, N, and O contents, followed by activation at high temperature (800-1000°C) in the presence of steam or oxidizing gases such as CO<sub>2</sub> [23]. Steam activation has a positive effect on specific surface area, pore volume, and pore size distribution, and might increase the oxygen content of the final product [24]. A number of factors such as the biomass type, activation time, and activation temperature affect the properties of activated carbons produced by physical activation method. [25]. Gasification is done usually to produce carbon with different porosities, which happens mainly by the removal of some of the carbon in the form of gaseous products according to following equations [26].



Iranmanseh *et al.* (2014) produced microporous activated carbon from sawdust by carbonization followed by physical activation with CO<sub>2</sub>. Carbonization consisted of heating sawdust under a constant flow of nitrogen for 2 hours at 550°C. The carbonized sawdust was then physically activated with CO<sub>2</sub> in the temperature range of 700 to 900°C for 1 hour. The total surface area of the resulting carbon products ranged from 397 to 731 m<sup>2</sup>/g, with burn offs up to 82% [27].

Bergna *et al.* (2018) investigated the effects of using two different processes in the production of activated carbon by physical activation of carbon produced from wood chips of spruce and birch. In one process, the chips were carbonized and the carbon formed was later activated by steam activation. In this process, the carbonization and

activation steps were separated in time. In the other process, the wood chips were carbonized and activated in a simultaneous one-stage sequence. While no significant differences were noticed regarding the total carbon content of the produced activated carbons in one-stage vs two-stage processes, small differences between the starting materials were observed. The carbon yield was apparently higher in the two-stage process, but the one-stage process produced activated carbon with higher surface areas [28].

In a study, Aworn *et al.* (2009) found that preparation of activated carbon from corn cobs by CO<sub>2</sub> activation was largely dependent on the temperature of activation; increasing temperature (in the range of 300 – 800°C) resulted in lower carbon yield but higher surface area [29]. In the preparation of activated carbon from oil palm stones by one-step CO<sub>2</sub> activation at different activation temperatures, Lua and Guo (2000) found that the particle size and the heating rate had no significant effects on the BET surface areas of the activated carbons whereas CO<sub>2</sub> flow rate, activation temperature, and hold time (duration of activation) had significant influence on BET surface area of the final products. Through evaluation of effects of time and temperature, an activation temperature of 850°C and a hold time of 2 hours were identified as optimal conditions for activation at which maximum BET and micropore surface areas were found to be 1410 and 942 m<sup>2</sup>/g, respectively. The pore size distributions of the activated carbons also confirmed these optimal conditions [30].

The effects of activation temperature (700, 720, 740 and 760 °C) and time (60, 90, and 120 min) on the mass yield and characteristics of the activated product in production of porous activated carbon from rubber wood sawdust was investigated by Mazian *et al.* (2016). The mass of activated carbon yield decreased with increasing carbonization temperature, but the carbon prepared at higher temperatures had improved surface area and pore volume and activation at 740 °C for 1 hour was recommended for CO<sub>2</sub> activation [31].

## 1.4.2. Chemical activation

Chemical activation is generally conducted by impregnating carbonaceous material with chemical agents such as alkali (KOH,  $K_2CO_3$ ), transition metals salts ( $AlCl_3$ ,  $ZnCl_2$ ,  $FeCl_3$ , etc), or certain acids ( $H_3PO_4$ ,  $H_2SO_4$ ), where the porosity is developed by dehydration reactions carried out by the activating reagents [32-39]. In a general procedure, the raw carbonaceous material is first impregnated with chemical agents. The impregnated sample is then carbonized under  $N_2$  atmosphere at a certain carbonization temperature. The experimental set-up for carbonization and activation is shown in (Figure 1.3). In contrary to physical activation (which is a two-step process), chemical activation is a one-pot or one-step process in which carbonization and activation proceed simultaneously. Chemically activated carbons generally show higher surface area than those of physically activated carbons [40]. Consequently, the chemical activation method has been regarded advantageous over thermal activation method due to a low energy consumption, high yield with well-developed porosity, and one-step accomplishment of carbonization and activation [22]. However, the main disadvantages of using chemical compounds as activator are that they are not environmentally friendly substances and are corrosive towards the equipment used for carbon preparation. Additionally, an acid washing step is needed after chemical activation in order to remove the side products/salts formed by chemical activating agent [36,38].

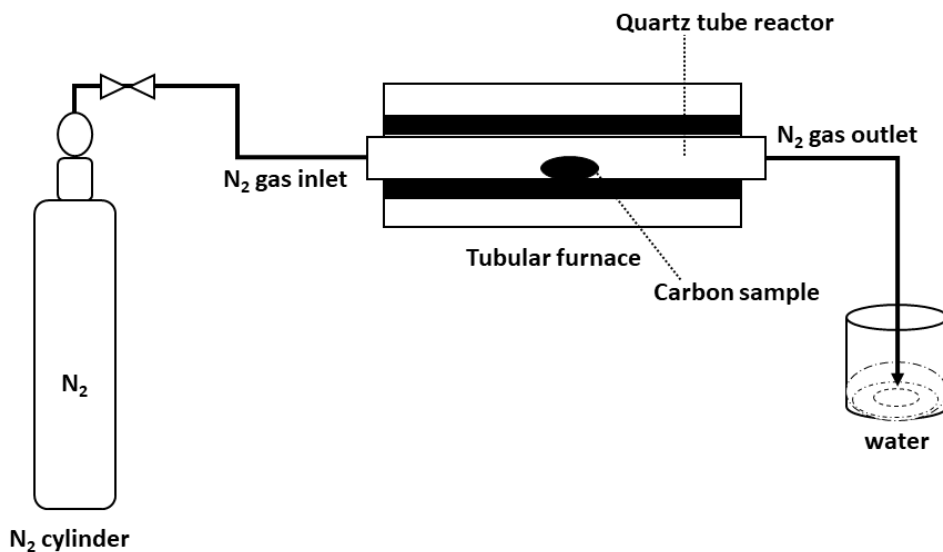
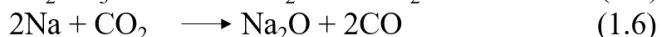
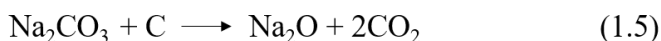
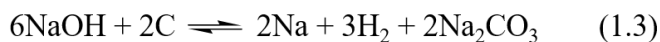


**Figure 1.3: Schematic diagram of the experimental set up used for carbonization and activation.**

The mechanism of carbonization in the presence of chemical activator is basically the decomposition and dehydration of raw materials preventing tar formation, and formation and removal of other volatile products. Pores are developed by dehydration and oxidation reactions affected by the chemicals. Lillo-Ródenas *et al.* have proposed the chemical reactions between carbon and alkaline metal hydroxides (NaOH and KOH), according to which the reactions produce metal, hydrogen, and metal carbonates. The following reaction can be described with Equations (1.3-1.6) [39-41].



In preparation of activated carbon by the chemical activation method, the type and amount of chemical activator, the ratio of weight of activator to that of carbonaceous material, and temperature of carbonization/activation are all important. In the production of activated carbon from tomato waste by ZnCl<sub>2</sub> activation, Sayğh and Güzel (2016) evaluated the effects of mass ratio of activator: substrate (1:1, 2:1, 4:1, 6:1 and 8:1),

carbonization temperature (400, 600 and 800 °C, and carbonization time (0.5, 1.0, 2.0 and 4 h) on the surface area and pore size of produced carbons. Results revealed that the BET surface area and pore volume of produced activated carbon were highest when mass ratio of activator: substrate (weight ratio of ZnCl<sub>2</sub>: carbonaceous material) was 6:1, carbonization temperature was 600 °C, and carbonization time was 1 h. The activated carbon produced at optimal conditions had the surface area of 1093 m<sup>2</sup>/g with the total pore volume of 1.569 cm<sup>3</sup>/g, and average pore diameter of 5.92 nm [42].

In preparation of low cost activated carbon from the grape stalk, Ozdemir *et al.* (2014) used chemical activation with ZnCl<sub>2</sub> under CO<sub>2</sub> atmosphere. Studies on the influence of carbonization temperatures and time, and mass ratio of activator: substrates on the pore development and yield of activated carbon revealed that the carbon yields decreased and BET surface area increased with increasing carbonization temperature and mass ratio of activator: substrate. The maximum (1411 m<sup>2</sup>/g) specific surface area of the activated carbon was achieved upon carbonization at 700°C for an activation duration of 2 hours and mass ratio of activator: substrate of 2:1 [43].

The effects of different chemical agents such as ZnCl<sub>2</sub>, K<sub>2</sub>CO<sub>3</sub>, NaOH and H<sub>3</sub>PO<sub>4</sub> in the production of activated carbon from biomass has also been investigated. Kthç *et al.* (2012) used carbon from *Euphorbia rigida* for these studies. The yields of activated carbons were decreased with increasing mass ratio of activator: substrate for all the activating reagents. In terms of specific surface area, porosity development, and surface morphology of the activated carbons, K<sub>2</sub>CO<sub>3</sub> was more effective than the other activating agents under identical conditions of carbonization and activation. On the other hand, NaOH was found to be an ineffective activating reagent with almost no pore formation and very little improvement in surface area after activation [44].

Foo *et al.* (2012) reported on a microwave induced activation process for production of coconut husk-based activated carbon using different activating agents. The effects of various factors, such as microwave power (90-800 W), radiation time (4-8 min) and activation agents/carbon ratio (0.25-2.00) on the activation were studied. Their results

revealed that KOH was a better activating agent, and the surface area of 1356.25 m<sup>2</sup>/g with carbon yield of 48% was achieved under the optimal conditions using microwave assisted KOH activation of coconut husk [45].

Lim *et al.* (2010) conducted activation of palm shells by using phosphoric acid as an activator. Under optimal conditions (activation at 425 °C for 30 minutes), the process resulted in activated carbon of The BET surface area 1100 m<sup>2</sup>/g, pore volume 0.903 cm<sup>3</sup>/g, and average pore diameter of 3.2 nm. Interestingly, the yield of activated carbon was not affected by the mass ratio of activator: substrate with phosphoric acid activation [46].

## 1.5. Functionalization of porous carbon

Modification of carbon with specific functional groups for a desirable application is an important area of research. Introducing nitrogen and/or nitrogen-containing functionalities on carbon has been proven to be an effective method to improve the performance of carbon materials in various applications such as adsorption, catalysis, and electrical conductivity [47-50]. For adsorption processes, N-containing functional groups act as adsorption sites and increase the electrostatic interaction between the adsorbent and adsorbate. In addition, nitrogen functionality, being polar in nature, enhances carbon's ability to interact with water through non-covalent interactions (such as H-bond and polar interactions), thus enhancing hydrophilicity and wettability. Through the studies of contact angle of N-doped mesoporous carbon, Wang *et al.* (2019) have demonstrated that the hydrophilicity of N-doped mesoporous carbon materials increased with increasing surface N content, and that the N-doped carbon showed enhanced adsorption capacity for a poorly water soluble antitumor drug hydroxycamptothecin (HCPT) [50]. Recent studies show that N-doping could promote polarization of  $\pi$  electrons on carbon surfaces and generate more  $\pi$ -electron-rich and  $\pi$ -electron-deficit sites for adsorption [51-54]. The existence of nitrogen-containing functional groups on the surface of carbon materials generally provides basic properties and electron-donor affinity, which improves the removal of polar compounds such as organic acids due to dipole-dipole interactions and

H-bonding [53,54]. For reasons as such, growing interest lies towards the development of bio-based carbon material grafted with nitrogen atoms and/or nitrogen containing functional groups.

There are several ways to introduce nitrogen to the surface of carbonaceous adsorbents, such as amine treatment, nitric acid treatment, and treating carbon with other nitrogen-containing compounds [55]. Niasar *et al.* (2016) demonstrated that carbon with basic characteristics could be produced by treating both commercial activated carbon and raw petroleum coke using  $\text{NH}_3$  and amines at elevated temperature [56]. Zhou *et al.* (2018) developed a one-step method of producing nitrogen containing porous carbon by carbonization of carbonaceous material with a nitrogen precursor and activating agent. Their study used potato waste residue as a carbon precursor, melamine as nitrogen source, and KOH as activating agent [57]. In a similar study, Ma *et al.* (2015) prepared nitrogen-doped carbon using sugar cane bagasse, urea, and KOH [58].

## 1.6. Applications of porous activated carbon

The activated carbon materials have excellent surface properties with the high degree of porosity and the high specific surface area. Due to the remarkable properties porous activated carbons are widely used in various applications [59,60]. For instance, application of activated carbon in environmental remediation, filtration, and separation technologies, as a sorbent of organic and inorganic pollutants from water and as a sorbent of hazardous gases, is well known. The activated carbons also have wide application in power engineering (as hydrogen storage material and the electrochemical capacitor), and catalyst supports.

## 1.7. Hemp fibers as potential precursor for carbon production

In recent years, hemp fibers (referred to as HFs hereafter) have received voluminous attention as a potential precursor for production of activated carbon due to the ease of availability and low-cost. As hemp fibers are considered as one of the strongest members of bast natural fibers family, hemp is primarily grown industrially for its fibers. The

fibers are obtained from the stalk of the plant. The hemp stalk contains two types of fibers – the long bast fibers found in the bark and the short fibers (hurds) located in the core of the stem. The long bast fibers, that typically constitute 20-30% of the stalk, are used for production of textiles and ropes. Lately, these fibers are attracting considerable attention for their application in composite materials.

The crop (hemp) is also grown for dual purposes – for producing fibers as well as seeds. Whilst the fibers are processed for their well-known applications, the seeds are used for food and cosmetic applications as hemp seed and hemp seed oil. The crop grown for dual purposes, however, yields relatively lower quality fibers than that of the crop grown specifically for fibers.

Hemp fibers are composed of three main fractions – cellulose, hemicellulose, and lignin. The long, best quality fibers are high in cellulose content (50-70%) and low in lignin content (about 7%) whereas the hurds are low in cellulose and high in lignin (typically 20-30%). The more lignified the fibers are, the less suitable they are for certain applications such as in textile industry. Thus, it is important to find alternate applications of the fibers that are deemed less suitable for their conventional use. Recent research has demonstrated that the chemical composition (of cellulose, hemicellulose, and lignin) and fibrous structure enable hemp fibers to be an attractive feedstock for carbon materials with specific structures and tunable properties [19, 33]. Despite this specific property of hemp fibers, the short type of fibers (hurds) are considered the waste by-product of bast fiber production. Additionally, substantial amounts of hemp stalks/fibers are still left in harvested fields without further utilization, resulting in the waste of valuable resource. Therefore, it is very important to convert this rich source of carbonaceous species into carbon materials.

## 1.8. Oil sands process-affected water (OSPW)

Canada's oil sands, located in Northern Alberta, are among the largest deposits of oil in the world attributing to more than 170 billion barrels of oil sands reserves [61]. Oil sand processing consists of bitumen extraction from sand and clay, which is done either by

open pit mining or by in-situ extraction using thermal recovery methods. In both methods, large quantities of water are needed for bitumen extraction of bitumen; requiring an average of 3 to 6 barrels of water for one barrel of crude oil produced [62,63]. Water used for the extraction process is discarded in the form of alkaline hot water or high pressure steam, which forms a large amount of what is known as oil sands process-affected water (OSPW) [64]. The oil sand process generated OSPW ends up as contaminated water in tailings ponds, the size of which is ever increasing thereby contaminating nearby water bodies and posing threats to environment.

### 1.8.1. Oil sands naphthenic acids

The oil sand process-affected water (OSPW) generated by processing of oil sand contains several contaminants such as polycyclic aromatic hydrocarbons (PAHs), (poly)phenols, cresols, benzene, toluene, thiophenols, and naphthenic acids [63,65,66]. Among these, naphthenic acids have been known to cause serious environmental problems and are detrimental to flora and fauna [65]. Naphthenic acids is a collective term used to describe the acidic components present in OSPW, and is a complex mixtures of alkyl-substituted acyclic and cycloaliphatic carboxylic acids [63,65,66]. The chemical structure of typical naphthenic acids consists of a carboxylic acid end connected in a hydrocarbon chain to one or more cyclopentyl or cyclohexyl carbon rings (an example is shown in Figure 1.4). They have the general chemical formula  $C_nH_{2n+z}O_2$ , where  $n$  specifies the number of carbon atoms and  $z$  is either zero or a negative even integer [67-69].

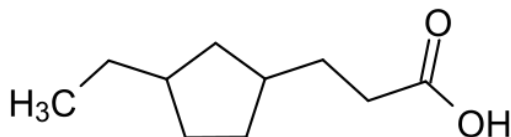


**Figure 1.4. Chemical structure of a representative naphthenic acid.**

Naphthenic acids are highly viscous liquids with characteristic odor, and have wide boiling point ranging between 250–350°C. Oil sands naphthenic acids typically have molecular weight greater than 120 g/mol. They are completely soluble in organic solvents and oils/lipids but are only sparingly soluble (<50 mg/L) or insoluble in water.

Chemically, naphthenic acids behave like usual carboxylic acids with dissociation constants between  $10^{-5}$  and  $10^{-6}$  and pKa values between 5 and 6. Solubility of naphthenic acids is dependent on pH, and can be increased under alkaline conditions (pH 8) [69-72]. Furthermore, due to both hydrophilic and hydrophobic constituents, naphthenic acids demonstrate surface active properties [71,72].

### 1.8.2. Toxicity of naphthenic acids

The concentration of naphthenic acids in tailings pond water ranges from 20-120 ppm [69-71]. High concentrations and the surface-active properties of naphthenic acids make them the most toxic compound in OSPW, and cause significant acute and chronic toxic concerns to aquatic organisms and algae [68]. Clemente and Fedorak (2005) found that the NA concentrations greater than 5 mg/L would be toxic to fish and surrounding wildlife [72]. Reportedly, naphthenic acid toxicity to aquatic animals comes from its surface active property leading to membrane disruption and the disruption of osmotic homeostasis to aquatic organisms [73,74]. Some investigations have suspected naphthenic acids as endocrine-disrupting substances [70, 73,75]. On the other side, high concentrations of naphthenic acids can potentially cause corrosion to the petroleum-refining operations at high temperatures [76,77]. Corrosion occurs through the formation of hydrogen gas at typical operating temperatures (200 to 400°C). Additionally, the carboxyl groups of these chemicals are able to react with metals and create functionalities that accelerate the corrosion process [78,79].

### 1.8.3. Model naphthenic acid compounds

The exact composition of OSPW is unknown, and it is very difficult to select the appropriate compounds that can be used to accurately model/mimic the behavior of OSPW. In several publications related to naphthenic acids, model naphthenic acids are used as representative compounds to mimic OSPW composition. These compounds were used either for calibration of analytical equipment, or for studies of environmental and/or and toxicological effects, or for evaluation of removal efficacy of adsorbents. The

commonly used model naphthenic acids that have been reported in the published literature are tabulated in Table 1.1.

**Table 1.1: List of model compounds identified in the literature survey**

Name	Formula	MW
Butanedioic, Succinic acid [92]	C <sub>4</sub> H <sub>6</sub> O <sub>4</sub>	118
Cyclopentane carboxylic acid	C <sub>6</sub> H <sub>10</sub> O <sub>2</sub>	114
Hexanoic acid [92]	C <sub>6</sub> H <sub>12</sub> O <sub>2</sub>	116
Benzoic acid [93]	C <sub>7</sub> H <sub>6</sub> O <sub>2</sub>	122
Cyclohexanecarboxylic acid [92-95]	C <sub>7</sub> H <sub>12</sub> O <sub>2</sub>	128
1,4-Cyclohexanedicarboxylic acid [92]	C <sub>8</sub> H <sub>12</sub> O <sub>4</sub>	128
3-methyl-1-cyclohexanecarboxylic acid [95]	C <sub>8</sub> H <sub>14</sub> O <sub>2</sub>	142
4-methyl-1-cyclohexane carboxylic acid [95]	C <sub>8</sub> H <sub>14</sub> O <sub>2</sub>	142
Adipic acid [92]	C <sub>6</sub> H <sub>6</sub> O <sub>4</sub>	142
3-Cyclohexanepropionic acid [93,96]	C <sub>9</sub> H <sub>16</sub> O <sub>2</sub>	156
4-Methycyclohexaneacetic acid (4MACH) [97]	C <sub>9</sub> H <sub>18</sub> O <sub>2</sub>	158
cyclohexane butyric acid (4-cyclohexylbutanoic acid) [98]	C <sub>10</sub> H <sub>18</sub> O <sub>2</sub>	170
4-propylcyclohexanecarboxylic acid [92]	C <sub>10</sub> H <sub>18</sub> O <sub>2</sub>	170
Citronellic acid [99]	C <sub>10</sub> H <sub>18</sub> O <sub>2</sub>	170
Decanoic acid [100]	C <sub>10</sub> H <sub>20</sub> O <sub>2</sub>	172
2-Naphthoic acid [101]	C <sub>11</sub> H <sub>8</sub> O <sub>2</sub>	172
1-Methyl-1-cyclohexanecarboxylic acid [102]	C <sub>8</sub> H <sub>14</sub> O <sub>2</sub>	172
1,2,3,4-tetrahydro-2-naphthoic acid [102]	C <sub>11</sub> H <sub>12</sub> O <sub>2</sub>	176
1-adamantane carboxylic acid [92], [102]	C <sub>11</sub> H <sub>16</sub> O <sub>2</sub>	180
Cyclohexanepentanoic acid [102]	C <sub>11</sub> H <sub>20</sub> O <sub>2</sub>	184
trans-4-tert-butylcyclohexanecarboxylic acid [102]	C <sub>11</sub> H <sub>20</sub> O <sub>2</sub>	184
1-adamantaneacetic acid [102]	C <sub>12</sub> H <sub>18</sub> O <sub>2</sub>	194
trans-4-pentylcyclohexane carboxylic acid [101],[102]	C <sub>12</sub> H <sub>22</sub> O <sub>2</sub>	198
Cyclohexylsuccinic acid [103]	C <sub>10</sub> H <sub>16</sub> O <sub>4</sub>	200

Lauric Acid; dodecanoic acid [104]	$C_{12}H_{24}O_2$	200
12-hydroxydodecanoic acid [102]	$C_{12}H_{24}O_3$	216
(4-cyclohexylphenyl)acetic acid	$C_{14}H_{18}O_2$	218
4-Heptyl benzoic acid [101]	$C_{14}H_{20}O_2$	220
3,5-Dimethyladamantane-1-acetic acid	$C_{14}H_{22}O_2$	222
Dicyclohexylacetic acid [102]	$C_{14}H_{24}O_2$	224
Diphenylacetic acid	$C_{14}H_{12}O_2$	212
4-Pentylbicyclo[2.2.2]octane-1-carboxylic acid	$C_{14}H_{24}O_2$	224
12-Methyltridecanoic acid	$C_{14}H_{28}O_2$	228
Myristic acid	$C_{14}H_{28}O_2$	228
(±)-6-Hydroxy-2,5,7,8-tetramethylchromane-2 carboxylic acid	$C_{14}H_{18}O_4$	250
(3aR)-(+)-Sclareolide	$C_{16}H_{26}O_2$	250
Palmitoleic acid [105]	$C_{16}H_{30}O_2$	254
hexadecanoic, Palmitic acid [104]	$C_{16}H_{32}O_2$	256
2-Hexyldecanoic acid [102]	$C_{16}H_{32}O_2$	256
Linolenic acid [105]	$C_{18}H_{30}O_2$	278
Linoleic acid [105]	$C_{18}H_{32}O_2$	280
Stearic acid [104]	$C_{18}H_{36}O_2$	284
1-pyrenebutyric acid [102]	$C_{20}H_{16}O_2$	288
12-hydroxysteric acid [102]	$C_{18}H_{36}O_3$	300
Abietic acid [102]	$C_{20}H_{30}O_2$	302
cis-4,7,10,13,16,19-Docosahexaenoic acid [105]	$C_{22}H_{32}O_2$	328

## 1.9. Removal of naphthenic acids by adsorption on activated carbon

During the last decades, researchers have devoted numerous efforts to develop suitable processes and materials for separation and removal of toxic naphthenic acids from the waste stream generated in oil sand processing. Among the traditional techniques,

adsorption is by far the most reliable, effective, and widely used technique for the removal of NAs from aqueous waste due to its simplicity, selectivity, scalability, and efficiency [74,80]. To date, studies performed to investigate the adsorption of organic contaminants have relied largely on the use of activated carbon (AC) and ion-exchange resins as adsorbents. Conventional activated carbon has undoubtedly been the most popular and widely used adsorbent to adsorb metal ions and organic molecules for the removal of pollutant species from liquids or gases [74,81-84]. The widespread applicability of activated carbon as adsorbent is due to its large specific surface area, large pore volume, multiple type of reactive surface sites, high chemical stability, easy availability, and low-cost preparation.

A number of studies have been performed to investigate the efficiency of activated carbon as adsorbents for naphthenic acid removal as well [85-88]. Mohamed *et al.* (2010) found that the sorption capacity of granular activated carbon (GAC) for naphthenic acids was much higher than that of polymeric sorbents [89]. Wu *et al.* (2001) demonstrated the adsorption of carboxylic acid-based surfactants with activated carbon [90]. Martinez-Iglesias *et al.* (2015) reported the adsorption of single and multicomponent model naphthenic acids on commercial granular activated carbon (GAC) [91]. Iranmanesh *et al.* (2014) produced activated carbons sawdust which were found to be effective for removal of NAs from aqueous solutions, demonstrating better performance than commercial AC sample [27]. Barnard used petroleum coke to produce AC using KOH as a chemical activation agent, which showed naphthenic acid removal efficiency of 80% from a solution of initial concentration of 41 ppm [75].

Niasar *et al.* (2016) introduced nitrogen-containing functional groups on the surface of both commercial activated carbon (AC) and raw petroleum coke. The adsorption performance of the surface modified AC and PAC towards model naphthenic acids was impressively enhanced by surface amination with nitrogen containing functional groups [56].

## 2.0. Statement of problems, research interest, and thesis outline

### **Statement of Problems**

Large volume of biomass is generated globally as agricultural and forestry residue. Despite being a sustainable resource of energy and materials, substantial amount of biomass is being disposed off through incineration or landfilling. This approach of biomass disposal (incineration and landfilling) not only contributes to air, water, and soil contamination, but also leads to emission of greenhouse gases. Increasing concerns and legislations to utilize renewable resources for reducing the global carbon footprints are driving research interests in the development of technology platforms for utilization of biomass feedstock for production of energy and materials.

The oil sands are one of Canada's largest industries, and drives Canada's economy. However, processing oil sands produces large volumes of oil sand process-affected water (OSPW) which is disposed off in tailing ponds. These tailing ponds contains several contaminants. Among such contaminants, naphthenic acids are notorious to pose toxic effects to environment, aquatic lives, and local flora and fauna. The concentration of naphthenic acids in tailings pond water ranges from 20-120 mg/L; whilst its concentration greater than 5 mg/L is considered to be toxic to aquatic animals and surrounding wildlife.

### **Research Objectives**

Conservation of energy and materials through reduce, re-use, and recycle of conventional resources, and efficient use of renewable resources is of utmost priority for sustainable development. Developing efficient ways for utilization of renewable resources (such as biomass) for production of biofuel and biomaterials is an integral area of research for combating with global challenges of energy and environment. One of the most important expertise of Charpentier group is hydrothermal treatment of biomass and production of advanced biofuel. This approach of biomass utilization produces hydrochar, which is

currently being used for a low-value application like soil amendment. Development of porous activated carbon with high specific surface area and appropriate pore distribution from a cheap and green route is an attractive way of producing value-added products from biowaste precursor(s). The main objective of this research is to utilize biomass as a renewable resource of carbon to make porous activated carbon, and investigate the potential of the produced carbon for environmental remediation.

A part of this thesis work conducted industry-driven problem-solving research activities by working in collaboration with a leading industry partner interested in biomaterials engineering and bio-based economy. Working in collaboration with the industry partner, one of the objectives of the present research was to help the industry partner characterize the biomaterial(s) they produce and also help them develop efficient technologies for valorization of their products/materials. Accordingly, the specific objectives of the present work are as follows:

1. To design and develop improved methods and/or products to develop high surface area porous activated carbons from a lignocellulose precursor material hemp fiber by simple, single-step carbonization method using a chemical activator.
2. To investigate the effects of carbonization temperature and the amount of activator (mass ratio of activator: substrate) on the surface area and surface properties of the produced carbons.
3. To prepare nitrogen-containing porous carbon from hemp fibers by chemical modification of hemp fibers with nitrogen-containing functional groups followed by activation and carbonization of chemically modified hemp fibers.
4. To characterize the prepared porous carbons with BET (Brunauer-Emmett-Teller) surface area, XRD (X-ray Diffraction), SEM (Scanning Electron Microscopy), HRTEM (High Resolution Transmission Electron Microscopy), Raman scattering, and elemental composition.
5. To explore the potential of prepared carbons as adsorbents for removal of naphthenic acids from contaminated aqueous solution.

6. To characterize the hydrothermal carbon (HTC) provided by our industry partner and develop high-value porous activated carbon from the provided hydrothermal carbon.

### **Thesis Outline**

Depending on the objective of research work and experiments accomplished, this thesis consists of six chapters.

**Chapter one** is the review of literature. This chapter provides general introduction of carbon materials, biomass resources, and methods of preparation of activated carbon from biomass. This chapter also discusses the ever-increasing issues of naphthenic acid contaminated oil sands tailings ponds of oil sand industry, and removal/remediation technologies.

**Chapter two** demonstrates a simple, single-step carbonization method for production of porous activated carbon by zinc chloride ( $\text{ZnCl}_2$ ) activation of hemp fibers (HFs), and describes the characterization of produced activated carbons.

**Chapter three** describes the preparation of nitrogen-containing porous activated carbon from hemp fibers by chemical modification of hemp fibers with N-aminoguanidine followed by activation and carbonization of chemically modified hemp fibers using  $\text{ZnCl}_2$  in inert atmosphere and characterization of prepared porous carbons.

**Chapter four** illustrates the potential applications of prepared porous carbons for the removal of model naphthenic acids from aqueous waste solution. This chapter also describes the investigations made to distinguish the adsorption mechanisms responsible for the removal of model naphthenic acids by the prepared porous carbons.

**Chapter five** describes the methods/methodologies used, and results of characterization of hydrothermal carbon (HTC) provided by the industry partner. The chapter also describes the method of preparation of porous activated carbon from the supplied HTCs.

**Chapter six** presents the conclusions and recommendations for future study.

## 2.1. References

- [1] G. Messina, S. Santangelo. Carbon: The future material for advanced technology applications: Springer; 2006.
- [2] J. Robertson, Amorphous carbon. *Adv. Phys.* 1986(36)317-374.
- [3] A. C. Ferrari, J. Robertson, Interpretation of Raman spectra of disordered and amorphous carbon. *Phys. Rev. B.* 2000(61)14095.
- [4] H. O. Pierson, Handbook of carbon, graphite, diamond, and fullerenes: properties, processing, and applications: Noyes Publications Park Ridge, NJ; 1993.
- [5] F. Tuinstra, J. L. Koenig, Raman spectrum of graphite. *J. Chem. Phys.* 1970(53)1126.
- [6] P.R. Wallace, The band theory of graphite. *Phys. Rev.* 1947(71)622.
- [7] A.H. Lettington, J. W. Steeds, Thin film diamond: Chapman and Hall;1994.
- [8] Y. Hirose, Y. Terasawa, Synthesis of diamond thin films by thermal CVD using organic compounds. *Jpn. J. Appl. Phys.* 1986(25)L519-L21.
- [9] S. Stankovich, D. A. Dikin, R. D. Piner, K. A. Kohlhaas, A. Kleinhammes, Y. Jia, Y. Wu, S. T. Nguyen, R. S. Ruoff, Synthesis of graphene-based nanosheets via chemical reduction of exfoliated graphite oxide. *Carbon* 2007(45)1558-1565.
- [10] A. K. Geim, Graphene: Status and prospects. *Science* 2009(324)1530-1534.
- [11] A. K. Geim, K. S. Konstantin, The rise of graphene. *Nat. Mat.* 2007(6)183-191.
- [12] M. Prato, Fullerene chemistry for materials science applications. *J. Mater. Chem.* 1997(7)1097-109.
- [13] F. Diederich, M. Gómez-López, Supramolecular fullerene chemistry. *Chem. Soc. Rev.* 1999(28)263-77.
- [14] P. M Ajayan, Q. Z Zhou, Applications of carbon nanotubes. *Carbon nanotubes: Springer* 2001, p.391-425.
- [15] R. Saitô, G. Dresselhaus, M. S. Dresselhaus, Physical properties of carbon nanotubes. London: Imperial College Press, c1998.
- [16] G. Zhou, L. Xu, G. Hu, L. Mai, Y. Cui, Nanowires for electrochemical energy storage. *Chem. Rev.* 2019(20)110402-11109.
- [17] J. M. Valente Nabais, C. Laginhas, M. M. I Ribeiro Carrott, P. J. M. Carrott, J. E. Crespo Amorós, A. V. Nadal Gisbert, Surface and porous characterization of activated

carbons made from a novel biomass precursor, the esparto grass. *Appl. Surf. Sci.* 2013(265)919-924.

[18] L. Khezami, A. Chetouani, B. Taouk, R. Capart, Production and characterization of activated carbon from wood components in powder: Cellulose, lignin, xylan, *Powder Technol.* 2005(157) 48-56.

[19] J.M. Rosas, J. Bedia, J. Rodríguez-Mirasol, T. Cordero, HEMP-derived activated carbon fibers by chemical activation with phosphoric acid, *Fuel* 88 (2009) 19–26.

[20] L. Shijie, H. Kuihua, Li. Jinxiao, Li. Ming, Lu. Chunmei, Preparation and characterization of super activated carbon produced from gulfweed by KOH activation, *Micropor. Mesopor. Mat.* 2017(243)291-300.

[21] R. C. Bansal, *Activated Carbon Adsorption*. London, CRC Press. ISBN: 0824753445(2005).

[22] R. Rajbhandari, L. K. Shrestha, B. P. Pokharel, and R. R. Pradhananga, Development of nanoporous structure in carbons by chemical activation with zinc chloride. *J. Nanosci. Nanotechnol.* 2013(13)2613–2623.

[23] R. T. Yang, *Adsorbents: Fundamentals and application*. New York, John Wiley & Sons Inc. ISBN: 9780471462415(2003).

[24] B. Wang, B. Gaob, J. Fang, Recent advances in engineered biochar productions and applications. *Crit. Rev. Environ. Sci. Technol.* 2017 (47)2158–2207.

[25] M.A. Tadda, A. Ahsan, A. Shitu, M. ElSergany, T. Arunkumar, B. Jose, M. AbdurRazzaque, N.N.N. Daud, A review on activated carbon: Process, application and prospects. *J. Adv. Civ. Eng. Pract. Res.* 2016(2)7–13.

[26] R.C. Bansal, J. Donnet, and F. Stoeckli, *Active carbon*. Marcel Dekker, Inc., New York. 1988, 482 pp.

[27] S. Iranmanesh, T. Harding, J. Abedi, F. Seyedyn-Azad, D. B. Layzell, Adsorption of naphthenic acids on high surface area activated carbons. *J. Environ. Sci. Heal. A* 2014(49)913-922.

[28] D. Bergna, T. Varila, H. Romar and U. Lassi, Comparison of the properties of activated carbons produced in one-stage and two-stage processes. *C* 2018(4)41-51.

- [29] A. Aworn, P. Thiravetyan and W. Nakbanpote, Preparation of CO<sub>2</sub> activated carbon from corncob for monoethylene glycol adsorption. *Colloids Surf. A: Physicochem. Eng. Asp.* 2009(333)19-25.
- [30] A. Lua, and J. Guo, Activated carbon prepared from oil palm stone by one-step CO<sub>2</sub> activation for gaseous pollutant removal. *Carbon* 2000(38)1089.
- [31] M. A. F. Mazlana, Y. Uemuraa, S. Yusupa, F. Elhassana, A. Uddinb, A. Hiwadab, M. Demiyab, Activated carbon from rubber wood sawdust by carbon dioxide activation. *Procedia Eng.* 2016(148)530-537.
- [32] Z. Gu, X. Wang, Carbon materials from high ash bio-char: a nanostructure similar to activated graphene. *Am. Trans. Eng. Appl. Sci.* 2013(2)15-34.
- [33] H. Wang, Z. Xu, A. Kohandehghan, Z. Li, K. Cui, X. Tan, T. J. Stephenson, C. K. King'ondeu, C. M. B. Holt, B. C. Olsen, J. K. Tak, D. Harfield, A. O. Anyia, and D. Mitlin, Interconnected carbon nanosheets derived from Hemp for ultrafast supercapacitors with high energy. *ACS nano* 2013 (6)5131–5141.
- [34] L. Shijie, H. Kuihua, Li. Jinxiao, Li. Ming, Lu. Chunmei, Preparation and characterization of super activated carbon produced from gulfweed by KOH activation. *Micropor. Mesopor. Mat.* 2017(243)291-300.
- [35] M. Kiliç, E. Apaydin-varol, A. Eren Pütün, Preparation and surface characterization of activated carbon from *Euphorbia rigida* by chemical activation with ZnCl<sub>2</sub>, K<sub>2</sub>CO<sub>3</sub>, NaOH and H<sub>3</sub>PO<sub>4</sub>. *Appl. Surf. Sci.* 2012(261)247-254.
- [36] S. Yorgun, D. Yildiz, Preparation and characterization of activated carbons from paulownia wood by chemical activation with H<sub>3</sub>PO<sub>4</sub>. *J. Taiwan Inst. Chem. E.* 2015(53)122-131.
- [37] R. Sivaraj, V. Rajendran and G. S. Gunalan, Preparation and characterization of activated carbons from *parthenium* biomass by physical and chemical activation techniques. *E-J. Chem.* 2010(7)1314-1319.
- [38] H. Teng, H.-C. Lin, Activated carbon production from low ash subbituminous coal with CO<sub>2</sub> activation. *AIChE J.* 1998(44)1170–1177.
- [39] R. T. Yang, *Adsorbents: Fundamentals and application.* (2003) New York, John Wiley & Sons Inc. ISBN: 9780471462415.

- [40] M. A. Lillo-Rodenas, D. Cazorla-Amoros, A. Linares-Solano, Understanding chemical reactions between carbons and NaOH and KOH: An insight into the chemical activation mechanism. *Carbon* 2003(41)267–275.
- [41] Ö. T. Şahin, C. Saka, Preparation and characterization of activated carbon from acorn shell by physical activation with H<sub>2</sub>O-CO<sub>2</sub> in two-step pretreatment. *Bioresour. Technol.* 2013(136)163–168.
- [42] H. sayğh, F. Güzel, High surface area mesoporous activated carbon from tomato processing solid waste by zinc chloride activation: process optimization, characterization and dyes adsorption. *J. Clean. Prod.* 2016(113)995-1004.
- [43] I. Ozdemir, M. Şahin, R. Orhan, M. Erdem, Preparation and characterization of activated carbon from grape stalk by zinc chloride activation. *Fuel Process. Technol.* 2014(125)200-206.
- [44] M. Kiliç, E. Apadin-Varol, A. E. Pütün, Preparation and surface characterization of activated carbons from *Euphorbia rigida* by chemical activation with ZnCl<sub>2</sub>, K<sub>2</sub>CO<sub>3</sub>, NaOH and H<sub>3</sub>PO<sub>4</sub>. *Appl. Surf. Sci.* 2012(261)247-254.
- [45] K.Y. Foo, B.H. Hameed, Coconut husk derived activated carbon via microwave induced activation: Effects of activation agents, preparation and adsorption performance. *Chem. Eng. J.* 2012(184)57-65.
- [46] W.C. Lim, C. Srivasakannan, N. Balasubramanian, Activation of palm shells by phosphoric acid impregnation for high yielding activated carbon. *J. Anal. Appl. Pyrol.* 2010(88)181-186.
- [47] M. Yang, L. Guo, G. Hu, X. Hu, L. Xu, J. Chen, W. Dai and M. Fan, highly cost-effective nitrogen doped porous coconut shell-based CO<sub>2</sub> sorbent synthesized by combining ammoxidation with KOH activation. *Environ. Sci. Technol.* 2015(49)7063-7070.
- [48] X. Wang, Y. Qin, L. Zhu and H. Tang, Nitrogen-doped reduced graphene oxide as a bifunctional material for removing bisphenols: Synergistic effect between adsorption and catalysis. *Environ. Sci. Technol.* 2015(49)6855-6864.
- [49] M. Zhou, F. Pu, Z. Wang and S. Guan, Nitrogen doped porous carbons through KOH activation with superior performance in supercapacitors. *Carbon* 2014(68)185-194.

- [50] X. Wang, H. Pan, Q. Lin, H. Wu, S. Jia, Y. Shi, One-Step synthesis of nitrogen-doped hydrophilic mesoporous carbons from chitosan-based triconstituent system for drug release. *Nanoscale Res. Lett* 2019(14)1-12.
- [51] W. Shen, W. Fan, Nitrogen-containing porous carbons: synthesis and application. *J. Mater. Chem. A* 2013(1)999-1013.
- [52] L. Wang, D. Zhu, J. Chen, Y. Chen, W. Chen, Enhanced adsorption of aromatic chemicals on boron and nitrogen co-doped single-walled carbon nanotubes. *Environ. Sci. Nano* 2017(4)558-564.
- [53] F. W. Shaarani, B. H. Hameed, Ammonia modified activated carbon for the adsorption of 2,4-dichlorophenol. *Chem. Eng. J.* 169(2011)180-185.
- [54] Z. Zhang, M. Xu, H. Wang, Z. Li, Enhancement of CO<sub>2</sub> adsorption on high surface area activated carbon modified by N<sub>2</sub>, H<sub>2</sub> and ammonia. *Chem. Eng. J.* 2010(160)571-577.
- [55] W. Shen, Z. Li, Y. Liu, Surface chemical functional groups modification of porous carbon. *Recent Patents Chem. Eng.* 2008(1)27-40.
- [56] S. N. Hojatallah, Li. Haning, V. R. K. Tirumala, Madhumita, B. R, Chunbao, X. Surface amination of activated carbon and petroleum coke for the removal of naphthenic acids and treatment of oil sands process-affected water (OSPW). *Chem. Eng. J.* 193(2016)189-199.
- [57] K. Zoua, Y. Deng, J. Chena, Y. Qiana, Y. Yangc, Y. Lia, G. Chend, Hierarchically porous nitrogen-doped carbon derived from the activation of agriculture waste by potassium hydroxide and urea for high-performance supercapacitors. *J. Power Sources* 2018(378)579-588.
- [58] G. Ma, Q. Yang, K. Sun, H. Peng, F. Ran, X. Zhao, Nitrogen-doped porous carbon derived from biomass waste for high performance supercapacitors. *Bioresour. Technol.* 2015(197)137-142.
- [59] J. Wang, H. L. Xin, D. Wang, Recent progress on mesoporous carbon materials for advanced energy conversion and storage. *Part. Part. Syst. Charact.* 2014(31)515-539.
- [60] Q. Li, R. Jiang, Y. Dou, Z. Wu, T. Huang, D. Feng, J. Yang, A. Yu, D. Zhao, Synthesis of mesoporous carbon spheres with a hierarchical pore structure for the electrochemical double-layer capacitor. *Carbon* 2011(49)1248-1257.

- [61] J.V. Headley, K. M. Peru, B. Fahlman, A. Colodey, and D. W. McMartin, Selective solvent extraction and characterization of the acid extractable fraction of Athabasca oils sands process waters by orbitrap mass spectrometry. *Int. J. Mass Spectrom.* 2013(345)104-108.
- [62] D.W. Schindler, and W.F. Donahue, An impending water crisis in Canada's western prairie provinces. *Proceedings of the National Academy of Sciences*, 2006(103)7210–7216.
- [63] E. Allen, Process water treatment in Canada's oil sands industry: I. Target pollutants and treatment objectives. *J. Environ. Eng. Sci.* 2008a (2)123-138.
- [64] J.C. Anderson, S.B. Wiseman, N. Wang, A. Moustafa, L. Perez-Estrada, M. Gamal El-Din, J.W. Martin, K. Liber, and J.P. Giesy, Effectiveness of ozonation treatment in eliminating toxicity of oil sands process-affected water to *Chironomus dilutus*. *Environ. Sci. Technol.* 2012(46)486-493.
- [65] E. Allen, Process water treatment in Canada's oil sands industry: II. A review of emerging technologies. *J. Environ. Eng. Sci.* 2008b (7)499-524.
- [66] H. S. Niasar, Treatment of oil sands process-affected water using activated and surface modified petroleum coke for organic compounds recovery. Ph.D thesis, 2017, Western University, London, Canada.
- [67] P. J. Quinlan, and K. C. Tam, Water treatment technologies for the remediation of naphthenic acids in oil sands process-affected water. *Chem. Eng. J.* 2015(279)696-714.
- [68] V.V. Rogers, K. Liber, and M.D. MacKinnon, Isolation and characterization of naphthenic acids from Athabasca oil sands tailings pond water. *Chemosphere* 2002(48) 519-527.
- [69] M. Bataineh, A. C. Scott, P. M. Fedorak, J. W. Martin, Capillary HPLC/QTOFMS for characterizing complex naphthenic acid mixtures and their microbial transformation. *Anal. Chem.* 2006(78)8354-8361.
- [70] D. M. Grewer, R. F. Young, R. M. Whittal, P. M. Fedorak, Naphthenic acids and other acid-extractables in water samples from Alberta: What is being measured? *Sci. Total Environ.* 2010(408)5997-6010.
- [71] X. Wang, K. L. Kasperski, Analysis of naphthenic acids in aqueous solution using HPLC-MS/MS. *Anal. Methods* 2010(2)1715-1722.

- [72] J. Clemente and P. Fedorak, A review of the occurrence, analyses, toxicity, and biodegradation of naphthenic acids. *Chemosphere* 2005(60)585-600.
- [73] Y. Shu, A. Dobashi, C. Li, Y. Shen, H. Uyama, Hierarchical porous carbon from greening plant shell for electric double-layer capacitor application. *Bull. Chem. Soc. Jpn.* 2017(90)44–51.
- [74] Y. Shu, J. Maruyama, S. Iwasaki, Y. Shen, H. Uyama, Activated carbon monolith derived from *Amygdalus pedunculata* shell and polyacrylonitrile for supercapacitors. *Bull. Chem. Soc. Jpn.* 2017(90)1333–1336.
- [75] Z. Barnard, Conversion of petroleum coke to activated carbon and its application to naphthenic acid removal from tailings pond water. M.Sc. Thesis, University of Alberta, Edmonton, Alberta, Canada, 2011.
- [76] A.C. Scott, W. Zubot, M. D. Mackinnon, D.W. Smith, and P. M. Fedorak, Ozonation of oil sands process water removes naphthenic acids and toxicity. *Chemosphere* 2008(71)156-160.
- [77] W. Zubot, M. D. MacKinnon, P. Chelme-Ayala, D. W. Smith, M. Gamal El-Din, Petroleum coke adsorption as a water management option for oil sands process affected water. *Sci. Total Environ.* 2012(364)427–428.
- [78] M. Arshad, M. A. Khosa, T. Siddique, A. Ullah, Modified biopolymers as sorbents for the removal of naphthenic acids from oil sands process affected water (OSPW). *Chemosphere* 2016(163)334–341.
- [79] S. Mishra, V. Meda, A. K Dalai, D. W. McMartin, J. V. Headley, K. M. Peru, Photocatalysis of naphthenic acids in water. *J. Water Resour. Prot.* 2010(2)644– 650 (2010).
- [80] M. Gamal El-Din, H. Fu, N. Wang, P. Chelme-Ayala, L. Pérez-Estrada, P. Drzewicz, J. W. Martin, W. Zubot, D. W. Smith, Naphthenic acids speciation and removal during petroleum-coke adsorption and ozonation of oil sands process-affected water. *Sci. Total Environ.* 2011(409)5119–25.
- [81] K. N. Aboua, Y. A. Yobeuet, K.B. Yao, D.L. Goné, A. Trokourey, Investigation of dye adsorption onto activated carbon from the shells of Macoré fruit. *J. Environ. Manag.* 2015(156)10–14.

- [82] B. Niu, F. Lu, H.-Y. Zhang, Y. Zhang, J. Zhao, Synthesis of nitriles from aerobic oxidation of amines catalyzed by ruthenium supported on activated carbon. *Bull. Chem. Soc. Jpn.* 2017(46)330–333.
- [83] E. H. Mohan, S. Anandan, B. V. A. Rao, T. N. Rao, Neem leaf-derived micro and mesoporous carbon as an efficient polysulfide inhibitor for sulfur cathode in a Li-S battery. *Bull. Chem. Soc. Jpn.* 2019(48)62–64.
- [84] B. Li, H. Zhang, D. Wang, H. Lv, C. Zhang, Agricultural waste-derived activated carbon for high performance lithium-ion capacitors. *RSC Adv.* 2017(7)37923–37928.
- [85] S. Iranmanesh, T. Harding, J. Abedi, F. Seyedeyn-Azad, D. B. Layzell. Adsorption of naphthenic acids on high surface area activated carbons. *J. Environ. Sci. Health, Part A* 2014(49)913-922.
- [86] C. Small, A. Ulrich, Z. Hashisho, Adsorption of acid extractable oil sands tailings organics onto raw and activated oil sands coke. *J. Environ. Eng.* 2012(138)833-840.
- [87] W. Zubot, M. D. MacKinnon, P. Chelme-Ayala, D. W. Smith, M. Gamal El-Din, Petroleum coke adsorption as a water management option for oil sands process affected water. *Sci. Total Environ.* 2012(427–428)364-372.
- [88] I. Md. Shahinoor, N. M. Kerry, A. M. Selamawit, L. Yang, Isotherm and kinetic studies on adsorption of oil sands process-affected water organic compounds using granular activated carbon. *Chemosphere* 202(2018)716-725.
- [89] M. H. Mohamed, L. D. Wilson, J. V. Headley, K. M. Peru, Sequestration of naphthenic acids from aqueous solution using  $\beta$ -cyclodextrin-based polyurethanes. *Phys. Chem. Chem. Phys.* 2010(13)1112-1122.
- [90] S. H. Wu, P. Pendleton, Adsorption of anionic surfactant by activated carbon: effect of surface chemistry, ionic strength, and hydrophobicity. *J. Colloid Interf. Sci.* 2001(243)306-315.
- [91] A. Martinez-Iglesias, H. S. Niasar, C. Xu, M. B. Ray. Adsorption of model naphthenic acids in water with granular activated carbon. *Adsorpt. Sci. Technol.* 2015(33) 881-893.
- [92] R. A. Frank. Naphthenic acids: Identification of structural properties that influence acute toxicity: The University of Guelph, Ph. D thesis, 2008.

- [93] A. Zhang, Q. Ma, K. Wang, Y. Tang, W. A. Goddard. Improved processes to remove naphthenic acids. Annual Technical Progress Report, California Institute of Technology 2005:1-24.
- [94] B. Wang, Y. Wan, Y. Gao, M. Yang, J. Hu. Determination and characterization of oxy-naphthenic acids in oilfield wastewater. *Environ. Sci. Technol.* 2013(47)9545-54.
- [95] R. Hindle, M. Noestheden, K. Peru, J. Headley. Quantitative analysis of naphthenic acids in water by liquid chromatography–accurate mass time-of-flight mass spectrometry. *J. Chromatogr. A* 2013(1286)166-74.
- [96] C. Leishman, E. E. Widdup, D. M. Quesnel, G. Chua, L. M. Gieg, M. A. Samuel, The effect of oil sands process-affected water and naphthenic acids on the germination and development of *Arabidopsis*. *Chemosphere* 2013(93)380-7.
- [97] J. Peng, J. Headley, S. Barbour, Adsorption of single-ring model naphthenic acids on soils. *Can. Geotech. J.* 2002(39)1419-26.
- [98] T-W. Yen, W. P. Marsh, M. D. MacKinnon, P. M. Fedorak, Measuring naphthenic acids concentrations in aqueous environmental samples by liquid chromatography. *J. Chromatogr. A* 2004(1033)83-90.
- [99] D. Jones, A. G. Scarlett, C. E. West, S. J. Rowland, Toxicity of individual naphthenic acids to *Vibrio fischeri*. *Environ. Sci. Technol.* 2011(45)9776-9782.
- [100] M. Nodwell, On the interactions between naphthenic acids and inorganic minerals. MASC Thesis, 2011, University of British Columbia.
- [101] K. D. Kennedy. Growth, survival, and community composition of Chironomidae (Diptera) larvae in selected Athabasca oil sands process-affected wetland waters of northeastern Alberta. MASC Thesis, 2012, University of Windsor.
- [102] W. A. Wurts, P. W. Perschbacher. Effects of bicarbonate alkalinity and calcium on the acute toxicity of copper to juvenile channel catfish (*Ictalurus punctatus*). *Aquaculture* 1994(125)73-9.
- [103] R. J. Kavanagh, R. A. Frank, B. K. Burnison, R. F. Young, P. M. Fedorak, K. R. Solomon, Fathead minnow (*Pimephales promelas*) reproduction is impaired when exposed to a naphthenic acid extract. *Aquat. Toxicol.* 2012(116)34-42.
- [104] F. M. Holowenko, M. D. MacKinnon, P. M. Fedorak, Methanogens and sulfate-reducing bacteria in oil sands fine tailings waste. *Can. J. Microbiol.* 2000(46)927-937.

[105] R. E. Madill, M. T. Orzechowski, G. Chen, B. G. Brownlee, N. J. Bunce, Preliminary risk assessment of the wet landscape option for reclamation of oil sands mine tailings: bioassays with mature fine tailings pore water. *Environ. Toxicol.* 2001(16)197-208.

## Chapter 2

# One-Step Preparation of Highly Porous Carbon Derived from Bio-Waste Hemp Fibers: Process Optimization

### Abstract

Highly porous carbon having high specific surface area was prepared using a single-step carbonization of hemp fibers using different chemical activators. The effects of carbonization temperature and mass ratio of activator: substrate of activator on pore structure/distribution and surface chemistry of the prepared carbons were investigated through the analysis of BET (Brunauer-Emmett-Teller) surface area, pore size and pore volume, X-ray diffraction (XRD), scanning electron microscopy (SEM) images, high resolution transmission electron microscopy (HRTEM) images, Fourier transform-infrared (FT-IR) spectra, and Raman scattering. Activating agent and mass ratio of activator: substrate (the mass ratio of activating agent: HFs, w:w) significantly affected the characteristics of the produced carbon, and  $\text{ZnCl}_2$  exhibited superior activation performance over KOH and other dehydrating/activating agents such as  $\text{K}_2\text{CO}_3$ ,  $\text{Na}_2\text{CO}_3$ , and  $\text{MgSO}_4$ . The optimal conditions leading to the conversion of hemp fibers to high surface area carbon were: carbonization temperature of  $500^\circ\text{C}$  for 1 h in presence of  $\text{ZnCl}_2$  as an impregnating agent at 2:1 mass ratio of  $\text{ZnCl}_2$  : hemp fibers. The BET surface area, pore volume, and pore size of the carbon prepared under optimal conditions were  $2518 \pm 19.59 \text{ m}^2/\text{g}$ ,  $1.546 \pm 0.047 \text{ cm}^3/\text{g}$  and  $24.56 \pm 0.725 \text{ \AA}$ , respectively, which are significantly higher than that of commercially available carbon products such as granular and porous activated carbons.

### *Keywords*

Hemp fibers, Porous carbon, Physical and chemical activation,  $\text{ZnCl}_2$  activation, Activated carbon, Granular activated carbon, Activation mechanism

## 2.1. Introduction

Due to their remarkable properties such as high surface area, high chemical and mechanical stability, and low toxicity, demand of porous carbon-based materials in various applications such as catalyst supports, gas storage, environmental remediation, and filtration, separation, and purification technology has been increasing in recent years [1-4]. Porous carbonaceous materials with tunable porosities, including activated carbons, carbon aerogels, and graphene-based materials, have been extensively investigated in such applications [5,6]. However, these carbon-based materials are relatively expensive and are largely derived from fossil-based, non-renewable resources. Consequently, in recent years, growing interest has been shifted to the production of cost-effective carbon products from renewable and sustainable resources. In this instance, utilization of biomass-based carbon sources such as forestry and/or agricultural by-products for production of porous carbons would be highly attractive [7-9].

Biomass is a promising carbon precursor due to its natural porous structure and suitability to deal with the problems of sustainability, economy, and availability [10,11]. The use of biowaste in carbon preparation provides a sustainable resource, and can help in reducing the cost of carbon preparation as an inexpensive and sustainable alternative to existing commercially available activated carbons, especially coal-based carbons, in many industrial applications [12-15]. Hemp fibers (referred to as HFs hereafter), derived from the hemp plant, are considered as one of the strongest members of bast natural fibers family. Reportedly, hemp fibers are composed of three main fractions – 67.0% cellulose, 16.1% hemicellulose, and 3.3% lignin; the ash content being 3.0%. In terms elemental composition, hemp fibers were analyzed to contain 43.17% carbon, 5.21% hydrogen, 0.63% nitrogen, and 50.99% oxygen [15]. This composition and fibrous structure enable HFs to be an attractive feedstock for carbon materials with specific structures and tunable properties [14-16]. Nevertheless, substantial amounts of hemp fibers are still left in harvested fields without further utilization, resulting in the waste of renewable resources. Therefore, it is very important to convert this rich source of carbonaceous species into carbon materials.

The production of porous activated carbon involves the pyrolysis of the raw carbonaceous materials in an inert gas environment. The process usually takes place in two steps: carbonization and activation. The main purpose of activation is to enlarge the diameter of the fine pores and also to create new pores [17]. Chemical and physical/thermal activation are the common ways of modifying the pore size and/or pore distribution of carbons prepared from biomass. By controlling the pyrolysis conditions such as temperature and duration of the carbonization process, it is possible to tune the carbon properties. Inert atmosphere carbonization of biomass at elevated temperature and pressure can enhance the surface properties of carbons by controlling aromatic rings instead of O-alkyl carbon [17]. Chemical activation method has been regarded advantageous over thermal activation method due to low energy consumption, high yield with well-developed porosity, and one-step accomplishment of carbonization and activation [17]. In chemical activation, the precursor raw material is impregnated with certain chemicals such as alkali (KOH, NaOH,  $K_2CO_3$ ), transition metals salts ( $AlCl_3$ ,  $ZnCl_2$ ,  $FeCl_3$ , etc) or certain acids ( $H_3PO_4$ ,  $H_2SO_4$ ), where the porosity is developed by dehydration reactions carried out by the activating reagents [13, 18-21].

Amongst the chemical activating agents,  $ZnCl_2$  has been widely used in the production of porous carbons from biomass resource by chemical activation method [18, 21, 22]. A number of literature reports are available for which  $ZnCl_2$  has been used as a chemical activator for the preparation of carbon materials from biomass resources [21, 23]. Reports indicate that, as an activating agent,  $ZnCl_2$ : i) promotes the decomposition of carbonaceous material, ii) lowers the carbonization temperature, iii) restricts/retards tar formation, and iv) increases the carbon yield [21, 23]. A few studies have been done on the preparation of porous carbon materials from HFs. For instance, Rosas *et al.* prepared hemp-derived activated carbon by chemical activation using KOH and  $H_3PO_4$  [15,16,24]. Wang *et al.* prepared interconnected graphene-like carbon nanosheets derived from hemp fiber using combined hydrothermal and activation process, and explored the potential application of the produced nanosheets in supercapacitors [16]. Recently, we reported on the application of chemical activators KOH and NaOH for enhancing the surface area of hemp fibers-based carbon (referred to as HFCs hereafter) by a two-step method: hydrothermal treatment followed by carbonization of hydrothermally treated product

[25]. In a continuation of our efforts to develop improved methods and/or products to develop porous activated carbon from hemp fiber, we investigated a single step process for the chemical activation of HFs with  $\text{ZnCl}_2$  as a chemical activator.

Herein, we report on the efficacy of  $\text{ZnCl}_2$  as an activating agent for conversion of HFs to HFCs. The effects of mass ratio of activator: substrate ( $\text{ZnCl}_2$ : HFs, w: w) and carbonization temperature on the surface area, pore size distribution, and pore volume of the activated carbon produced by  $\text{ZnCl}_2$  activation of HFs were systematically evaluated, and the optimal conditions of HFC preparation were identified from the studies of structural morphology including BET surface area, pore size, and pore volume of the produced HFCs.

## 2.2. Experimental

### 2.2.1. Materials and Chemicals

Hemp fibers were supplied by American Hemp, Winston Salem, NC, USA. The obtained samples of hemp fibers were cut into smaller pieces with scissors, thoroughly washed several times with de-ionized water to clean off the dirt, and dried in vacuum oven at  $100^\circ\text{C}$  for 24 h. The dried raw materials were then crushed and ground in an electric grinder (CGOLDENWALL, model: DF-15 Grinder). Following chemicals were obtained from Sigma-Aldrich, Oakville, ON, Canada:  $\text{ZnCl}_2$  (> 98% purity), anhydrous  $\text{K}_2\text{CO}_3$  (ACS reagent grade,  $\geq 99\%$  purity),  $\text{MgSO}_4$  anhydrous ( $\geq 99\%$  purity), anhydrous  $\text{Na}_2\text{CO}_3$  (ultrapure,  $\geq 99.5\%$  purity), powdered activated charcoal (DARCO, 12–20 mesh) and granular activated charcoal (20-40) mesh. The chemicals KOH (99% purity) and 37% HCl were obtained from Caledon Laboratories Ltd., Canada. Deionized (DI) water (18.2  $\text{M}\Omega$ ) was obtained from a compact ultrapure water system (EASY pure LF, Mandel Scientific Co., Guelph, ON, Canada, model BDI-D7381). Ultra high pure (UHP) nitrogen gas of 99.999% purity, provided by Praxair (Oakville, ON, Canada), was used for experiments conducted in inert atmosphere. Millipore filter water was used to prepare solutions. All chemicals/reagents were used as received.

## 2.2.2. Methods

### 2.2.2.1. Preparation of hemp derived porous carbon materials (HFC<sub>S</sub>)

Three (3.0) grams of pretreated (washed, dried, ground) HFs powder was soaked in 50 mL of ZnCl<sub>2</sub> solution for 1 h at room temperature. The mass ratio of activator: substrate (ZnCl<sub>2</sub>: HFs, w:w) was varied as 1:1, 2:1 and 3:1, which was calculated as the ratio of the weight of ZnCl<sub>2</sub> to the weight of the used raw HFs powder. The impregnated sample was oven dried at 115°C for 24 h in a vacuum oven. A weighted amount of impregnated sample was carbonized under N<sub>2</sub> atmosphere at a heating rate of 3°C/min in a tubular furnace (21100 tube furnace). Activation time was 1 h after the onset of desired temperature, and the carbonization temperature was varied in the range of 400-700°C. After completion of the carbonization at each temperature, the obtained carbonized product was washed several times with 2 M (M = mol/litre) HCl followed by deionized water until the pH of the filtrate was neutral. The washed carbon was dried in an oven at 115°C for 24 h and stored in glass containers for advanced characterization and application studies. The carbon samples were named as HFC-X-Y where, X corresponds to the mass ratio of activator: substrate and the Y correspond to the carbonization temperature. For instance, HFC-3-500 represents the HFC prepared with mass ratio of activator: substrate of 3:1 (ZnCl<sub>2</sub>: HFs) and carbonization temperature of 500°C. A control product (for control experiments) was prepared by the carbonization of HFs without ZnCl<sub>2</sub>, and this product was named as HFC-0-500 (where 0 indicates no activating agent was used, and 500 indicates the carbonization temperature).

### 2.2.2.2. Optimization of parameters for preparation of porous HFCs

The parameters such as carbonization temperature and time, and mass ratio of activator: substrate (ZnCl<sub>2</sub>: HFs, w: w) affect the property of carbon prepared from HFs. Consequently, the effects of these factors on the properties of the final product were

thoroughly examined. At first, the effects of carbonization temperature were evaluated in the temperature range of 400 to 700°C at an mass ratio of activator: substrate of 3:1 (ZnCl<sub>2</sub>:HFs, w:w) keeping the carbonization time and heating rate same (3°C/min heating rate and 1 h carbonization time). From these experiments, 500°C was found to be the most effective carbonization temperature. Accordingly, the effects of mass ratio of activator: substrate were examined by varying the mass ratio of activator: substrate at constant carbonization temperature of 500°C and 1 h carbonization time. Triplicate experiments were conducted to evaluate the effect of each parameter, and the results are presented as average ± standard deviation of triplicate analysis.

### 2.2.2.3. Yield of porous carbon and burn-off

The yield of carbon samples and burn-off were calculated using the following formulae:

$$\text{Yield of carbon sample(w\%)} = \frac{W_{\text{carbon}}}{W_0} \times 100$$

$$\text{Burn-off} = \frac{W_0 - W_{\text{carbon}}}{W_0} \times 100$$

$W_0$  = weight of raw material impregnated (g)

$W_{\text{carbon}}$  = weight of carbon obtained after carbonization (g)

### 2.2.2.4. Characterization of HFs and obtained HFCs

The surface area and porosity of the prepared HFCs were characterized by N<sub>2</sub> adsorption-desorption isotherms at -193°C in a constant volume using 99.995% pure N<sub>2</sub> gas. Tristar II 3020 (Micromeritics Instrument Corporation) was used to determine the surface area and total pore volume of the samples. The N<sub>2</sub> adsorption-desorption isotherms were analyzed to characterize the nature of the pores. Before performing the N<sub>2</sub> adsorption experiment, the samples were subjected to degassing at 150°C for 8 h to remove residual moisture and any adsorbed gases. BET and BJH plots were analyzed to calculate the specific surface area and average pore diameter.

Surface functional groups of the carbon materials were analyzed by FT-IR (Fourier transform infrared) spectra using an ATR-FTIR spectroscope (Nicolet 6700 FTIR, ThermoFisher Scientific, Waltham, MA, USA) obtained at room temperature. The percentage of transmission of samples was recorded in the range of 600 to 4000  $\text{cm}^{-1}$ . Surface morphology of raw material and the prepared HFCs was studied using Scanning Electron Microscopy (Hitachi FlexSEM, model SU 1000) with secondary electron detector. High resolution transmission electron microscopic (HRTEM) images were obtained with a JEOL 2010F microscope.

Crystallinity and amorphous nature/structure of the raw material as well as the prepared HFCs were determined by X-ray diffraction analysis using a Bruker D2 PHASER desktop diffractometer with Cu  $K\alpha$  radiation (30 kV, 10 mA and  $\lambda=1.54 \text{ \AA}$ ). The X-ray diffraction patterns were collected with scan rate of  $0.1^\circ$  per second, and the diffraction angle was varied from  $10^\circ$  to  $70^\circ$ . Raman spectra were obtained with Renishaw InVia Reflex Raman Spectrometer with an excitation wavelength of 633 nm as the light source.

## 2.3. Results and Discussion

### 2.3.1. Evaluation of optimal parameters for preparation of HFCs

#### 2.3.1.1. Effect of carbonization temperature

The carbonization temperature is an important parameter in controlling the surface area and pore volume of the carbon materials. Hence, the effect of carbonization temperature on pore size distribution, pore volume, and specific surface area of the prepared carbons was evaluated in the range of 400 to 700°C at  $\text{ZnCl}_2$ : HF's ratio of 3:1. The BET surface area (Figure 2.1a), pore volume (Figure 2.1b), and pore size (Figure 2.1c) of the obtained HFCs increased with increasing the carbonization temperature, reached a maximum at 500°C, and then exhibited slightly decreasing trend with further increasing the temperature beyond 500°C. A similar trend of decrease in the surface area and pore volume with increasing carbonization temperature was observed by Qian *et al.* for activation of manure compost, and by Hayashi *et al.* for carbonization of lignin by using  $\text{ZnCl}_2$  as an activator (26,27). The increase in the specific BET surface area on increasing

the carbonization temperature from 400 to 500°C is attributable to the removal of volatile substances while the decrease in surface area at higher temperature is likely due to the widening and destruction of pores due to excessive heating. Reports indicate that heat shrinkage of the material leading to narrowing and closing up of some of the pores results in reduction of surface area and pore volume in the case of activation at temperature above 500°C (22,23). It is also postulated that the crosslinking of carbon atoms at higher temperature reduces the space between atoms and reduces porosity and accessibility to adsorbate gases (22,23). The BET surface area, pore volume, and pore size of the carbon prepared at 500°C carbonization temperature were  $2325 \pm 8.89 \text{ m}^2/\text{g}$ ,  $1.853 \pm 0.132 \text{ cm}^3/\text{g}$  and  $31.96 \pm 2.319 \text{ \AA}$ , respectively, which is significantly higher than that of the carbon prepared at lower (400°C) or higher (700°C) temperatures. Consequently, carbonization temperature of 500°C was chosen for subsequent experiments.

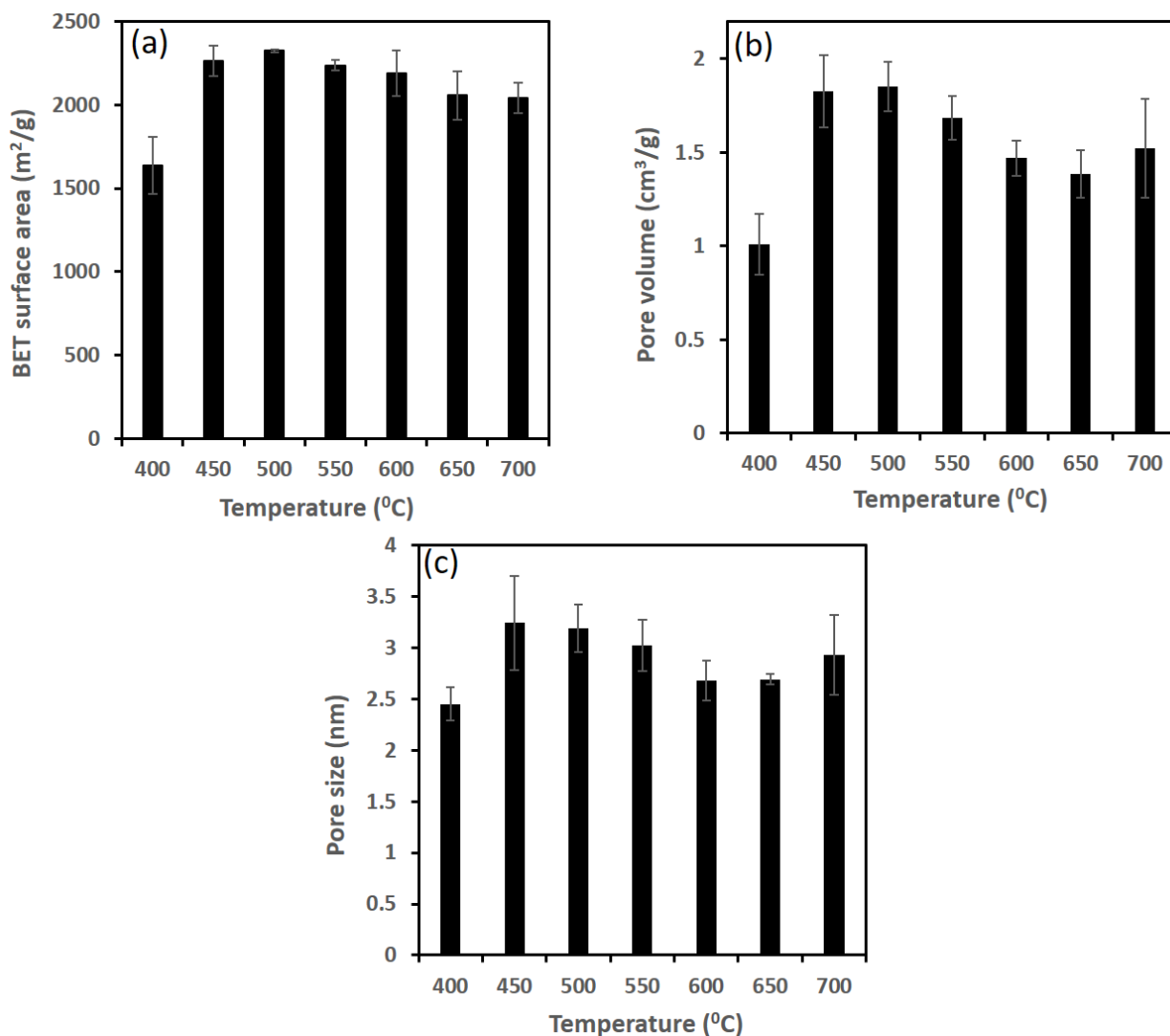


**Figure 2.1. Effect of carbonization temperature on surface areas (a), pore volume (b) and pore size (c) of hemp derived porous carbons (HFCs). Conditions: mass ratio of activator: substrate ( $\text{ZnCl}_2$ : HF<sub>s</sub> = 3:1, w: w), heating rate = 3°C/min, holding time = 1 h. Results are presented as average  $\pm$  standard deviation of analysis of triplicate samples. Error bars represent the standard deviation.**

### 2.3.1.2. Effect of activator: substrate ( $\text{ZnCl}_2$ : HF<sub>s</sub>) ratio

The effect of mass ratio of activator: substrate of  $\text{ZnCl}_2$  (an activating agent) on the BET surface area, pore volume, and pore size of resulting HFCs was evaluated by varying the ratio of weight of  $\text{ZnCl}_2$  to the weight of HF<sub>s</sub> at 500°C carbonization temperature (Table

2.1). Also shown in table 2.1 is the result of surface property analysis of HFC carbonized at 500°C without ZnCl<sub>2</sub> activation (control sample, named as HFC-0-500). Carbonization of HFs without ZnCl<sub>2</sub> activation resulted in HFC of very low surface area and pore volume (Table 2.1), indicating that ZnCl<sub>2</sub> activation has significant effect on improving the porous characteristics of carbon.

It is obvious from the results of Table 2.1 that the mass ratio of activator: substrate has a remarkable influence on porosity development. Carbonization of HFs with mass ratio of activator: substrate of 2: 1 (ZnCl<sub>2</sub>:HFs, w:w) resulted in carbon that has remarkably higher BET surface area than the carbon produced at 1:1 and 3:1 ratios, thus inferring that the ZnCl<sub>2</sub>: HFs ratio of 2:1 is likely the optimal condition for producing porous carbon from HFs. These results are in agreement with the results obtained from the chemical activation of lignin, waste potato residue, and cattle manure compost raw materials with ZnCl<sub>2</sub> (26,27,28). As an activator, ZnCl<sub>2</sub> is reported to inhibit tar formation and promote the release of volatiles, thus assisting in preparing the micropores. However, excess ZnCl<sub>2</sub> would lead to damaging the pore walls, widening of pores, and increase of pore volume due to violent reactions, causing microporous to be destroyed by collapsing or merging into mesopores (27,29), which was also observed in our case (Table 2.1). Results indicate that the carbon prepared at ZnCl<sub>2</sub> mass ratio of activator: substrate of 1:1 mainly contains micropores; higher amount of ZnCl<sub>2</sub> leading to formation of mesoporous material.

**Table 2.1. Effect of mass ratio of activator: substrate (ZnCl<sub>2</sub>: HFs) on surface areas of porous carbons produced**

HFCs samples <sup>1</sup>	Mass ratio of activator: substrate (ZnCl <sub>2</sub> : HFs)	BET surface area <sup>2</sup> (m <sup>2</sup> g <sup>-1</sup> )	Pore volume <sup>2</sup> (cm <sup>3</sup> /g)	Pore size <sup>2</sup> (Å°)
HFC-1-500	1:1	1828 ± 129	0.609 ± 0.523	19.50 ± 0.385
HFC-2-500	2:1	2518 ± 19.6	1.546 ± 0.047	24.56 ± 0.725
HFC-3-500	3:1	2325 ± 8.89	1.853 ± 0.132	31.96 ± 2.319
HFC-0-500	without activator	6.684 ± 1.56	0.007 ± 0.0006	50.10 ± 14.15

<sup>1</sup>Carbonization temperature = 500°C, heating rate = 3°C/min, holding time = 1 h

<sup>2</sup> Results are presented as average ± standard deviation of analysis of triplicate samples.

The pore size distribution results of  $\text{ZnCl}_2$  activated HFC samples presented in Table 2.1 were further confirmed by BJH method. As can be seen in Figure 2.2, the prepared HFCs have pores in the in the range of 2-4 nm. The pore size distribution curves shown in Figure 2.2 indicate that the pores of HFC-1-500 are mostly nanoporous, and those of HFC-2-500 and HFC-3-500 are mostly mesoporous. It is interesting to note that the average pore diameter was largely dependent on the ratio of  $\text{ZnCl}_2$ : HFs. As the mass ratio of activator: substrate increased, the average pore diameter increased for the carbonization temperature of  $500^\circ\text{C}$ ; thus allowing for tuning the pore size of the final product.

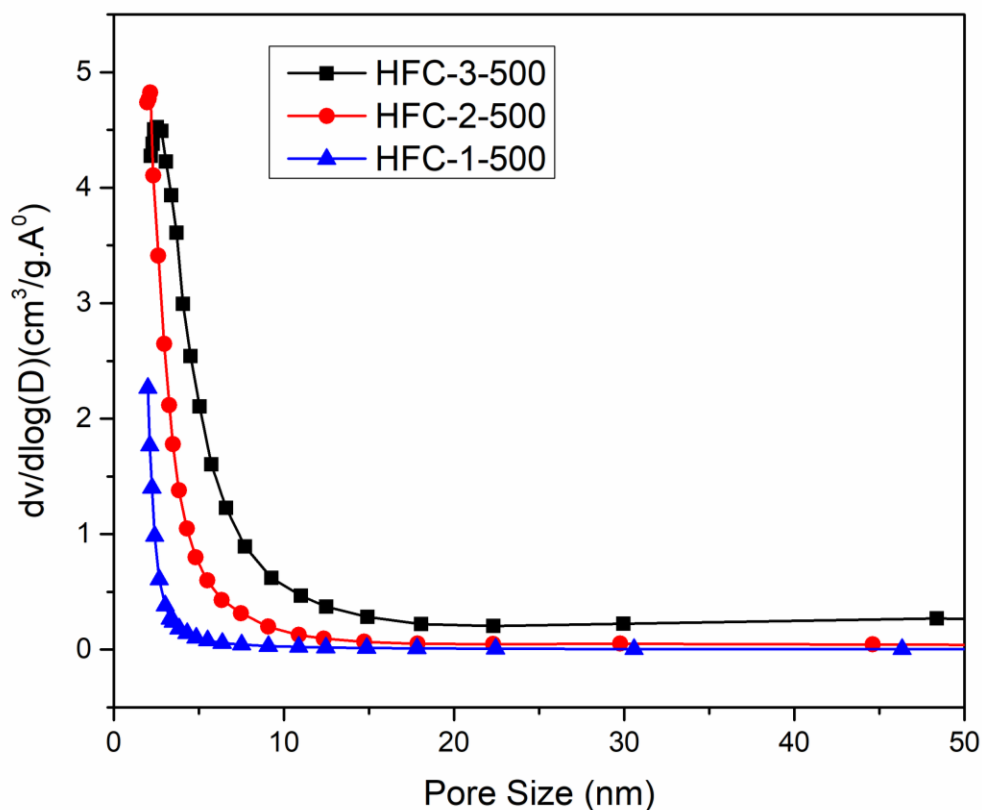


**Figure 2.2.** The pore size distribution of HFCs determined by the BJH method. Carbons were prepared by varying the mass ratio of activator: substrate at carbonization temperature of  $500^\circ\text{C}$ .

### 2.3.1.3. Carbon yield and burn-off

The carbonization temperature and mass ratio of activator: substrate also play an important role on the yield of carbon materials and burn-off. As seen in Table 2.2, it is found that the yield of carbon materials decreased continuously with increasing carbonization temperature. This is attributed to the removal of volatile compounds resulting from the decomposition of lignocellulosic materials in the form of CO, CO<sub>2</sub> and CH<sub>4</sub> [21]. Our findings are in agreement with those of Ndi *et al.* [30]. As evident from Table 2.2, as the carbonization temperature increased from 400 to 700 °C, the yield of carbon materials decreased from 13 to 10 %. When the carbon yield decreased, burn-off of activated carbons increased with increasing carbonization temperature.

Yields of carbons with low ZnCl<sub>2</sub>: HF<sub>s</sub> ratio of 1.0 gets a higher value 21.53 % at 500 °C carbonization temperature. As the mass ratio of activator: substrate increases from 1.0 to 3.0, more carbon burn-off occurred and micropore widening into mesopore by extra ZnCl<sub>2</sub>, resulting in lower yield values [31]. Higher mass ratio of activator: substrate restrict the formation of tars and volatiles and produce a deeper dehydration and elimination reactions, breaking the bonds C-O-C and C-C of the raw material, thus decreasing the carbon yield, as previously observed by Quin *et al.* and Sait *et al.* [26,31].

### 2.3.1.4. Effect of other activating agents

Using ZnCl<sub>2</sub> as an activating agent, the carbonization conditions of 2:1 (w:w) ratio of ZnCl<sub>2</sub>: HF<sub>s</sub> (w:w), 500°C carbonization temperature, and 1 h carbonization time yielded HFC with the highest surface area ( $2518 \pm 19.59$  m<sup>2</sup>/g), pore volume ( $1.546 \pm 0.047$  cm<sup>3</sup>/g) and pore size ( $24.56 \pm 0.725$  Å). Accordingly, these conditions were considered ideal for preparation of porous activated carbon from HF<sub>s</sub>. Hence, the efficacy of other activating and/or dehydrating agents for preparation of HFCs from HF<sub>s</sub> was also evaluated under these conditions. Table 2.3 summarizes the BET surface area, pore volume, and pore size distribution of the carbon materials prepared from HF<sub>s</sub> using different activating agents. From the comparison of results of Table 2.1 and 2.3, it is

apparent that ZnCl<sub>2</sub> demonstrated significantly better efficacy as an activator for preparation of porous carbon from HF<sub>s</sub>.

**Table 2.2. Effect of temperature and mass ratio of activator: substrate on carbon yield (%) and burn off (%) in preparation of porous activated carbon from HF<sub>s</sub> using ZnCl<sub>2</sub> activating agent.**

Carbonization temp. (°C)	Mass ratio of activator: substrate (ZnCl <sub>2</sub> : HF <sub>s</sub> )	Carbon yield (%)	Burn-off (%)
450	3:1	13.00	87.00
500	3:1	12.57	87.42
550	3:1	12.11	87.89
600	3:1	11.40	88.60
700	3:1	10.34	89.66
500	1:1	21.53	78.47
500	2:1	16.25	83.75

**Table 2.3. BET surface area, average pore diameter and pore volume of HFCs prepared by using different activators.**

Activator <sup>1</sup>	BET surface area <sup>2</sup> (m <sup>2</sup> g <sup>-1</sup> )	Pore volume <sup>2</sup> (cm <sup>3</sup> /g)	Pore size <sup>2</sup> (Å)
K <sub>2</sub> CO <sub>3</sub>	550.6 ± 47.02	0.281 ± 0.022	20.45 ± 0.081
Na <sub>2</sub> CO <sub>3</sub>	206.5 ± 10.46	0.164 ± 0.005	31.81 ± 1.953
MgSO <sub>4</sub>	422.6 ± 14.69	0.223 ± 0.007	21.16 ± 0.093
KOH	638.0 ± 56.20	0.325 ± 0.026	22.09 ± 0.505
ZnCl <sub>2</sub>	2518 ± 19.59	1.546 ± 0.047	24.56 ± 0.725

<sup>1</sup> Activator ratio: HF<sub>s</sub> = 2:1, carbonization temperature = 500°C, heating rate = 3°C/min, holding time = 1 h.

<sup>2</sup> Results are presented as average ± standard deviation of analysis of triplicate samples.

### 2.3.1.5. Comparative evaluations

Table 2.4 compares the BET surface area of HFC of this study with porous carbon derived from ZnCl<sub>2</sub> activation of other biomasses. It is obvious that the hemp fibers yield carbon which has much higher surface area than the carbon produced from several biomasses, and comparable BET surface area to the carbon produced from wood.

**Table 2.4. Comparison of surface area of HFC with similar nanoporous carbon materials derived from other biomass-based wastes by chemical activation method with ZnCl<sub>2</sub> activating agent.**

Precursor	Activating agents	CT (°C)	Activator: substrate (w:w)	Ct (h)	BET surface area (m <sup>2</sup> /g)	Ref.
Pomegranate						
Seed	ZnCl <sub>2</sub>	600	2:0	1.0	978.8	[42]
Tomato						
waste	ZnCl <sub>2</sub>	600	6:1	1.0	1093	[6]
Grape stalk	ZnCl <sub>2</sub>	700	2:1	2.0	1411	[18]
Tamarind						
wood	ZnCl <sub>2</sub>	300	1:1	0.6	1322	[46]
Kraft lignin	ZnCl <sub>2</sub>	500	1:1	1.0	1347	[47]
<i>Enteromorpha</i>						
<i>Prolifera</i>	ZnCl <sub>2</sub>	500	1:1	1.0	1688	[48]
Sugar beet	ZnCl <sub>2</sub>	500	1:1	1.0	1697	[49]
Cherry						
stones	ZnCl <sub>2</sub>	500	4:1	2.0	1971	[50]

Sunflower	ZnCl <sub>2</sub>	600	2:1	1.0	2240	[35]
Sugar cane						
Bagasse	ZnCl <sub>2</sub>	500	2:1	1.0	2289	[35]
<b>Hemp fibers</b>	<b>ZnCl<sub>2</sub></b>	<b>500</b>	<b>2:1</b>	<b>1.0</b>	<b>2518<sup>1</sup></b>	This work

<sup>1</sup>The average value of triplicate studies presented

CT= Carbonization temperature, Ct = Carbonization time

The BET surface area, pore volume, and pore size distribution properties of the HFC prepared in this study under the optimal conditions were also compared with that of some commercial products (Table 2.5). The ZnCl<sub>2</sub> activated HFC displayed an average BET surface area of 2518 m<sup>2</sup>/g, which is much higher than that of the granular and powdered activated carbons studied. In fact, the BET surface area of most of the commercially available activated carbons are in the range of 500 – 2000 m<sup>2</sup>/g [33-35]. It is interesting to note that the carbon prepared in this study had substantially higher surface area and pore volume than the commercial activated carbons and silica-alumina adsorbent. This remarkable surface area of HFC of this study makes this product highly suitable as an adsorbent.

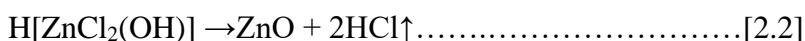
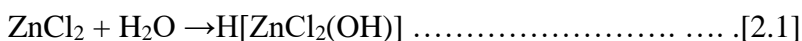
**Table 2.5. Comparison of characteristics of HFC of this study with that of commercial activated carbons**

Carbon samples	BET surface area (m <sup>2</sup> /g)	Pore volume (cm <sup>3</sup> /g)	Pore size (Å)
HFC-2-500	<b>2518</b>	<b>1.546</b>	<b>24.56</b>
Granular activated charcoal (841-420 μm pore size)	1005	0.487	19.41
Powdered activated carbon (DARCO, 1680-841 μm pore size)	876.0	0.648	29.59

## 2.3.2. Activation mechanism

### 2.3.2.1. ZnCl<sub>2</sub> activation

The ZnCl<sub>2</sub> activation mechanism is described in detail in the literature. Raw HF is a complex material composed of natural polymers cellulose, lignin, and hemicellulose. Reportedly, activation with ZnCl<sub>2</sub> solution first results in degradation of the cellulosic materials, thus allowing the activating agent to enter into the interior of the HF and increase contact between the activating agent and the carbon precursor [36]. It is believed that reactions (2.1) – (2.4) shown below are the major reactions occurring in ZnCl<sub>2</sub> activation of carbonaceous materials. During the drying process (typically at around 100°C for 12 h in an oven), the ZnCl<sub>2</sub> preloaded onto the raw HFs would be initially hydrolyzed to H[ZnCl<sub>2</sub>(OH)]. It is proposed that as the activation reaction proceeds, a part of ZnCl<sub>2</sub> gets converted to ZnO, which is then loaded on to the carbon resulting in ZnO-loaded carbon [36]. The dehydration reaction occurring in carbonization step results in charring and aromatization of the carbon skeleton, which imparts porous structure. The porous nature is also believed to be governed by the removal of ZnO either due to its reaction with interior carbon atoms during the pyrolysis process or during post-processing washing.



### 2.3.2.2. Activation with alkali metal carbonates and hydroxides

Alkali metal carbonate (eg, potassium carbonate,  $K_2CO_3$ ) activation is believed to involve the reactions (2.5) to (2.9). A plausible mechanism is the decomposition and/or reduction of  $K_2CO_3$  under inert condition to form K,  $K_2O$ , CO and  $CO_2$ . The  $K_2O$  formed as a result of decomposition of  $K_2CO_3$  then combines with carbon resulting in formation and evolution of CO, thus generating pores and increasing surface area. Additionally, the produced alkaline metals, that are intercalated in the carbon matrix, are responsible for both stabilization and widening of the spaces between the carbon atomic layers.

Activation with alkali metal carbonate is also believed to restrict the formation of tar and intensify the formation of cross-links by dehydration [37,38].



On the other hand, activation with alkaline hydroxide is believed to involve the redox reaction and carbon oxidation to generate porosity. During the activation process, formation and decomposition of alkali carbonate, evolution of CO,  $CO_2$ , and water vapours will likely occur according to the possible reactions (3.0) – (3.3) leading to the generation of porous carbon [39].



### 2.3.3. N<sub>2</sub> adsorption-desorption isotherms

The nitrogen adsorption-desorption isotherm plots for the ZnCl<sub>2</sub> activated HFCs prepared at 500°C carbonization temperature and different mass ratio of activator: substrates are shown in Figure 2.3. The results demonstrate that the HFC-2-500 and HFC-3-500 samples exhibited a similar trend of a sharp rise in N<sub>2</sub> adsorption at lower relative pressure ( $P/P^\circ$ ), which later increased slowly with increasing relative pressure ( $P/P^\circ$ ). This adsorption is followed by desorption hysteresis loop at higher relative pressures. A notable increase of nitrogen adsorption at lower relative pressure with a hysteresis loop at higher relative pressures is a typical sorption isotherm of porous materials containing mesopore structures, and the materials displayed Type-IV adsorption isotherms according to IUPAC classification (40,41). The observance of hysteresis loop in the adsorption-desorption process inferring the presence of mesoporosity is frequent in the activated carbons (41, 42). The commercial GAC, on the other hand, displayed a less steep Type I isotherm with a slightly sloped-up plateau which is characteristics of an activated carbon with a microporosity. The carbon sample HFC-1-500 displayed similar adsorption-desorption isotherm as that of commercial granular activated carbon, but with notably higher nitrogen adsorption capacity. Nitrogen adsorption capacity of control sample

(HFC-0-500) is very low indicating low porosity development in this sample.

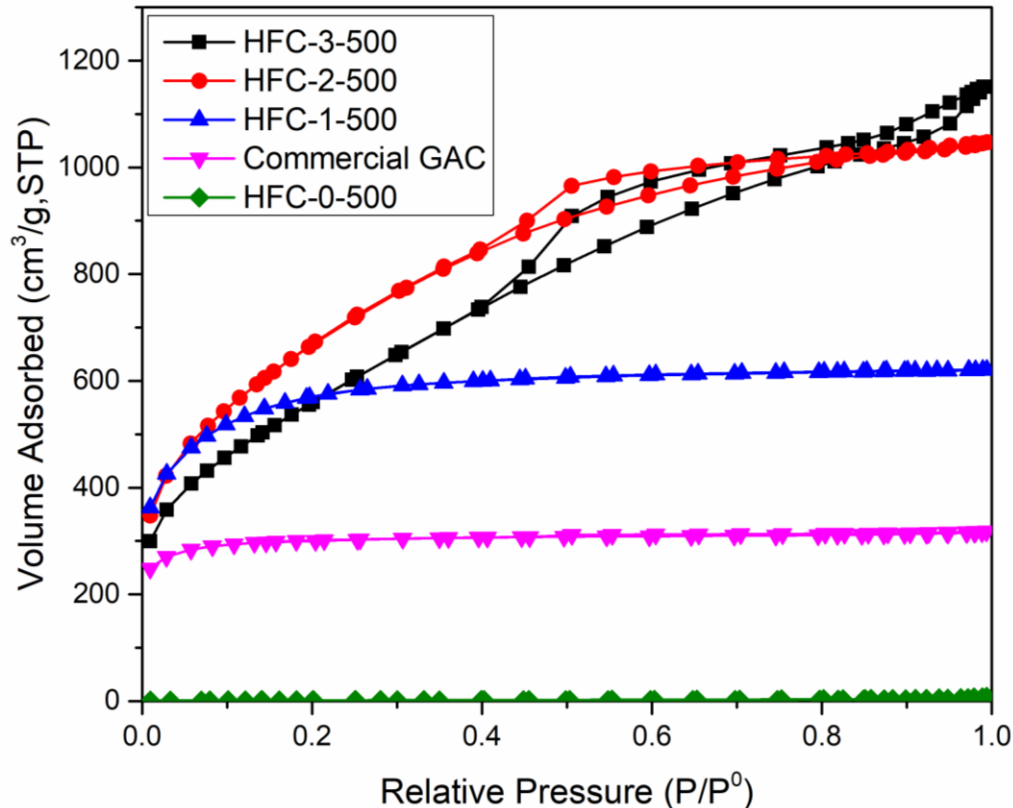


**Figure 2.3. Nitrogen adsorption-desorption isotherms at 77 K for  $\text{ZnCl}_2$  activated porous carbons prepared at variable mass ratio of activator: substrate (carbonization temperature =  $500^\circ\text{C}$ ) and that of commercial granular activated carbon (commercial GAC).**

#### 2.3.4. FT-IR Spectra

Functional groups determine the surface properties of the carbons and their quality, and are thus very important characteristics of the porous carbons. FT-IR spectroscopy was used to analyze the surface functional groups present on pretreated HFs (chopped, washed, dried, and milled) and the prepared HFCs. The FT-IR spectra of pretreated HFs and HFCs prepared at  $500^\circ\text{C}$  carbonization temperature with and without  $\text{ZnCl}_2$  activation are shown in Figure 2.4. For comparison, FT-IR spectra of commercially available granular activated carbon (commercial GAC) were also analyzed. The HFs, being lignocellulosic materials, show many bands in FT-IR spectrum related to bending

and stretching vibrations of O-H, C-O and C-C bonds reflecting the functional groups present in cellulose and hemicellulose [43]. For instance, a broad and strong band located in the range of 3200-3400  $\text{cm}^{-1}$  is attributable to the O-H stretching vibration of alcohol (may also be due to adsorbed water), a small absorption band at 2922  $\text{cm}^{-1}$  is attributable to C-H stretching vibrations of -CH<sub>2</sub>- and -CH<sub>3</sub> groups, the bands at 1637 and 1727  $\text{cm}^{-1}$  arise due to the stretching vibrations of carbonyl groups, the band at 1559  $\text{cm}^{-1}$  is associated with C-O stretching vibrations, the bands at about 1416, 1314 and 1232  $\text{cm}^{-1}$  are associated to C-H bending of alkanes and O-H bending of alcohols, and the band at 1036  $\text{cm}^{-1}$  is associated with C-O stretching vibration of alcohols and ether [35].

The IR spectra of HFC-0-500 and HFC-2-500 are different from that of the HFs in that many bands disappeared after activation and carbonization. The reduction in the intensity of the broad band around 3349  $\text{cm}^{-1}$  and the disappearance of the band at 1036  $\text{cm}^{-1}$  is attributable to the removal of H<sub>2</sub>O molecules after carbonization. The disappearance of IR bands associated with bending and stretching vibrations of functional groups of HFs after activation and carbonization indicates that thermal and/or chemical activation led to decomposition of functional groups and breakage of many bonds leading to the elimination of light and volatile substrates [6]. The IR spectrum of HFC-2-500 is similar to that of commercially available granular activated carbon.

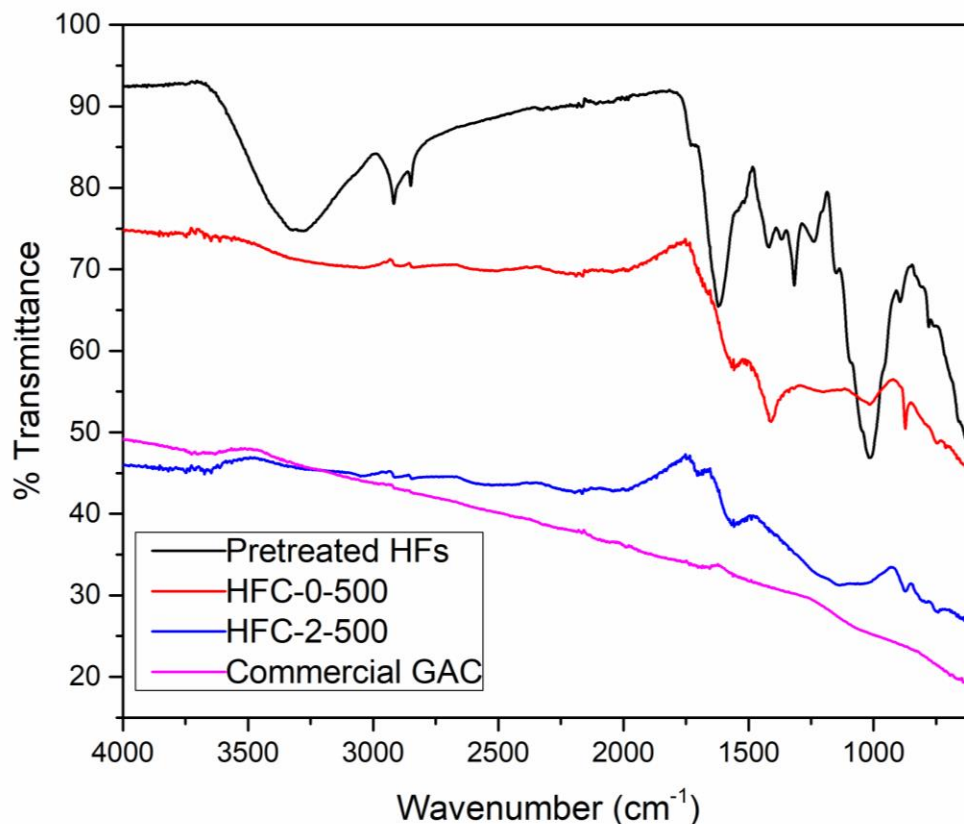


**Figure 2.4. Comparison of FT-IR spectra of the pretreated HFs, HFCs and commercial GAC.**

### 2.3.5. SEM analysis

Scanning electron microscopy (SEM) images were studied to evaluate the surface morphology of the carbon samples. Figure 2.5 shows the SEM micrographs of pretreated HFs, HFCs and commercial GAC. Significant differences were observed in the surface morphology of HFs and HFCs. The surface of HFs is rough, and has micrometer-sized tube-like fibrous structure (Figure 2.5a). Upon carbonization at 500°C, few pores or cracks were developed on the surface of HFC-0-500 (Figure 2.5b). It can be seen from the micrograph of Figure 2.5c that the external surface of HFC-2-500 is irregular and full of cavities as a result of activation. The SEM image of commercial GAC is similar to that of HFC-2-500, with relatively smaller pores appearing on the surface.

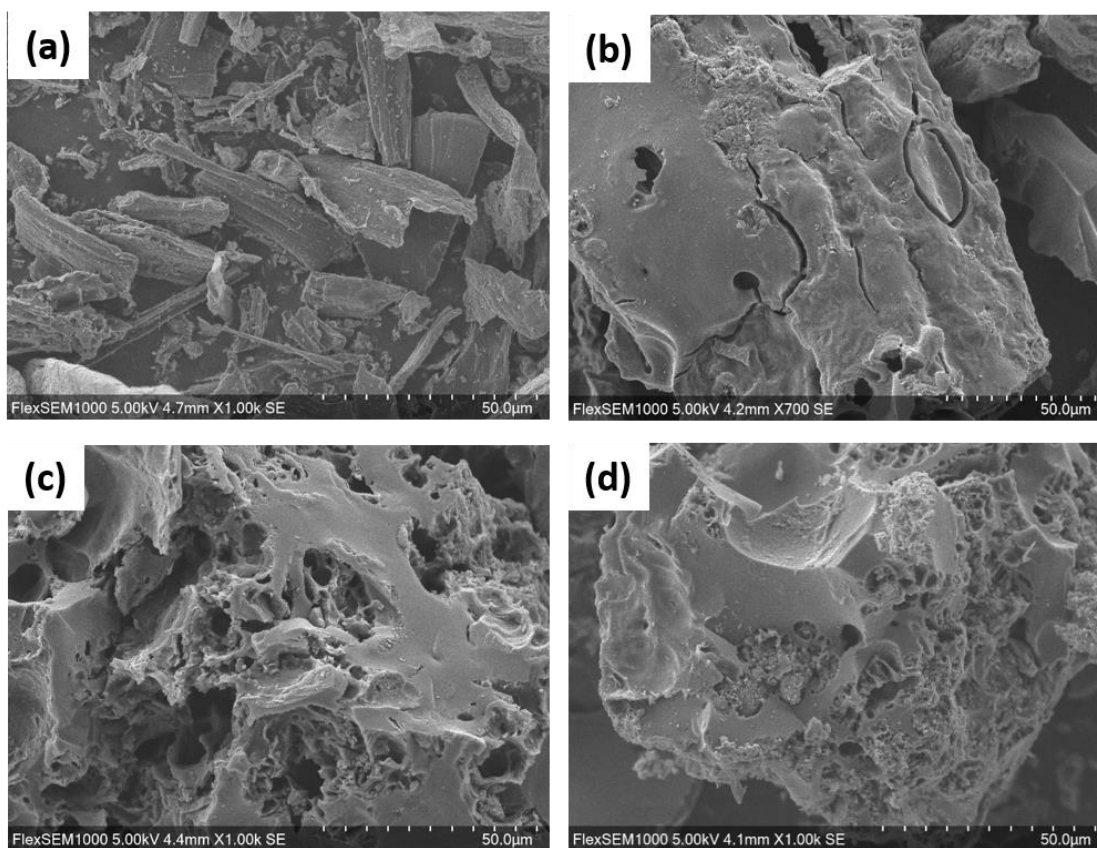


**Figure 2.5. SEM images of pretreated HFs (a), HFC-0-500 (b), HFC-2-500 (c) and commercial GAC (d).**

### 2.3.6. XRD analysis

The XRD patterns of pretreated HFs, two different HFCs, and commercial GAC are shown in Figure 2.6. HFs exhibited a broad peak centered at  $2\theta=22.5$  (002), which is indicative of crystalline portion of cellulose, and another peak at about  $2\theta=18.7$  (101), which is indicative of amorphous part (cellulose, hemicellulose and lignin) of lignocellulosic materials. Upon carbonization, the peak for crystalline cellulose became less prominent due to destruction of crystalline structure. The carbon sample HFC-2-500 and commercial GAC exhibited similar XRD patterns with the appearance of broad and low intensity peaks at around  $2\theta=23$  and  $2\theta=44$ , which correspond to the diffraction of (002) and (100) plane of graphite lattice of graphitic carbon with amorphous character.

Appearance of two broad peaks at  $2\theta=23.4$  and  $2\theta=43.9$  is also indicative of the absence of crystalline silica in the sample.

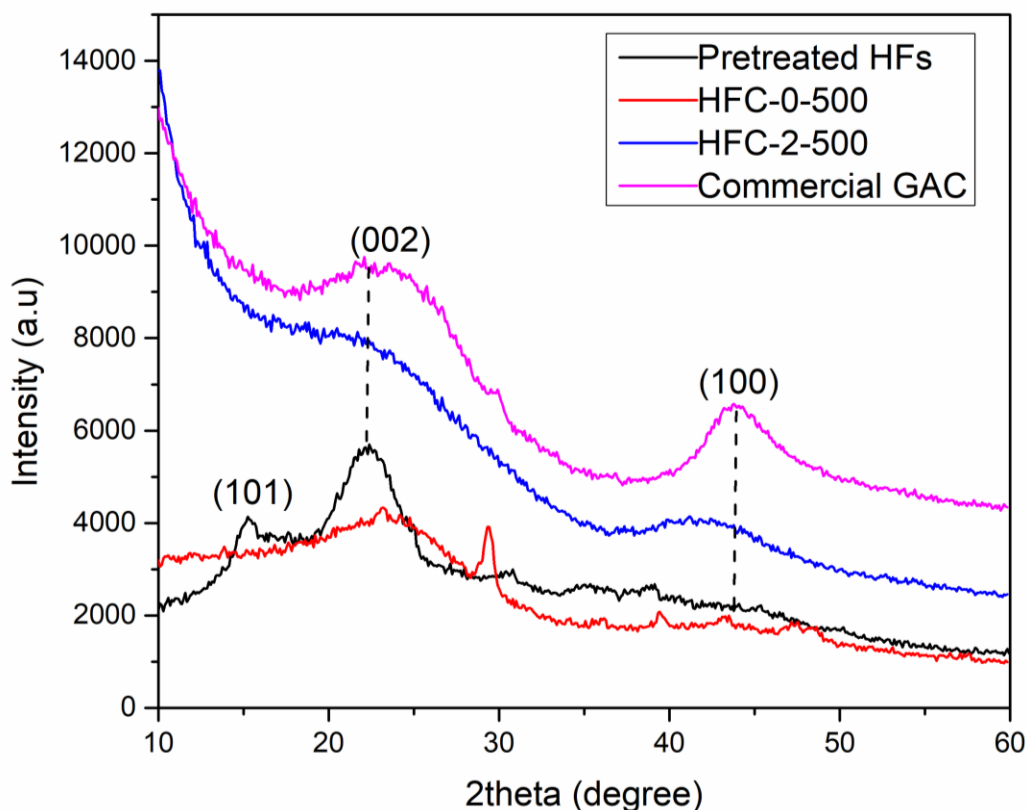


**Figure 2.6. XRD patterns of pretreated HFs, HFCs and commercial GAC.**

### 2.3.7. Raman spectra

Figure 2.7 shows the Raman spectra of HFCs prepared by carbonization at  $500^{\circ}\text{C}$  with and without  $\text{ZnCl}_2$  activation. The  $\text{ZnCl}_2$  activated sample (Figure 2.7b) displayed two distinct bands – one relatively broad band centered at  $1332\text{ cm}^{-1}$  indexed to the D band; and the other sharp G band at about  $1587\text{ cm}^{-1}$ . Generally, the intensity/height of the D band represents the concentration of disordered carbon in the sample, while the intensity of the G peak indicates the concentration of graphitized carbon [44]. In both the samples, intensity of G band is higher than that of the D band indicating that substantial amount of carbon is graphitized in the samples analyzed. The intensity ratio ( $I_D/I_G$ ) of the D and G bands reflects the ratio of disordered carbon and ordered graphitized carbon in the Raman

spectra of carbon samples. The relative intensity of the G and D bands ( $I_D/I_G$ ) is remarkably high for HFC-2-500 ( $I_D/I_G$  ca.  $0.93 \pm 0.025$ ) than that for HFC-0-500 ( $I_D/I_G$  ca.  $0.78 \pm 0.020$ ), which indicates that  $ZnCl_2$  activation led to higher degree of graphitization. The enhanced degree of graphitization suggests that the process of  $ZnCl_2$  activation not only created pores but also enhanced the concentration of graphitized carbon in HFCs.

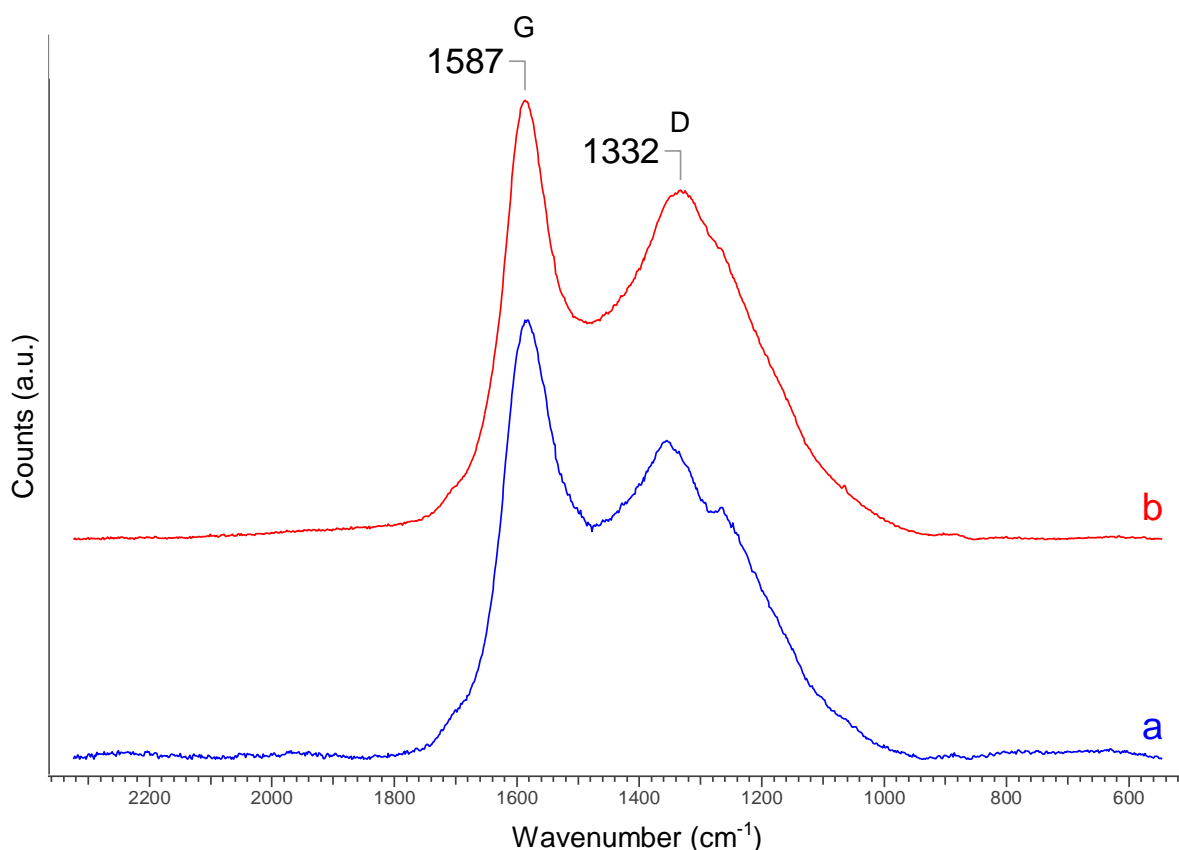


**Figure 2.7. Raman spectra of HFC-0-500 (a) and HFC-2-500 (b).**

### 2.3.8. High resolution transmission electron microscopy (HRTEM) image

Due to a higher level of graphitization, as indicated by Raman spectra, in HFC-2-500 sample, this carbon sample was further characterized by HRTEM (Figure 2.8). HRTEM image reveals that HFC-2-500 was made up of random assembly of nanometer-sized sheets. However, the ordered graphene layers are not fully developed, which is in agreement with the results of XRD and Raman scattering. Presumably, the lower

activation temperature is the reason why the graphitic layers are not fully developed resulting in partial graphitization. Sharp XRD peaks followed by ordered graphitic layers can be observed upon heating carbon precursors at a very high temperature of 2000°C [45].

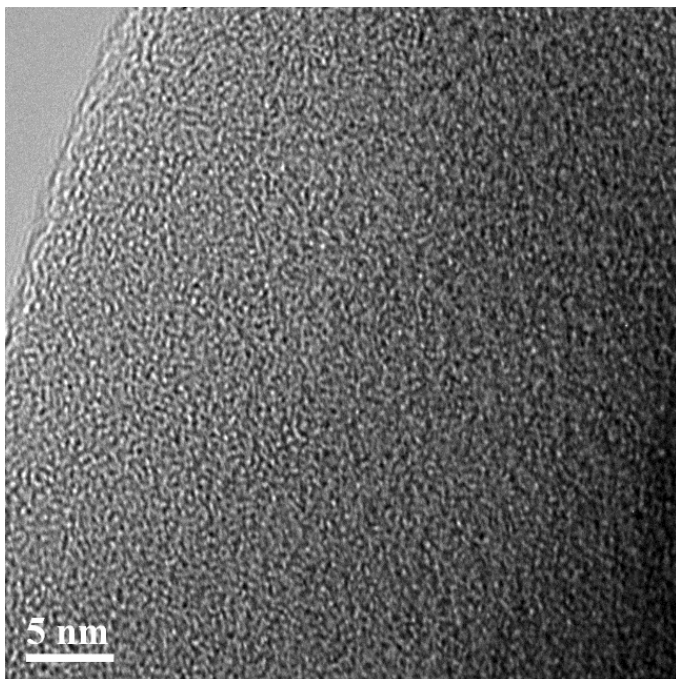


**Figure 2.8. HRTEM image of HFC-2-500.**

## 2.4. Conclusions

We have successfully prepared high surface area porous carbons (HFCs) from a lignocellulose precursor material hemp fiber by simple, single-step carbonization method using zinc chloride ( $\text{ZnCl}_2$ ) activation. A systematic evaluation of effect of carbonization temp in the range of at 400 to 700°C and effects of  $\text{ZnCl}_2$  mass ratio of activator: substrate on the surface properties of the porous carbons indicated that a carbonization temperature of 500°C and mass ratio of activator: substrate of 2:1 (w/w;  $\text{ZnCl}_2$ : HF) were ideal for preparation of high surface area activated carbon. Our systemic evaluation also demonstrated that the surface properties (surface area, pore size distribution, and pore volume) of the HFCs derived from HFs can be controlled by  $\text{ZnCl}_2$  mass ratio of

activator: substrate and carbonization temperature. Since the starting material is low-cost bio-waste, scalable production of high surface area porous carbon material would be attractive for sustainable utilization of the waste of hemp industry and development of water and wastewater treatment technology.

## 2.5. Acknowledgements

The present work was financially supported by Natural Sciences & Engineering Research Councils (NSERC) of Canada and Mitacs Accelerate grant, the later in association with Sarnia-based industry.

## 2.6. References

- [1] C. Merlet, B. Rotenberg, P. A. Madden, P.-L. Taberna, P. Simon, Y. Gogotsi and M. Salanne, On the molecular origin of supercapacitance in nanoporous carbon electrodes. *Nat. Mater.* 2012(11)306-310.
- [2] Y. Zhang, A. Wang and T. Zhang, A new 3D mesoporous carbon replicated from commercial silica as a catalyst support for direct conversion of cellulose into ethylene glycol. *Chem. Commun.* 2010(46)862-864.
- [3] M. S. Mauter and M. Elimelech, Environ. Environmental applications of carbon-based nanomaterials. *Sci. Technol.* 2008(42)5843-5859.
- [4] A. V. Herrera-Herrera, M. Á. González-Cubelo, J. Hernández-Borges and M. Á. Rodríguez-Delgado, Carbon nanotubes applications in separation science: A review. *Anal. Chim. Acta*, 2012(734)1-30.
- [5] P. Veslelá, V. Slovák, N-doped carbon xerogels prepared by ammonia assisted pyrolysis: Surface characterization, thermal properties and adsorption ability for heavy metal ion. *J. Anal. Appl. Pyrol.* 2014(109)266-271.
- [6] H. Saygin, F. Güzel, High surface mesoporous activated carbon from tomato processing solid waste by  $ZnCl_2$  activation: process optimization, characterization and dye adsorption. *J. Clean. Prod.* 2016(113)995-1004.

- [7] A. K. Santra, T. K. Pal & S. Datta, Removal of metanil yellow from its aqueous solution by fly ash and activated carbon produced from different sources. *Sep. Sci. Technol.* 2008(43)1434–1458.
- [8] P. K. Mallik, Use of activated carbons prepared from sawdust and rice husk for adsorption of acid dyes: a case study of acid yellow 36. *Dyes pigments* 2003(56)239-249.
- [9] M. Auta, B. H. Hameed, Optimized waste tea activated carbon for adsorption of methylene blue and acid blue 29 dyes using response surface methodology. *Chem. Eng. J.* 2011(175)233-243.
- [10] J. M. Valente Nabais, C. Laginhas, M. M. I Ribeiro Carrott, P. J. M. Carrott, J. E. Crespo Amorós, A. V. Nadal Gisbert, Surface and porous characterization of activated carbons made from a novel biomass precursor, the esparto grass. *Appl. Surf. Sci.* 2013(265)919-924.
- [11] L. Khezami, A. Chetouani, B. Taouk, R. Capart, Production and characterization of activated carbon from wood components in powder: Cellulose, lignin, xylan. *Powder Technol.* 2005(157) 48-56.
- [12] L. Muniandy, F. Adam, A. R. Mohamed, Eng-Poh Ng, The synthesis and characterization of high purity mixed microporous/mesoporous activated carbon from rice husk using chemical activation with NaOH and KOH. *Micropor. Mesopor. Mater.* 2014(197)316-323.
- [13] L. Shijie, H. Kuihua, Li. Jinxiao, Li. Ming, Lu. Chunmei, Preparation and characterization of super activated carbon produced from gulfweed by KOH activation. *Micropor. Mesopor. Mater.* 2017(243)291-300.
- [14] J. M. Rosas, J. Bedia, J. Rodríguez-Mirasol, T. Cordero, Preparation of Hemp-derived activated carbon monoliths. Adsorption of water vapor, *Ind. Eng. Chem. Res.* 2008(47)1288-1296.
- [15] J. M. Rosas, J. Bedia, J. Rodríguez-Mirasol, T. Cordero, HEMP-derived activated carbon fibers by chemical activation with phosphoric acid. *Fuel* 2009(88)19–26.

- [16] H. Wang, Z. Xu, A. Kohandehghan, Z. Li, K. Cui, X. Tan, T. J. Stephenson, C. K. King'ondeu, C. M. B. Holt, B. C. Olsen, J. K. Tak, D. Harfield, A. O. Anyia, and D. Mitlin, Interconnected carbon nanosheets derived from Hemp for ultrafast supercapacitors with high energy. *ACS nano* 2013 (6)5131–5141.
- [17] R. Rajbhandari, L. K. Shrestha, B. P. Pokharel, and R. R. Pradhananga, Development of nanoporous structure in carbons by chemical activation with zinc chloride. *J. Nanosci. Nanotechnol.* 2013(13)2613–2623.
- [18] I. Ozdemir, M. Sahin, R. Orhan, M. Erdem, Preparation and characterization of activated carbon from grape stalk by zinc chloride activation. *Fuel Process. Technol.* 2014(125)200-206.
- [19] A. L. Cazetta, A. M.M Vargas, E. M. Nogami, M. H. Kunita, M. R. Guiherme, A. C. Martins, T. L. Silva, J. C.G. Moraes, V. C. Almeida, NaOH-activated carbon of high surface area produced from coconut shell: Kinetics and equilibrium studies from the methylene blue adsorption. *Chem. Eng. J.* 2011(174)117-125.
- [20] M. Kiliç, E. Apaydin-varol, A. Eren Pütün, Preparation and surface characterization of activated carbon from *Euphorbia rigida* by chemical activation with  $ZnCl_2$ ,  $K_2CO_3$ , NaOH and  $H_3PO_4$ . *Appl. Surf. Sci.* 2012(261)247-254.
- [21] Z. Liu, Y. Huang, G. Zhao, preparation and characterization of activated carbon fibers from liquefied wood by  $ZnCl_2$  activation. *Bioresource* 2016(11)3178-3190.
- [22] S. Yorgun, D. Yildiz, preparation and characterization of activated carbons from paulownia wood by chemical activation with  $H_3PO_4$ . *J. Taiwan Inst. Chem. Eng.* 2015(53)122-131.
- [23] S. Yorgun, N. Vural, H. Demiral, Preparation of high-surface area activated carbons from Paulownia wood by  $ZnCl_2$  activation. *Micropor. Mesopor. Mater.* 2009(122)189–194.
- [24] R. Yang, G. Liu, X. Xu, M. Li, J. Zhang, X. Hao, Surface texture, chemistry and adsorption properties of acid blue 9 of hemp (*Cannabis sativa* L.) bast-based activated

carbon fibers prepared by phosphoric acid activation. *Biomass and energy* 2011(35)437-445.

[25] M. Z. Hossain, W. Wu, W. Z. Xu, M. B. I. Chowdhury, A. K. Jhavar, D. M. and P. A. Charpentier, High-surface-area mesoporous activated carbon from Hemp Bast Fiber using hydrothermal processing. *C* 2018(4)38.

[26] Q. Qian, M. Mochida, H. Tatsumoto, Preparation of activated carbons from cattle-manure compost by zinc chloride activation. *Bioresour. Technol.* 2007(98)353-360.

[27] J. Hayashi, A. Kazehaya, K. Muroyama, A. P. Watkinson, Preparation of activated carbon from lignin by chemical activation. *Carbon* 2000(38)1873-1878.

[28] Z. Zhanga, X. Luoa, Y. Liub, P. Zhoua, G. Maa, Z. Lei, L. Leia, A low cost and highly efficient adsorbent (activated carbon) prepared from waste potato residue. *J. Taiwan Inst. Chem. Eng.* 2015 (49)206-211.

[29] J. Yang, K. Qiu, development of high surface area mesoporous activated carbon from herb residue. *Chem. Eng. J.* 2011(167)148-154.

[30] N. J. Ndi, M. J. Ketcha, G. S. Anagho, N. J. Ghogomu, E. P. Belibi. Physical and chemical characteristics of activated carbon prepared by pyrolysis of chemically treated Kola nut (*Cola acuminata*) Shell wastes and its ability to adsorb organics. *Int. J. Adv. Chem. Technol.* 2014(3)1.

[31] A. Kumar, H. Mohan Jene, High surface area microporous activated carbons prepared from Fox nut (*Euryale ferox*) shell by zinc chloride activation. *Appl. Surf. Sci.* 2015(356)753-761.

[32] A. H. Bastam V. Fierro, H. EI- Saied, A. Celzard, 2-Steps KOH activation of rice straw: an efficient method for preparing high-performance activated carbon. *Bioresour. Technol.* 2009 (100)3941-3947.

- [33] A. Arami-Niya, W. M. A. W. Daud, F. S. Mijalli, using granular activated carbon prepared from oil palm shell by  $ZnCl_2$  and physical activation for methane adsorption. *J. Anal. App. Pyrol.* 2010(89)197-203.
- [34] P.T. Williams, A. R. Reed, Development of activated carbon pore structure via physical and chemical activation of biomass fiber waste. *Biomass Bioenergy* 2006(30)144.
- [35] T. Liou, Development of mesoporous structure and high adsorption capacity of biomass-based activated carbon by phosphoric acid and zinc chloride activation. *Chem. Eng. J.* 2010(158)129–142.
- [36] D. Honga, J. Zhoua, C. Hub, Q. Zhoua, J. Maoa, Q. Qina, Mercury removal mechanism of AC prepared by one-step activation with  $ZnCl_2$ . *Fuel* 235(2019)326–335.
- [37] D. Adinata, W.M. Wan-Daud, and M.K. Aroua. Preparation and characterization of activated carbon from palm shell by chemical activation with  $K_2CO_3$ . *Bioresour. Technol.* 2007(98)145.
- [38] D.W. Mckee, Mechanisms of the alkali metal catalysed gasification of carbon. *Fuel* 1983(62)170-175.
- [39] E. Raymundo-Piñero, P. Azaïs, T. Cacciaguerra, D.Cazorla- Amorós, A. Linares-Solano, F. Béguin, KOH and NaOH activation mechanisms of multiwalled carbon nanotubes with different structural organization. *Carbon* 2005(43)786-795.
- [40] J. Lee, J. Kim, T. Hyeon, Recent progress in the synthesis of porous carbon materials. *Adv. Mater.* 2006(18)2073–2094.
- [41] T.-Y. Ma, L. Liu, Z.-Y. Yuan, Direct synthesis of ordered mesoporous carbons. *Chem. Soc. Rev.* 2013(42)3977–4003.
- [42] S. Ucar, M. Erdem, T. Tay. S. Karago, Preparation and characterization of activated carbon produced from pomegranate seeds by  $ZnCl_2$  activation. *Appl. Surf. Sci.* 2009(255)8890-8896.

- [43] A. Gundogdu, C. Duran, H. B. Senturk, M. Soylak, M. İmamoglu, Y. Onal, Physicochemical characteristics of a novel activated carbon produced from tea industry waste. *J. Anal. Appl. Pyrol.* 2013(104)249-259.
- [44] P. Hao, Z. Zhao, Y. Leng, J. Tian, Y. Sang, R. I. Boughton, C. P. Wong, H. Liu, B. Yang, graphene-based nitrogen self-doped hierarchical porous carbon aerogels derived from chitosan for high performance supercapacitors. *Nano Energy* 2015(15)9–23.
- [45] L. K. Shrestha, R.G. Shrestha, Y. Yamauchi, J.P. Hill, T. Nishimura, K. Miyazawa, T. Kawai, S. Okada, K. Wakabayashi, K. Ariga, Nanoporous carbon tubes from fullerene crystal as the  $\pi$ -electron carbon source. *Angew. Chem. Int. Ed.* 2015(54)951–955.
- [46] J. Acharaya, J. N. Sahu, B. K. Sahoo, C. R. Mohanty, B. C. Meikap, Removal of chromium (IV) wastewater by activated carbon developed from Tamarind wood activated with  $ZnCl_2$ . *Chem. Eng. J.* 2009(150)25-39.
- [47] E. Gonzalez-Serrano, T. Cordero, J. Rodrı́guez-Mirasol, and J. J. Rodrı́guez, Development of porosity upon chemical activation of kraft lignin with  $ZnCl_2$ . *Ind. Eng. Chem. Res.* 1997(36)4832-4838.
- [48] Y. Li, Q. Du, X. Wang, P. Zhang, D. Wang, Z. Wang, Y. Xia, Removal of lead from aqueous solution by activated carbon prepared from *Enteromorpha prolifera* by  $ZnCl_2$  activation. *J. Hazard. Mater.* 2010(183)583-589.
- [49] Y. Önal, C. Akmil-Başar, Ç. Sarci-Özdemir, S. Erdoğan, Textural development of sugar beet bagasse activated with  $ZnCl_2$ . *J. Hazard. Mater.* 2007(142)138-143.
- [50] M. Olivares-Marín, C. Fernández-González, A. Macías-García, Preparation of activated carbon from cherry stones by chemical activation with  $ZnCl_2$ . *Appl. Surf. Sci.* 2006 (252)5967-5971.

## Chapter 3

# Preparation of Nitrogen-doped Hemp Fibers-Based Mesoporous Carbon

### Abstract

In this study, nitrogen-functionalized mesoporous carbon materials derived from hemp fibers (N-HFCs) were prepared by simultaneous activation and carbonization of hemp fibers modified with nitrogen containing functional group. The prepared N-HFCs employed hemp fibers as the carbon source,  $ZnCl_2$  as the activating agent for carbonization, and N-aminoguanidine as the nitrogen source. The process consisted of two steps - i) immobilization of nitrogen-containing functional groups (N-aminoguanidine) on the surface of hemp fibers (HFs), and ii) activation and carbonization of nitrogenized hemp fibers using  $ZnCl_2$  activator in inert atmosphere. The prepared N-HFCs were characterized by the study of BET (Brunauer-Emmett-Teller) surface area, XRD (X-ray Diffraction), SEM (Scanning Electron Microscopy), HRTEM (High Resolution Transmission Electron Microscopy), Raman Scattering, and elemental composition. The obtained N-HFCs demonstrated the BET surface areas in the range of 561.40 to 753.98  $m^2/g$  and nitrogen content of up to 12.3 w%.

### *Keywords*

Hemp fibers, Nitrogen-functionalized porous carbon, N-Aminoguanidine,  $ZnCl_2$  activation, Immobilization, Doped, Nitrogen content

### 3.1. Introduction

Mesoporous carbon materials are widely used in many fields of science and technology, including catalysis [1,2], separation [3-5], and energy storage/conversion [6,7] due to their outstanding physicochemical properties including large specific surface area, developed internal porosity, excellent thermal stability, and environmental acceptability. Considerable efforts have been made aiming to synthesize a variety of carbon-based materials, such as high specific area activated carbon (AC), carbon nanotube (CNT), graphene, and graphite to improve their performance in various applications.

Modification of carbon with specific functional groups for a desirable application is an important area of research. Functionalization with nitrogen is an effective method to improve the performance of carbon materials in various applications such as adsorption [8], catalysis [9], and electrical conductivity [10]. Heteroatom functionalization is one of the ways to enhance the physicochemical properties of the materials, and then extend the range of application. For example, nitrogen functionalized mesoporous carbon could improve various performances such as conductivity, basicity, oxidation stability, catalytic activity, and adsorption capacity [11]. For the adsorption processes, N-containing functional groups could not only act as adsorption sites increasing the electrostatic interaction between the adsorbent and adsorbate, but also raise the hydrophilicity of the adsorbent to improve the adsorption capacity [11]. The approach of introduction of surface functional groups has been proved to be promising for improving the surface wettability as well as adsorption capacity of carbon materials. A recent study shows that N-doping could promote polarization of  $\pi$  electrons on carbon surfaces and generate more  $\pi$ -electron-rich and  $\pi$ -electron-deficit sites for adsorption [11,12]. It is believed that the existence of nitrogen-containing functional groups on the surface of carbon materials generally provides basic properties and electron-donor affinity, which improves the removal of polar compounds, such as organic acids, due to dipole-dipole interactions and H-bonding [13,14].

Covalent interactions between epoxy matrix and nucleophilic functional groups on the carbon fibers is an area of increasing interest in composite materials. Reports are

available on which nucleophilic groups (eg, amines) were immobilized on carbon surface [15-17]. Reportedly, grafting of polymers onto carbon surface was possible through the graft polymerization of vinyl monomers initiated by azo group immobilized carbon [18]. A similar concept can be used in chemical modifications of activated carbon surfaces to enhance the adsorption of metal ions, organic acids, and environmental pollutants [19,20]. Therefore, fabrication of nitrogen grafted carbon materials with high specific surface area and appropriate pore distribution from a sustainable route will be an attractive approach for production of carbon materials that have improved efficiency and wide applicability. For this reason, growing interest lies on the development of bio-based carbon materials grafted with nitrogen atoms and/or nitrogen containing functional groups.

Approaches for introduction of nitrogen containing functionalities on carbon include – i) treatment of activated carbon with nitrogen containing reagents such as  $\text{NH}_3$ , nitric acid, amines, etc. at high temperature, or ii) activation of carbon/carbon precursor and nitrogen containing precursors (such as urea, melamine, etc.) with activating agents [11,21-24]. For instance, Niasar *et al.* treated both commercial activated carbon (AC) and raw petroleum coke (PC) using  $\text{NH}_3$  and amines at elevated temperature to obtain carbon with basic characteristics [25]. Zhou *et al.* prepared the nitrogen-doped porous carbon by one-step process using potato waste residue as a carbon precursor, melamine as nitrogen source, and KOH as activating agent [25]. In a similar study, Ma *et al.* prepared nitrogen-doped carbon using sugar cane bagasse, urea, and KOH [26]. The approach of heating the mixture of carbon source with nitrogen source and activator, however, produces carbon with nitrogen being doped only in the range of 6.20-6.70 presumably due to the reason that covalent linking of nitrogen-containing functional groups onto carbon precursor/surface is not possible in this approach.

Herein, we propose an alternate approach of making nitrogen-doped carbon from biomass resources. Our approach includes immobilization of nitrogen-containing functional group on the surface of carbon precursor followed by activation of nitrogen functionalized carbon precursor. This chapter describes the preparation of nitrogen-containing porous carbon from hemp fibers by chemical modification of hemp fibers with N-

aminoguanidine followed by activation and carbonization of chemically modified HFs using  $\text{ZnCl}_2$  in inert atmosphere. In this method, hemp fibers (HFs) are utilized as carbon precursor, N-aminoguanidine (AG) is used as a nitrogen source, and  $\text{ZnCl}_2$  acts as an activator in carbonization step. The prepared nitrogen-containing hemp fiber-based carbons (referred to as N-HFCs hereafter) were characterized through the studies of elemental composition,  $\text{N}_2$  adsorption-desorption, X-ray Diffraction (XRD), High Resolution Transmission Electron Microscopy (HRTEM), Scanning Electron Microscopy (SEM), and Raman Scattering.

## 3.2. Experimental

### 3.2.1. Materials and Chemicals

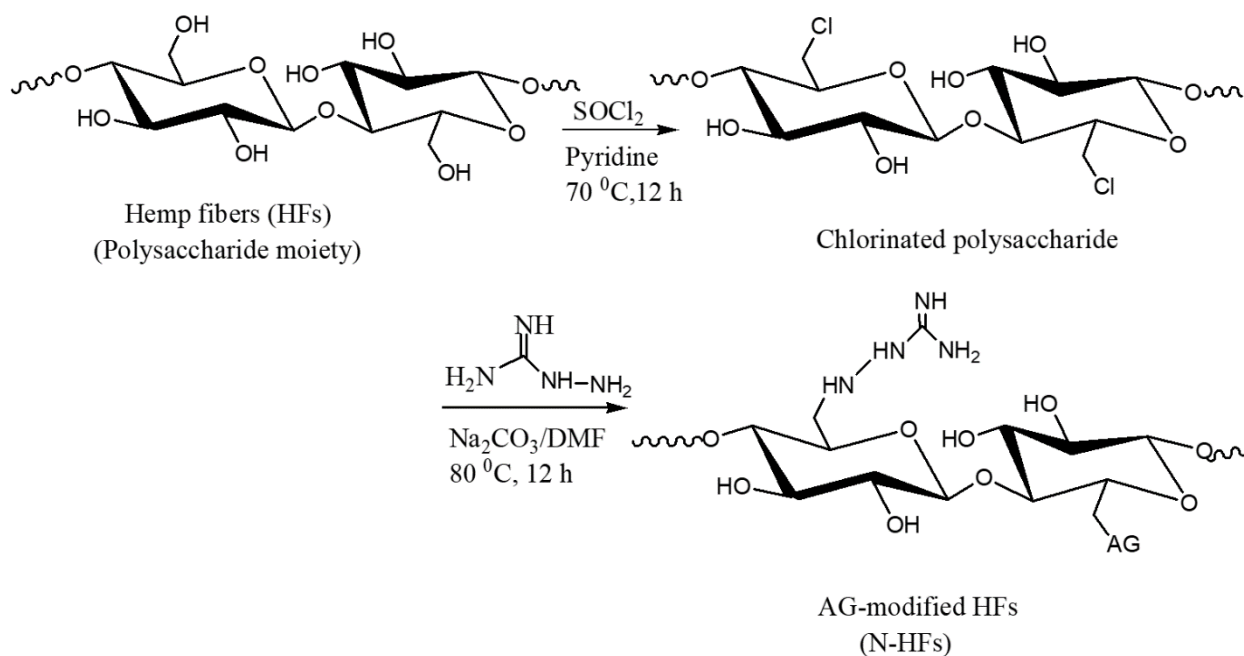
Hemp fibers were supplied by American Hemp, Winston Salem, NC, USA. The obtained samples of hemp fibers were cut into smaller pieces with scissors, thoroughly washed several times with de-ionized water to clean off the dirt, and dried in vacuum oven at  $100^\circ\text{C}$  for 24 h. The dried raw materials were then crushed and ground in an electric grinder (CGOLDENWALL, model: DF-15). N-aminoguanidine hydrochloride ( $\text{CH}_6\text{N}_4\cdot\text{HCl}$ ;  $\geq 98\%$  purity), zinc chloride ( $\text{ZnCl}_2$ ;  $\geq 98\%$  purity), thionyl chloride ( $\text{SOCl}_2$ ;  $\geq 99\%$  purity), dimethyl formamide (DMF; 99.8% purity), and sodium carbonate ( $\text{Na}_2\text{CO}_3$ ;  $\geq 99.5\%$  purity) used in the present study were purchased from Sigma Aldrich (Oakville, ON, Canada) and were used without further purification.

### 3.2.2. Methods

#### 3.2.2.1. Preparation of N-HFCs

Preparation of N-HFCs from hemp fibers consisted of two steps – i) preparation of N-aminoguanidine modified hemp fibers (N-HFs), and ii) carbonization of N-HFs in presence of  $\text{ZnCl}_2$  activator to yield nitrogen-doped hemp fiber-derived activated carbon (N-HFCs).

**Preparation of N-HFs:** Surface modification of pretreated HFs with N-aminoguanidine was carried out according to the reaction sequence shown in Scheme 3.1[28]. In a typical run, 20 mL thionyl chloride was slowly added in ice-cold condition to a stirred suspension of 13.0 g pre-treated HFs in 100 mL of pyridine over a period of 2 h. After the addition of thionyl chloride, the reaction mixture was first allowed to come to room temperature and then slowly heated to a temperature of 70°C, which was maintained overnight with continuous stirring. Then, 30 mL of ice-cold water was slowly added, vacuum filtration was applied, and the filter cake was collected. The filter cake was repeatedly washed with water, followed by 95% ethanol (100 mL) and again with water. After drying of the residue (100°C, 24 h) chlorinated product was obtained. In the next step, a slurry consisting of 6.0 g chlorinated HFs, 3.53 g Na<sub>2</sub>CO<sub>3</sub>, and 5.0 g N-aminoguanidine hydrochloride in 80 mL dimethylformamide (DMF) was stirred at 80°C for 24 h. Upon cooling, water (50 mL) was added, and the solid was collected by filtration. The residue was washed repeatedly with distilled water until the filtrate was neutral toward pH indicators. The filter cake was then washed with 95% ethanol (100 mL) followed by water. Drying overnight in vacuum oven at 100°C yielded the chemically modified HFs material, which was named as N-HFs.



**Scheme 3.1: Preparation route of N-aminoguanidine modified HFs (N-HFs).**

**Preparation of N-HFCs:** For carbonization of N-HFs, the optimal conditions of carbonization of HFs (chapter 2, section 2.2.2.2) were employed. In a typical run, the prepared N-HFs powder sample was thoroughly mixed with  $\text{ZnCl}_2$  using mortar and pestle at mass ratio of 1:1, 2:1, and 3:1 (w: w), separately. A mixture of weighted amounts of N-HFs and  $\text{ZnCl}_2$  was carbonized under  $\text{N}_2$  atmosphere in a tubular furnace for 1 h at temperature of  $500^\circ\text{C}$ . The heating rate  $3^\circ\text{C}/\text{min}$ , and the holding time (1 h) started after the onset of set temperature  $500^\circ\text{C}$ . After being cooled to room temperature, the products were washed thoroughly with 2 M HCl followed by deionized water to neutral PH value, and dried at  $100^\circ\text{C}$  for 12 h in a convection oven. The obtained N-HFC samples were labeled as N-HFC-x, where x represents the mass ratio of  $\text{ZnCl}_2$  and N-HFs in the corresponding sample. The dried samples were used for characterization.

### 3.2.2.2. Surface characterization

Brunauer–Emmett–Teller (BET) surface area analysis, Scanning Electron Microscopy (SEM), X-ray diffraction (XRD), Raman spectra and high-resolution transmission electron microscopy (HRTEM) were used to characterize the properties of the material. Tristar II 3020 (Micromeritics Instrument Corporation) was used to determine the surface area and pore size of solid materials by nitrogen adsorption-desorption isotherm at 77 K. Samples were subjected to degassing for 8 h at  $150^\circ\text{C}$  to remove the moisture and other adsorbed gases from the surface before the measurements were recorded. Elemental analysis was carried out on a CHN elemental analyzer (Flash EA1112, Thermo Electron Corporation).

The SEM images were recorded by using Hitachi FlexSEM (model SU 1000). XRD patterns were obtained by using a Bruker D2 PHASER desktop diffractometer with  $\text{Cu K}\alpha$  radiation (30 kV, 10 mA and  $\lambda=1.54 \text{ \AA}$ ). The diffraction angle was varied from  $10^\circ$  to  $70^\circ$ . The HRTEM images were obtained with a JEOL Model JEM-2100F operating at 200 kV. Raman measurements were performed with Kaiser Optical Systems RXNI-785 with an excitation wavelength of 785 nm.

### 3.3. Results and Discussion

#### 3.3.1. Elemental composition analysis

The results of C, H, and N analysis of pretreated HFs (without immobilization of AG) and different N-HFCs are listed in Table 3.1. The nitrogen content of pretreated HFs was found to be only 2.04% whereas the HFCs contained remarkably higher proportion of nitrogen (8.70 to 12.3%). The high content of nitrogen in all N-HFC samples as compared to HFs is due to the immobilization of nitrogen containing functional groups on the surface of feed material (N-HFs) prior to carbonization. Increasing the amount of ZnCl<sub>2</sub> activator to 3:1 ratio (ZnCl<sub>2</sub>: N-HFs) substantially lowered the nitrogen content of final product (Table 3.1) as compared to the product of 2:1 and 1:1 ratio of ZnCl<sub>2</sub>: N-HFs. This observation is consistent with the results reported by Yue *et al.* and Liu *et al.* on which some N-containing moieties were decomposed during the ZnCl<sub>2</sub> activation process [29-31]. A plausible reason for excess amount ZnCl<sub>2</sub> leading to the reduction of nitrogen content of nitrogen-doped carbon is that the excess activator reacts with the functional groups through chemical interactions leading to formation of water-soluble products which are possibly leached out in washing step.

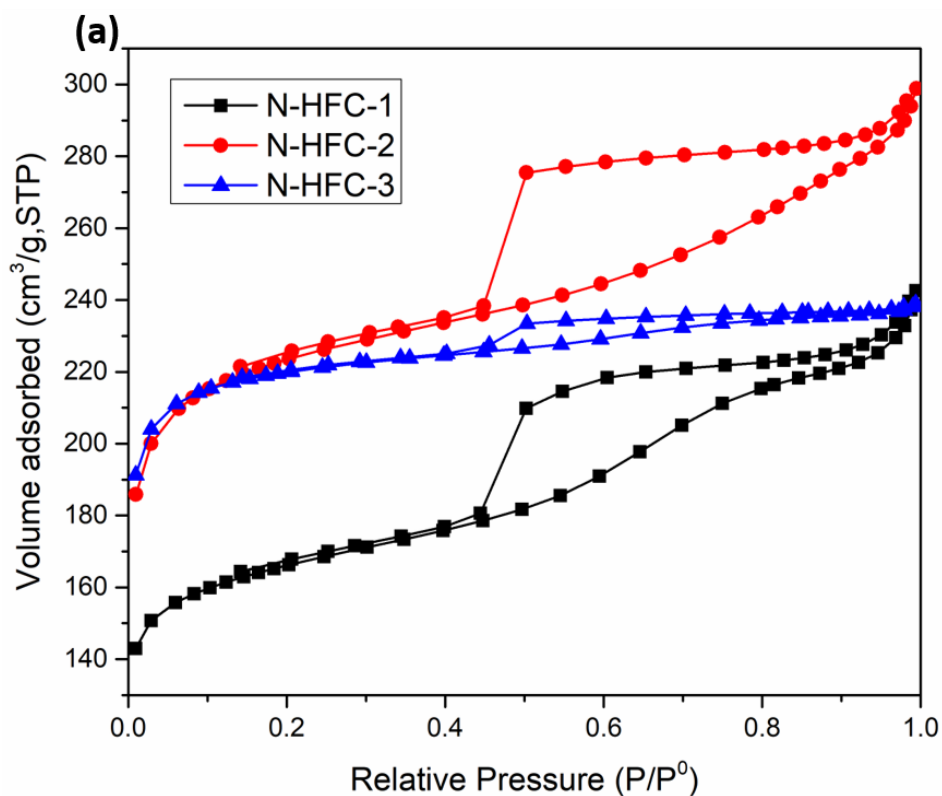
**Table 3.1. Elemental composition of HFs without chemical modification, and N-HFCs obtained by carbonization of N-HFs at different ratio of ZnCl<sub>2</sub> activator.**

Sample	ZnCl <sub>2</sub> : N-HF ratio	Elemental Composition (%)		
		C <sup>1</sup>	H <sup>1</sup>	N <sup>1</sup>
HFs	N/A	40.7±0.07	5.94±0.08	2.04±0.01
N-HFC-1	1:1	50.1±0.16	3.25±0.18	12.2±0.05
N-HFC-2	2:1	49.2±0.12	3.19±0.22	12.3±0.03
N-HFC-3	3:1	56.6±0.26	2.02±0.31	8.70±0.95

<sup>1</sup> Results are presented as average ± standard deviation of analysis of triplicate samples.

### 3.3.2. Nitrogen adsorption-desorption isotherms

The specific surface area and pore structures of N-HFCs were evaluated by nitrogen adsorption–desorption isotherm measurements. Figure 3.1a shows the N<sub>2</sub> adsorption–desorption isotherms and BJH (Barrett-Joyner-Halenda) pore size distribution of the N-HFC samples. All the isotherm plots of the N-HFC samples exhibit type-IV adsorption–desorption isotherms with a distinct hysteresis loop at relative pressure ( $P/P^{\circ}$ ) between 0.48 and 1.0. The shape of the isotherm is due to capillary condensation, indicating the presence of mesopores (IUPAC definition 2–50 nm) [32]. These results of pore size distribution of the samples obtained by BJH method shown in Figure 3.1b also indicate the presence of mesopores in N-HFC samples. All the samples have pore distribution peaks between 2.0 and 2.5 nm, which suggests the presence of mesopores.



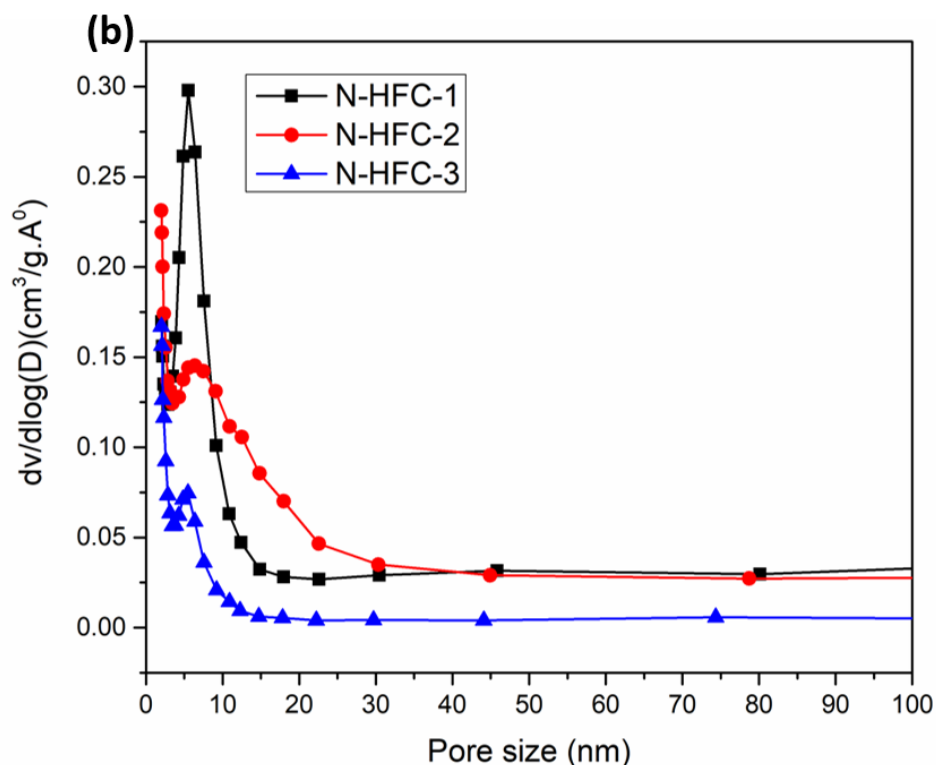


**Figure 3.1. Nitrogen adsorption-desorption isotherms at 77 K (a), and (b) pore-size distribution (b) of N-HFCs.**

The surface properties (surface area and pore size distribution) of the N-HFC samples are summarized in Table 3.2. The specific surface area of N-HFC increased notably with increasing the  $\text{ZnCl}_2$ : N-HFs ratio from 1:1 to 2:1 (increased from 561 to 754). However, further increasing the  $\text{ZnCl}_2$ : N-HFs ratio to 3:1 has no substantial change on the surface area or pore size distributions. The carbon product obtained from surface functionalization of HFs with N-aminoguanidine treatment has lower specific surface area than that of the product without surface modification (eg, HFC-2-500 had specific surface area of 2518; chapter 2). The decrease is likely attributable to the weight gain as a result of functionalization of feed material [29,30].

**Table 3.2. Surface characteristics of pretreated HFs as well as N-HFC materials.**

Sample	Surface area (m <sup>2</sup> g <sup>-1</sup> )	Pore volume (cm <sup>3</sup> g <sup>-1</sup> )	Pore size (nm)
N-HFC-1	561	0.35	2.53
N-HFC-2	754	0.38	2.43
N-HFC-3	734	0.36	2.00

### 3.3.3. Comparative evaluation

Among the prepared materials, N-HFC-2 has a higher surface content of nitrogen (12.3 w%), indicating the presence of higher amount of surface nitrogen containing functional groups. This is comparable with or higher than the percentage of nitrogen reported in N-enriched carbons prepared from various precursors (Table 3.3) which is very likely due to the reason that in this study the nitrogen-containing functional groups were covalently bonded to carbon precursor prior to carbonization.

**Table 3.3. Comparison of surface area and N-content of N-HFC-2 with N-enriched porous carbons prepared from various precursors.**

Carbon precursors	Nitrogen precursors	Activating agents	BET surface area (m <sup>2</sup> /g)	N content (w%)	Reference
Coconut shell	urea	KOH	1023	1.35	[30]
Lotus leaf	-	NaNH <sub>2</sub>	1924	3.64	[39]
Willow catkin	thiourea	KOH	1547	4.14	[37]
Phenol-formaldehyde resin	melamine	NaOH	1159	4.27	[34]
Biochar	NH <sub>3</sub>	-	418.7	5.69	[35]
Potato waste	melamine	ZnCl <sub>2</sub>	1052	6.20	[25]

Coconut shell	NH <sub>3</sub>	KOH	879	6.16	[31]
Sugar cane bagasse	urea	CaCl <sub>2</sub>	945.8	6.70	[26]
Sucrose	urea	KOH	1745	7.7	[33]
Glucose and glucosamine		-	327	-	[36]
Pomelo peels	diammonium hydrogen Phosphate	-	807.7	-	[38]
D-Glucose	urea	K <sub>2</sub> CO <sub>3</sub>	933	12.27	[29]
<b>Hemp Fibers</b>	<b>N-Amino guanidine</b>	<b>ZnCl<sub>2</sub></b>	<b>754.0</b>	<b>12.3</b>	This work

---

### 3.3.4. X-ray diffraction analysis

The XRD patterns of the prepared N-HFC samples are shown in Figure 3.2. The two broad and weak peaks at  $2\theta = 22.3$  and  $43.8^\circ$  can be ascribed respectively to (002) and (100) reflections of the disordered carbon layer [29]. The broad and weak peak of (002) reflection in all samples indicates a less ordered graphitic structure possibly due to strong chemical activation by ZnCl<sub>2</sub> during the thermal treatment. The absence of sharp peaks reveals that all N-HFCs prepared from HFs are devoid of crystalline materials. The amorphous nature of the materials developed in this study is an advantageous property for well-defined adsorbents.

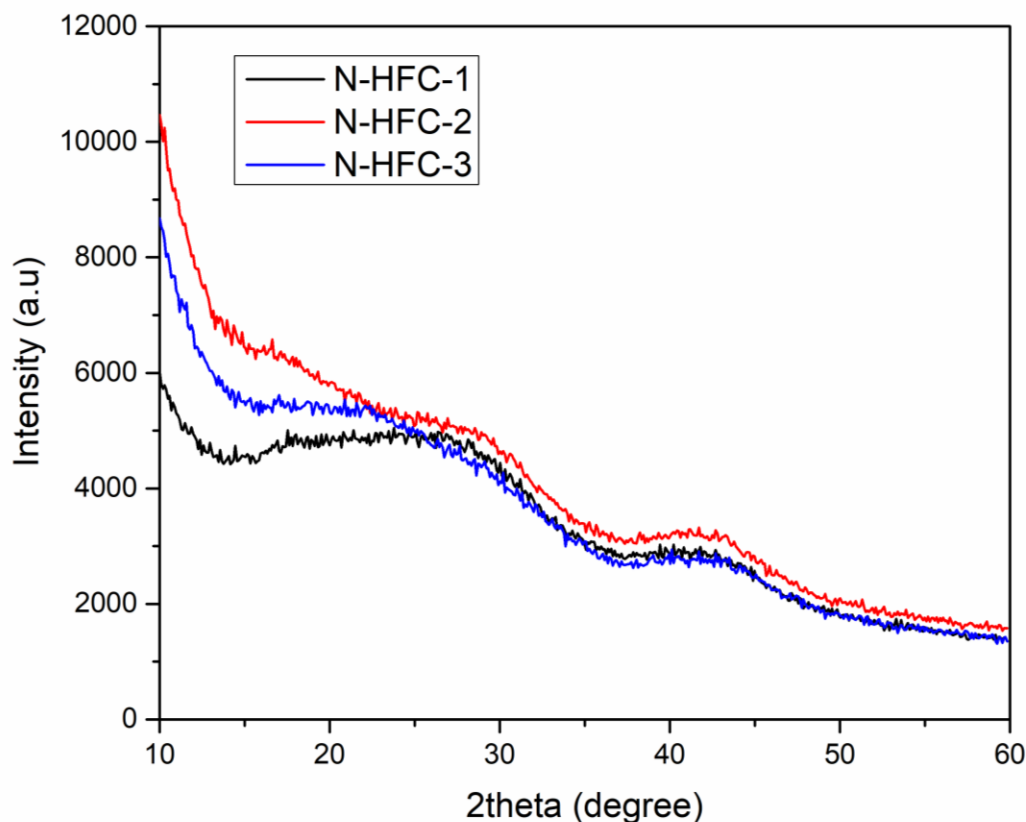


**Figure 3.2. XRD analysis of N-HFC samples.**

### 3.3.5. Spectroscopic analysis

The structure of the N-HFC-2 was further studied by Scanning Electron Microscopy (SEM), Raman Spectroscopy, and HRTEM, and the results are shown in Figure 3.3(a-c), respectively. The SEM image of N-HFC-2 (Figure 3.3a) reveals that N-HFC-2 contains large number of honeycomb-like pores on the surface, indicating the porous nature of the material.

The Raman spectrum of N-HFC-2 shows the D band at  $1365\text{ cm}^{-1}$  attributable to the degree of disorderness, and the G band at  $1586\text{ cm}^{-1}$  corresponding to graphitic orderness in the structure (Figure 3.3b) [30,31]. The intensity ratio ( $I_D/I_G$ ) can be used to qualitatively investigate the degree of graphite disorder or defects in the carbon materials. The intensity ratio,  $I_D/I_G = (1.128 \pm 0.051)$  of N-HFC-2 is greater than  $I_D/I_G = (0.9 \pm 0.025)$  of  $\text{ZnCl}_2$  activated HFs (chapter 2, section 2.3.7), which means that NHFC-2 has

more disorderness and defected structure than  $\text{ZnCl}_2$  activated HFs. The relative low degree of orderness of N-HFC-2 observed in Raman spectrum is also in consistent with broad (002) and (100) XRD peaks for relatively low degree of orderness. A high-resolution TEM image of the NHFC-2 shown in Figure 3.3 c also corroborates the existence of disordered carbon.

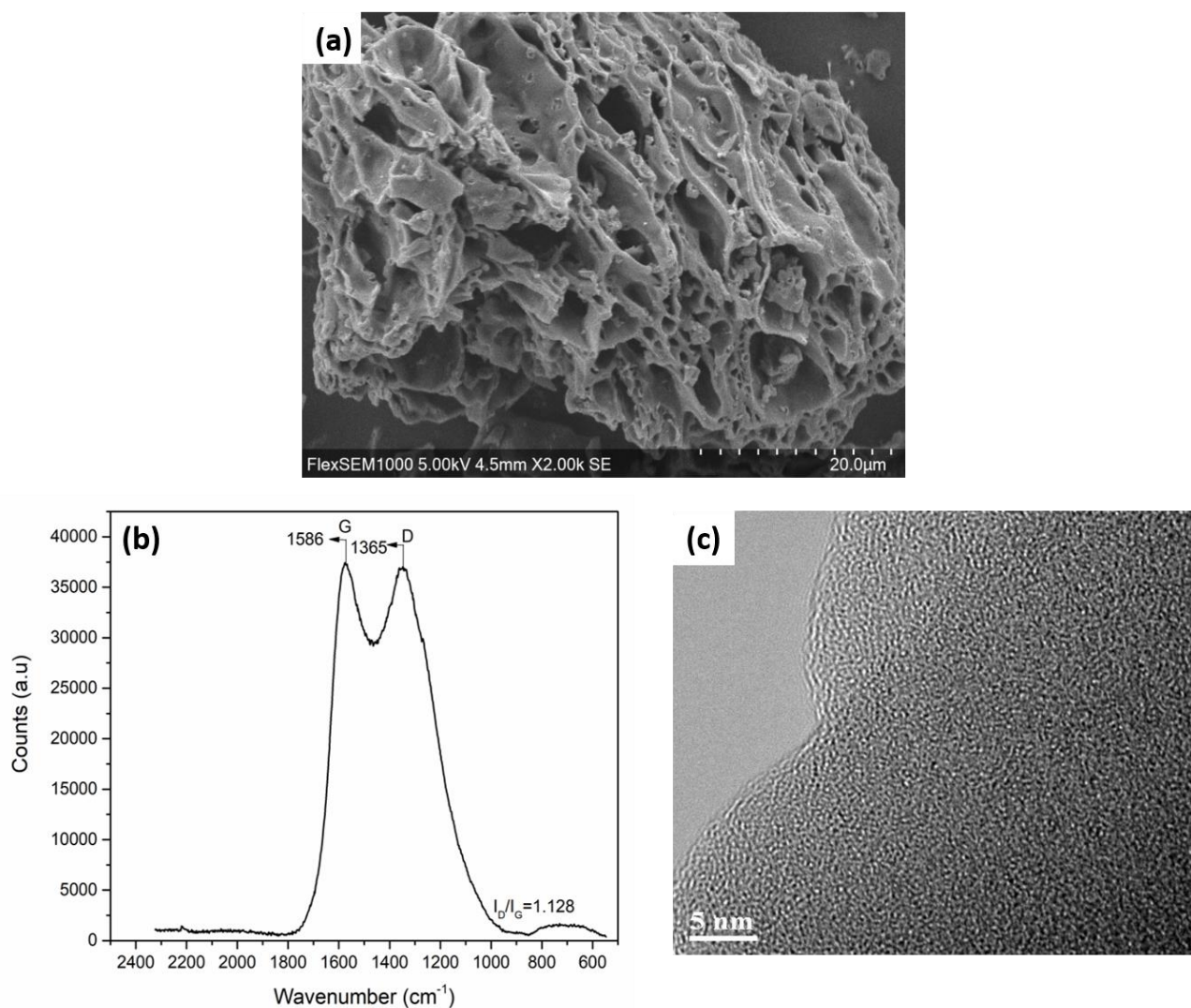


**Figure 3.3. SEM image (a), Raman spectra (b), and high-resolution TEM spectrum (c) of N-HFC-2.**

### 3.4. Conclusions

Nitrogen-containing hemp fiber-derived mesoporous carbon materials (N-HFCs) have been successfully prepared using hemp fibers as carbon source, N-aminoguanidine as nitrogen precursor, and  $\text{ZnCl}_2$  as an activator in carbonization. Introduction of nitrogen precursor on the surface of HFs through covalent linkages led to nitrogen-doped carbon with nitrogen content of 13%, which is remarkably higher than the nitrogen content of nitrogen-doped carbons prepared by the carbonization of mixture of carbon precursor, nitrogen precursor, and activator. The high amount of nitrogen doped may induce the enhancement of electron conductivity and surface wetting ability of carbon materials. Additionally, the presence of substantial amount of accessible basic sites like nitrogen-containing functional groups on the surface of N-HFCs materials should play crucial role in influencing the adsorption performance for adsorption of metal ions and acidic species. The innovative work reported here offers an effective yet extremely simple, low-cost, and eco-friendly method for the scalable synthesis of nitrogen-containing mesoporous carbon derived from biomass.

### 3.5. References

- [1] Z. Li, J. Liu, C. Xia, F. Li, Nitrogen-functionalized ordered mesoporous carbons as multifunctional supports of ultrasmall pd nanoparticles for hydrogenation of phenol. *ACS Catal.* 2013 (11)2440–2448.
- [2] F. Goettmann, A. Fischer, M. Antonietti, A. Thomas, Chemical synthesis of mesoporous carbon nitrides using hard templates and their use as a metal-free catalyst for friedel-crafts reaction of benzene. *Angew. Chem. Int. Ed.* 2006(45)4467–4471.
- [3] M. R. Awual, A novel facial composite adsorbent for enhanced copper(II) detection and removal from wastewater. *Chem. Eng. J.* 2015(266)368–375.
- [4] M. R. Awual, T. Yaita, Y. Okamoto, A novel ligand based dual conjugate adsorbent for cobalt(II) and copper(II) ions capturing from water. *Sensor Actuat B* 2014(203)71–80.

- [5] M. R. Awual, M. Ismael, T. Yaita, SA. El-Safty, H. Shiwaku, Y. Okamoto, S. Suzuki, Trace copper(II) ions detection and removal from water using novel ligand modified composite adsorbent. *Chem. Eng. J.* 2013(222)67–76.
- [6] J. Wang, HL. Xin, D. Wang, Recent progress on mesoporous carbon materials for advanced energy conversion and storage. *Part. Part. Syst. Charact.* 2014(31)515–539.
- [7] Q. Li, R. Jiang, Y. Dou, Z. Wu, T. Huang, D. Feng, J. Yang, A. Yu, D. Zhao, Synthesis of mesoporous carbon spheres with a hierarchical pore structure for the electrochemical double-layer capacitor. *Carbon* 2011(49)1248–1257.
- [8] M. Yang, L. Guo, G. Hu, X. Hu, L. Xu, J. Chen, W. Dai and M. Fan, highly cost-effective nitrogen doped porous coconut shell-based CO<sub>2</sub> sorbent synthesized by combining ammoxidation with KOH activation. *Environ. Sci. Technol.* 2015(49)7063-7070.
- [9] X. Wang, Y. Qin, L. Zhu and H. Tang, Nitrogen-doped reduced graphene oxide as a bifunctional material for removing bisphenols: Synergistic effect between adsorption and catalysis. *Environ. Sci. Technol.* 2015(49)6855-6864.
- [10] M. Zhou, F. Pu, Z. Wang and S. Guan, Nitrogen doped porous carbons through KOH activation with superior performance in supercapacitors. *Carbon* 2014(68)185-194.
- [11] W. Shen, W. Fan, Nitrogen-containing porous carbons: synthesis and application. *J. Mater. Chem. A* 2013(1)999-1013.
- [12] L. Wang, D. Zhu, J. Chen, Y. Chen, W. Chen, Enhanced adsorption of aromatic chemicals on boron and nitrogen co-doped single-walled carbon nanotubes. *Environ. Sci. Nano* 2017(4)558-564.
- [13] F. W. Shaarani, B. H. Hameed, Ammonia modified activated carbon for the adsorption of 2,4-dichlorophenol. *Chem. Eng. J.* 169(2011)180-185.

- [14] Z. Zhang, M. Xu, H. Wang, Z. Li, Enhancement of CO<sub>2</sub> adsorption on high surface area activated carbon modified by N<sub>2</sub>, H<sub>2</sub> and ammonia. *Chem. Eng. J.* 2010(160)571-577.
- [15] E. Fitzer, K.H. Geigl, W. Huttner, R. Weiss, Chemical interactions between the carbon-fiber surface and epoxy-resins. *Carbon* 1980(18)389–393.
- [16] B. Barbier, J. Pinson, G. Desarmot, M. Sanchez, Electrochemical bonding of amines to carbon-fiber surfaces toward improved carbon-epoxy composites. *J. Electrochem. Soc.* 1990(137)1757–1764.
- [17] D.A. Buttry, J.C.M. Peng, J.B. Donnet, S. Rebouillat, Immobilization of amines at carbon fiber surfaces. *Carbon* 1999(37)1929–1940.
- [18] N. Tsubokawa, M. Koshihara, Grafting of polymers onto activated carbon surface: Graft polymerization of vinyl monomers initiated by azo groups that were introduced onto the surface. *J. Macromol. Sci. Pure.* 1997(A34 12)2509–2524.
- [19] W. Yantasee, Y. Lin, K. L. Alford, B. J. Busche, G. E. Fryxell., M. H. Engelhard, Electrophilic aromatic substitutions of amine and sulfonate onto fine-grained activated carbon for aqueous-phase metal ion removal. *Sep. Sci. Technol.* 2004(39)3263–3279.
- [20] S. S. Mohammad, M. A.W.D. Wan, H. Amirhossein, S. Ahmad, A review on surface modification of activated carbon for carbon dioxide adsorption. *J. Anal. Appl. Pyrol.* 89(2010)143-151.
- [21] T. C. Drage, A. Arenillas, K. M. Smith, C. Pevida, C. E. Snape, Preparation of carbon dioxide adsorbents from the chemical activation of urea–formaldehyde and melamine–formaldehyde resins. *Fuel* 2007(86)22-31.
- [22] F. Stoeckli, T. A. Centeno, A. B. Fuertes and J. Mukzb, Porous structure of polyacrylamide-based activated carbon fibers. *Carbon* 1996(34)1201-1206.
- [23] R. J. J. Jansen and H. V. Bekkum, Amination and ammoxidation of activated carbons. *Carbon* 1994(32)1507-1516.

- [24] C. L. Mangun, K. R. Benak, J. Economy, K. L. Foster, Surface chemistry, pore sizes and adsorption properties of activated carbon fibers and precursors treated with ammonia. *Carbon* 2001(39)1809-1820.
- [25] H. S. Niasar, H. Li, T. V. R. Kasanneni, M. B. Ray, C. Xu, Surface amination of activated carbon and petroleum coke for the removal of naphthenic acids and treatment of oil sands process-affected water (OSPW). *Chem. Eng. J.* 193(2016)189-199.
- [26] K. Zoua, Y. Deng, J. Chena, Y. Qiana, Y. Yangc, Y. Lia, G. Chend, Hierarchically porous nitrogen-doped carbon derived from the activation of agriculture waste by potassium hydroxide and urea for high-performance supercapacitors. *J. Power Sources* 2018(378)579–588.
- [27] G. Ma, Q. Yang, K. Sun, H. Peng, F. Ran, X. Zhao, Nitrogen-doped porous carbon derived from biomass waste for high performance supercapacitors. *Bioresour. Technol.* 2015(197)137–142.
- [28] K. Khunathai, K. Inoue, K. Ohto, H. Kawakita, M. Kurata, K. Atsumi, H. Fukuda, and S. Alam, Adsorptive recovery of palladium(II) and platinum(IV) on the chemically modified microalgal residue. *Solv. Extr. Ion Exch.* 2013(31)320–334.
- [29] L. Yue, L. Rao, L. Wang, L. An, C. Hou, C. Ma, H. DaCosta, and X. Hu, Efficient CO<sub>2</sub> adsorption on nitrogen-doped porous carbons derived from D-Glucose. *Energy Fuels* 2018(32)6955–6963.
- [30] J. Chen, J. Yang, G. Hu, X. Hu, Z. Li, S. Shen, M. Radosz, M. Fan, Enhanced CO<sub>2</sub> capture capacity of nitrogen-doped biomass-derived porous carbons. *ACS Sustain. Chem. Eng.* 2016(3)1439–1445.
- [31] M. Yang, L. Guo, G. Hu, X. Hu, L. Xu, J. Chen, W. Dai, M. Fan, Highly cost-effective nitrogen-doped porous coconut shell based CO<sub>2</sub> sorbent synthesized by combining ammoxidation with KOH activation. *Environ. Sci. Technol.* 2015(49)7063–7070.

- [32] H. Liu, K. Wang, H. Teng, A simplified preparation of mesoporous carbon and the examination of the carbon accessibility for electric double layer formation. *Carbon* 2005(43)559–566.
- [33] D. L. Sivadas, S. Vijayan, R. Rajeev, K.N. Ninan, K. Prabhakaran, Nitrogen-enriched microporous carbon derived from sucrose and urea with superior CO<sub>2</sub> capture performance. *Carbon* 109(2016)7-18.
- [34] K. Li, J. Cao, H. Li, J. Liu, M. Lu, D. Tang, Nitrogen functionalized hierarchical microporous/mesoporous nitrogen content for enhanced lead(II) adsorption. *RSC Adv.* 2016 (6)92186–92196.
- [35] W. Yu, F. Lian, G. Cui, Z. Liu, N-doping effectively enhances the adsorption capacity of biochar for heavy metal ions from aqueous solution. *Chemosphere* 2018(193)8-16.
- [36] H. Qu, X. Zhang, J. Zhan, W. Sun, Z. Si, and H. Chen, Biomass-based nitrogen-doped hollow carbon nanospheres derived directly from glucose and glucosamine: structural evolution and supercapacitor properties. *ACS Sustain. Chem. Eng.* 2018(6)7380–7389.
- [37] Y. Li, G. Wang, T. Wei, Z. Fan, P. Yan, Nitrogen and sulfur co-doped porous carbon nanosheets derived from willow catkin for supercapacitors. *Nano Energy* 2016(19)165-175.
- [38] Z. Wang, Y. Tana, Y. Yang, X. Zhao, Y. Liua, L. Niu, B. Tichnell, L. Konga, L. Kanga, Z. Liu, F. Rana, Pomelo peels-derived porous activated carbon microsheets dual-doped with nitrogen and phosphorus for high performance electrochemical capacitors. *J. Power Sources* 2018(378)499–510.
- [39] S. Liu, P. Yang, L. Wang, Y. Li, Z. Wu, R. Ma, J. Wu, and X. Hu, Nitrogen-doped porous carbons from lotus leaf for CO<sub>2</sub> capture and supercapacitor electrodes. *Energy Fuels* 2019(33) 6568–6576.

## Chapter 4

# Utilization of Hemp Fibers-Based Carbon for Adsorptive Removal of Model Naphthenic Acids (NAs) from Aqueous Solution

### Abstract

This chapter describes the removal of two model naphthenic acids, namely 2-naphthoic acid and benzoic acid, from aqueous solutions by using hemp fibers derived carbon as adsorbent. The adsorbents were prepared either by simple one step method of carbonization and activation (described in chapter 2) or by introduction of nitrogen-containing functional groups on surface of hemp fibers followed by activation and carbonization (described in chapter 3), and were named as HFC and N-HFC, respectively. Batch adsorption studies were conducted to evaluate the effect of various parameters such as pH, adsorbent dose, contact time, and initial NAs concentration on naphthenic acid removal. Based on the adsorption experiments, N-HFC exhibited higher removal efficiency than HFC from basic solution of both the model compounds. In the adsorption kinetic experiment, adsorption of 2-naphthoic acid and benzoic acid reached equilibrium within 60 min for both the adsorbents. Adsorption kinetics was analyzed using pseudo-first-order and pseudo-second-order kinetic models, and were found to follow a pseudo-second-order kinetic model. Both adsorbents exhibited remarkable adsorption capacity towards 2-naphthoic acid followed by benzoic acid. The effectiveness of the HFs derived carbons were also compared with commercially available granulated carbon (GAC) for the removal of NAs from acidic and basic conditions. Comparative evaluations demonstrated that the mesoporous carbonaceous materials derived from hemp fibers is an attractive adsorbent for removal of such contaminants from contaminated aqueous streams.

## *Keywords*

Hemp fibers, ZnCl<sub>2</sub> activated porous carbon, Nitrogen-functionalized porous carbon, Adsorptive removal, Model naphthenic acids, Oil sand process-affected water (OSPW), Kinetic models.

### 4.1. Introduction

Canada has the world's second largest resources of petroleum products, which is located in Northern Alberta, and is known as Oil Sand Industry [1,2]. Processing of oil sand produces substantial amounts of wastewater known as oil sand process-affected water (OSPW), that contains several contaminants [3,5]. The dissolved organic acids, collectively known as naphthenic acids (NAs), are one of the major contaminants of OSPW [3,5]. Structurally, NAs are the complex mixtures of alkyl-substituted acyclic and cycloaliphatic carboxylic acids. They are released and concentrated in tailing ponds during oil sand processing and petroleum refining. Concentrations of NAs in natural water of Northern Alberta are typical below 1 mg/L. In OSPW, however, the concentration of NAs can reach up to 120 mg/L, which is enough to pose toxic effects to aquatic lives [5]. High concentration of NAs in OSPW also causes equipment corrosion during oil sand operation [6,7]. Consequently, NAs have become a very anxious problem due to their toxic effect leading to serious threats and hazards to the ecological system and human health. Due to the toxicity of NAs and increasingly strict regulations for environmental protection and saving the lives of aquatic, removal of NAs from wastewater is not only of increasing interest, but also a must [8].

During the last decade, researchers have put numerous efforts to develop suitable process and materials for better separation of toxic NAs from the waste solution generated in the oil sand processing. Among the traditional techniques, adsorption is by far the most effective and widely used technique for the removal of NAs from aqueous waste due to its simplicity, selectivity, and efficiency [9,10]. To date, extensive studies performed to investigate the adsorption process of organic acids relies largely on activated carbons and ion-exchange methods [9,10-13]. Conventional activated carbon has undoubtedly been

the most popular and widely used as an adsorbent to adsorb metal ions and organic molecules, and catalyst supports for the removal of pollutant species from gases or liquids [14-19] due to its large specific surface area, large pore volume, multiple type of reactive surface sites, high chemical stability, and easy of availability. Several studies have been performed to investigate the efficacy of activated carbon as adsorbents for NAs removal [13, 20-22]. Mohamed et al., (2010) found that the sorption capacity of granular activated carbon (GAC) for NAs was much greater than that of polymeric sorbents [6]. Wu et al., (2001) demonstrated enhanced adsorption of carboxylic acid-based surfactants with activated carbon adsorbent [23]. Martinez-Iglesias et al., (2015) demonstrated the applicability of commercial granular activated carbon (GAC) on adsorption of single and multicomponent model NAs [24].

Specific surface area and pore structure of carbon are important characteristics for adsorption performance. In addition, surface functionalization of carbon plays a crucial role for the adsorption of ionic species [25]. In general, carbon materials are of relatively inert nature. They also lack functional groups, and have poor surface wettability which impedes the penetration of adsorbate into the pores of carbons and limits their practical applications. Compared to common carbon materials, nitrogen functionalized mesoporous carbon has been considered a promising candidate for adsorption and removal of organic pollutants. For the adsorption processes, N-containing functional groups not only act as active adsorption sites by increasing the electrostatic interaction between the adsorbent and adsorbate, but also raise the surface wettability of the adsorbent and enhance the adsorption capacity [26, 27].

It is believed that the existence of nitrogen-containing functional groups on the surface of carbon materials provides basic properties and electron-donor affinity, which improves the removal of polar compounds such as organic acids, due to dipole-dipole interactions and H-bonding [15,16]. For instance, the adsorption performance of the surface modified AC and PAC towards model NAs was notably enhanced by surface amination with nitrogen containing functional groups [28]. Therefore, sustainable production of nitrogen grafted carbon materials with high specific surface area and appropriate pore distribution will be attractive for treatment of OSPW by adsorption-based methods.

Fabrication of nitrogen-containing carbon materials with high specific surface area and appropriate pore distribution from a cheap and green route, such as using biowastes as a precursor, is of significant interest. Taking this into consideration, the aim of this work is to explore the possibility of HFs derived carbons as adsorbents in the removal of NAs from aqueous solution, and evaluate the removal efficacy of the prepared carbon with that of commercial granular activated carbon. For this purpose, 2-naphthoic acid and benzoic acid were selected as a model compounds.

## 4.2. Experimental

### 4.2.1. Materials and Chemicals

Hemp fibers were supplied by American Hemp, Winston Salem, NC, USA. The obtained samples of hemp fibers were cut into smaller pieces by scissors. The collected pieces were thoroughly washed several times with de-ionized water to clean off the dirt, and dried in vacuum oven at 100°C for 24 h. The dried raw materials were then crushed and grinded in an electric grinder (CGOLDENWALL, model: DF-15 Grinder). N-aminoguanidine hydrochloride ( $\text{CH}_6\text{N}_4\cdot\text{HCl}$ ,  $\geq 98\%$  purity) and zinc chloride ( $\text{ZnCl}_2$ ,  $\geq 98\%$  purity) used in the present study were purchased from Sigma Aldrich, Canada and were used without further purification. The compounds 2-naphthoic acid (VWR international,  $\geq 98\%$  purity, chemical formula:  $\text{C}_{10}\text{H}_7\text{COOH}$ ,  $M_w$ : 172.18 g/mol,  $\lambda_{\text{max}} = 265$  nm) and benzoic acid (Alfa Aesar,  $\geq 99.5\%$ , chemical formula:  $\text{C}_6\text{H}_5\text{COOH}$ ,  $M_w$ : 122.12 g/mol,  $\lambda_{\text{max}} = 225$  nm) were used as the model adsorbates. The stock solutions (70 mg/L) of 2-naphthoic acid and benzoic acid were prepared individually by dissolving an appropriate quantity of model compound in de-ionized water. Working solutions of desired concentration were prepared by successive dilution.

### 4.2.2. Methods

#### 4.2.2.1. Preparation of hemp fibers-derived mesoporous carbons

Preparation of the mesoporous carbon HFC was carried out by carbonization of pretreated (cleaned and dried) hemp fibers using  $\text{ZnCl}_2$  activator as described in chapter 2, section 2.2.2.1. The carbon prepared at  $500^\circ\text{C}$  carbonization temperature and ratio of  $\text{ZnCl}_2$  to HFs is 2:1 was used in this study for adsorption process. The nitrogen-containing carbon, named N-HFC, was prepared by nitrogen functionalization of pretreated hemp fibers followed by carbonization as described in chapter 3 of section 3.2.2.1.

#### 4.2.2.2. Batch adsorption experiments

Batch adsorption experiments were performed to study the effect of parameters such as adsorbent dose, initial concentration, contact time, and solution pH for the removal of model NAs with HFC and N-HFC. In a typical experiment, definite volume of test solutions containing known concentration of model NAs was mixed with pre-weighed adsorbent in 50 mL of Erlenmeyer flasks, and the samples were shaken in a orbital shaker at 200 rpm under ambient temperature conditions until the equilibrium time was reached.

To evaluate the effect of adsorbent dose on adsorption of model NAs, different amounts of adsorbent varying from 0.005 to 0.02 g were added into the adsorbate solutions of initial concentration of 40 mg/L, and the mixtures were shaken in a shaker at 200 rpm for 24 hrs. In experiments conducted to study the effect of initial concentration, the solutions of known initial concentrations (40-70 mg/L) were mixed with 0.01 g or 0.02 of adsorbent, and the mixture was shaken for 48 h at ambient conditions. In this case, the solutions of model NAs were used without any pH adjustment (pH of the solutions was nearly 4.4).

After adsorption, the mixture was filtered immediately with  $0.45\ \mu\text{m}$  nylon syringe and the concentrations of model NAs in the filtrates were measured by a UV-vis spectrophotometer (UV-3600, Shimadzu) at  $\lambda_{\text{max}}$  of 265 and 225 nm, respectively for 2-naphthoic acid and benzoic acid. Triplicate sets were carried out for each adsorption experiment, and the average values of three results were taken into consideration.

From the measured initial ( $C_i$ ) and equilibrium ( $C$ ) concentrations, percentage of the adsorbate (model NAs) adsorbed on the adsorbent were calculated according to the relation,

$$\% \text{ Adsorption} = \frac{C_i - C}{C_i} \times 100 \dots\dots\dots[4.1]$$

where  $C_i$  and  $C$  are the NAs concentration in the test solution, before and after adsorption (mg/L), respectively.

The adsorption kinetics tests were carried out to find the optimum time required to attain the equilibrium of adsorption of model NAs on HFs-derived carbon materials. For this, 50 mg (0.05 g) of adsorbent was shaken with 100 ml solution of 40 mg/L initial concentration of model NAs prepared in de-ionized water. Definite volume (5 mL) of the shaking mixture was sampled at different time intervals for the analysis of residual concentration of NAs in the solution. From the measured initial concentration and the concentration at any time,  $t$ , the amount of model NA adsorbed,  $q_t$ , was calculated by using the following relation,

$$q_t = \frac{C_i - C_t}{W} \times V \dots\dots\dots[4.2]$$

where,  $C_i$  and  $C_t$  are the initial and remaining NAs concentrations at any time  $t$  (mg/L), respectively,  $W$  is the weight of the adsorbent (g) and  $V$  is the volume of the test solution (L).

#### 4.2.2.3. Control experiment

A control/blank experiment was performed in which the mixture of adsorbent and de-ionized water was shaken under the same conditions as the test experiment, and the filtrate of this blank experiment was subjected to UV-vis measurement to see if any organic matter present in activated carbons will be leached out into the solution and interfere with the UV-vis measurement. The filtrate of control experiment displayed no

UV-vis absorption signal/peak inferring that no organic material was leached out from the adsorbent that interferes with analysis of 2-naphthoic acid and benzoic acid.

### 4.3. Results and Discussions

#### 4.3.1. Effect of adsorbent dose on adsorption of model NAs

The effect of adsorbent dose on percentage adsorption of 2-naphthoic acid and benzoic acid from synthetic aqueous solutions (pH 4.4) on HFC and N-HFC, was studied at different adsorbent doses (5-20 mg/10 mL) using model NA solutions of 40 mg/L initial concentrations. The result shown in Figures 4.1a and b indicate that N-HFC is more effective than HFC for adsorption of both the model compounds.

For adsorption of 2-naphthoic acid, quantitative adsorption was achieved with N-HFC at adsorbent dose of as low as 0.5 mg/mL whereas HFC needed an adsorbent dosage of 1.5 mg/mL to achieve quantitative adsorption. This remarkable efficiency of N-HFC compared to HFC is attributable to the presence of nitrogen functionality which, at pH 4.4, is converted to positively charged centers and electrostatic interactions are in play for adsorption of naphthoic acid in their dissociated (anionic) form.

For benzoic acid adsorbate, initially the percentage of adsorption increased rapidly with increase in adsorbent dose for both the adsorbents. This may happen due to increased surface area of adsorption and enhanced number of adsorption active sites with an increase in amount of adsorbent [29, 30]. Saturation of N-HFC with 95% adsorption of benzoic acid occurred at an adsorbent dose of 1.5 mg/mL, and 82% adsorption of benzoic acid on HFC was achieved at an adsorbent dose of 2 mg/mL. The superior performance of N-HFC compared to HFC is likely due to the presence of positively charged kernels in N-HFC at pH 4.4 which contribute to adsorption of anionic species of benzoic acid.

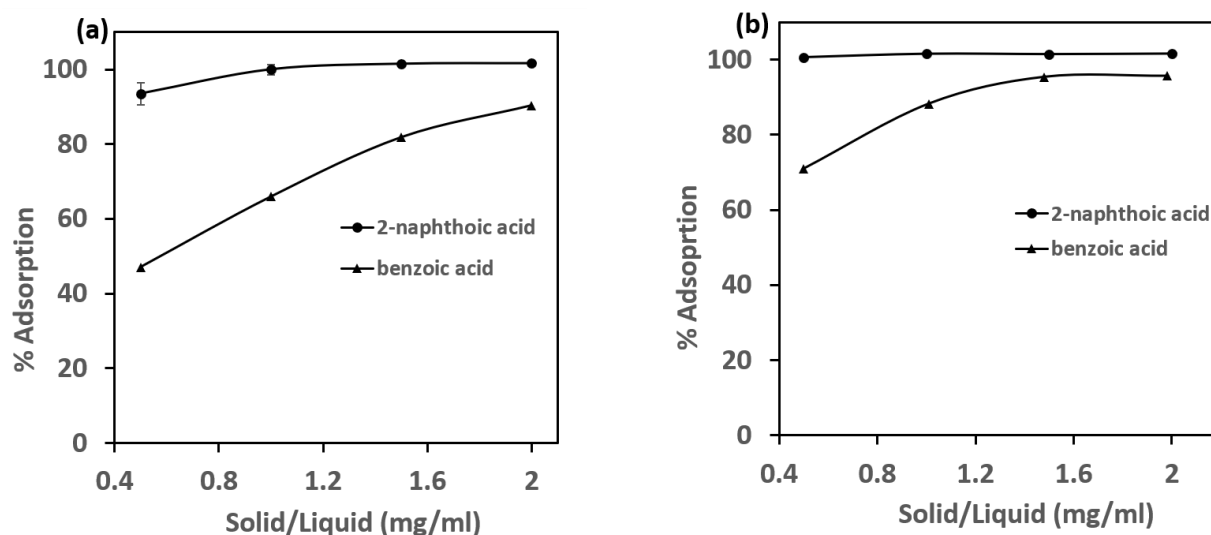


**Figure 4.1. Effect of adsorbent dose for removal of 2-naphthoic acid and benzoic acid from aqueous solution at pH 4.4 with (a) HFC and (b) N-HFC. Initial concentration of model NAs = 40 mg/L, volume of test solution = 10 mL, shaking time = 48 h, temperature =  $25 \pm 2^\circ\text{C}$ , shaking speed = 200 rpm.**

#### 4.3.2. Adsorption efficiency in various initial concentrations of adsorbate

Figures 4.2a and b illustrate the efficiency of the adsorbents for adsorption of 2-naphthoic acid and benzoic acid from aqueous solutions of varying initial concentration. Both the adsorbents demonstrated remarkable efficiency for adsorption of 2-naphthoic acid over a wide range of concentrations ranging from 40 to 70 mg/L. The results of figure 4.2b further suggest that N-HFC also holds appreciable efficiency for removal (with near quantitative adsorption) of benzoic acid in the initial concentration range of 40 to 70 mg/L. The HFC, on the other hand, was effective only for removal of nearly 80% benzoic acid from solutions of 50 to 70 mg/L concentrations. This indicates that nitrogen functionality on carbon surfaces enhanced adsorption of model naphthenic acids under weakly acidic condition (pH 4.4).

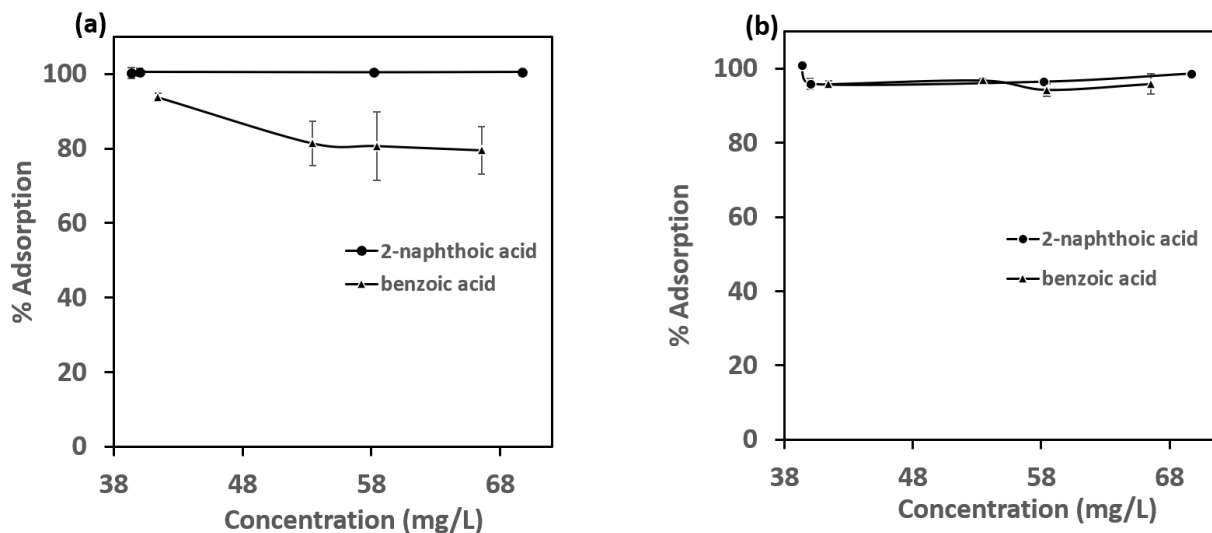


**Figure 4.2. Adsorption efficiency of (a) HFC and (b) N-HFC with varying initial concentrations of model NAs. Initial concentration of NAs = 40 to 70 mg/L, volume of test solution = 10 mL, wt. of adsorbent = 10 mg for adsorption of 2-naphthoic acid and 20 mg for adsorption of benzoic acid, shaking time = 48 h, temperature =  $25 \pm 2^\circ\text{C}$ , shaking speed = 200 rpm.**

### 4.3.3. Adsorption isotherm

The adsorption isotherm (adsorption capacity) of HFC and N-HFC towards 2-naphthoic acid and benzoic acid was evaluated in terms of adsorption isotherm. Figure 4.3(a) shows the adsorption isotherm of 2-naphthoic acid and benzoic acid on HFC, and figure 4.3(b) shows the adsorption isotherm of 2-naphthoic acid and benzoic acid on N-HFC. The amount of adsorption of 2-naphthoic acid and benzoic acid on both the adsorbents increases with increasing concentration of adsorbate solution, and tends to approach a plateau in higher concentration. The maximum adsorption capacity of HFC was evaluated as 70 and 27 mg/g for 2-naphthoic acid and benzoic acid, respectively. Likewise, the maximum adsorption capacity of N-HFC for 2-naphthoic acid and benzoic acid was found to be 71 and 33 mg/g. It must, however, be noted that as the solubility of 2-naphthoic acid and benzoic acid posed problems for preparing the adsorbate solutions of more than 70 ppm, these experiments were conducted using up to 70 ppm solutions.

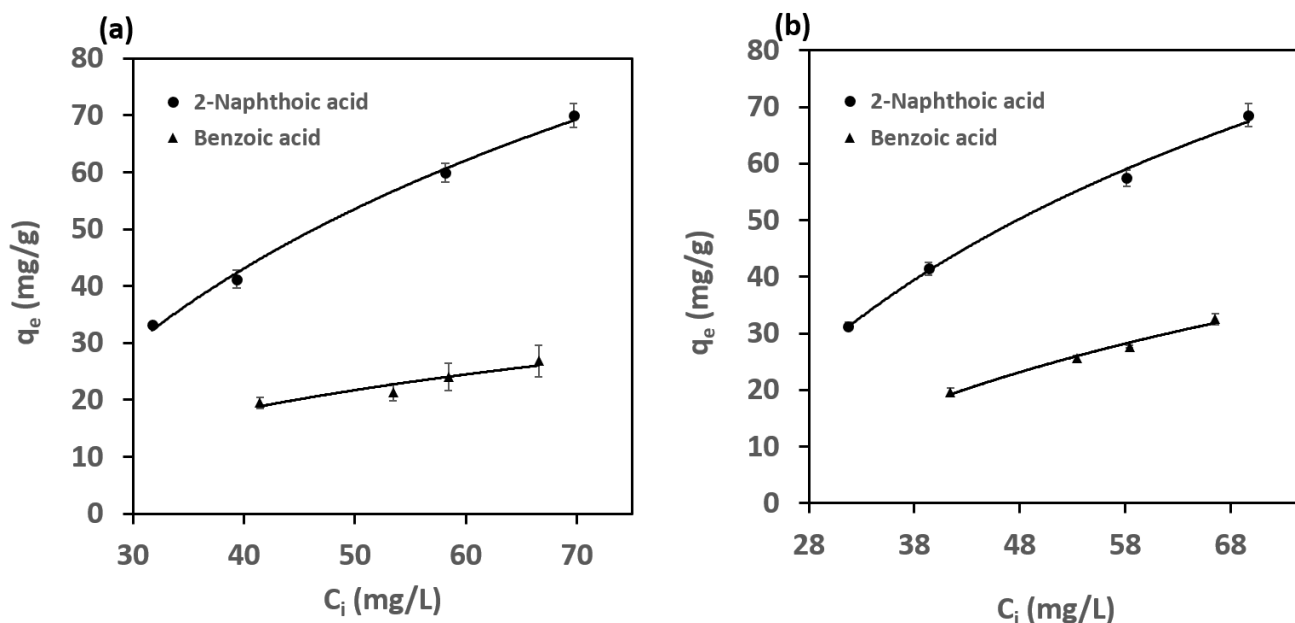


**Figure 4.3.** Adsorption isotherm of (a) HFC and (b) N-HFC with varying initial concentrations of model NAs. Initial concentration of NAs = 40 to 70 mg/L, volume of test solution = 10 mL, wt. of adsorbent = 10 mg for adsorption of 2-naphthoic acid and 20 mg for adsorption of benzoic acid, shaking time = 48 h, temperature =  $25 \pm 2^\circ\text{C}$ , shaking speed = 200 rpm.

#### 4.3.4. Adsorption kinetics

Investigation of adsorption kinetics allows the evaluation of adsorbent's performance and gives insight into the underlying mechanisms of adsorption. The time dependence of adsorption of 2-naphthoic acid and benzoic acid on HFC and N-HFC was studied with adsorbate concentration of 70 mg/L at pH 4.4. As shown in Figures 4.4a and c, the adsorption rate of 2-naphthoic acid on both the adsorbents was quick, and more than 95% adsorption was achieved within 10 minutes of contact time. Equilibrium of adsorption of 2-naphthoic acid was achieved in 30 minutes for N-HFC (Figure 4.4c), and in 1 h for HFC (Figure 4.4a). As evident from the Figures 4.4a and c, adsorption of benzoic acid on N-HFC was remarkably faster than on HFC at initial stage of adsorption, which resulted in better adsorption efficiency of N-HFC over HFC for adsorption of benzoic acid. The notable fast kinetics of adsorption of these model compounds on N-HFC reflects the great

potentiality of hemp derived porous carbon materials for adsorptive removal of NAs from contaminated natural water and from aqueous environment at weakly acidic conditions.

Figures 4.4b and d illustrate the amount of model NAs adsorbed on HFC and N-HFC, respectively. In both cases, initial adsorption was higher for 2-naphthoic acid than that of benzoic acid. This indicated remarkably higher affinity/selectivity of the adsorbents for 2-naphthoic acid over benzoic acid, which is more pronounced for HFC (Figure 4.4b). Regardless of the initial adsorption selectivity, progressive adsorption of model NAs led to saturation of the adsorbents when approached equilibrium (indicated by plateau state in Figure 4.4b and d). The progressive increase in adsorption and consequent attainment of equilibrium of adsorption is due to progressive mass transfer of the adsorbate molecules from the bulk liquid to the surface of the adsorbent followed by saturation of adsorption sites and limited internal mass transfer within the adsorbent. The plots of time vs  $qt$  (Figure 4.4b and d) are smooth and continuous towards saturation, indicating the formation of monolayer coverage of adsorbate molecules on carbon surface [28].

Under the experimental conditions (specified in figure legend), the adsorption capacity of both the carbon materials for NAs increased gradually with extending time. In 240 minutes, the adsorption capacity of HFC reached 116 mg/g for 2-naphthoic acid and 105 mg/g for benzoic acid, respectively. Similarly, the adsorption capacity of N-HFC for 2-naphthoic acid and benzoic acid were 118 mg/g and 118 mg/g, respectively.

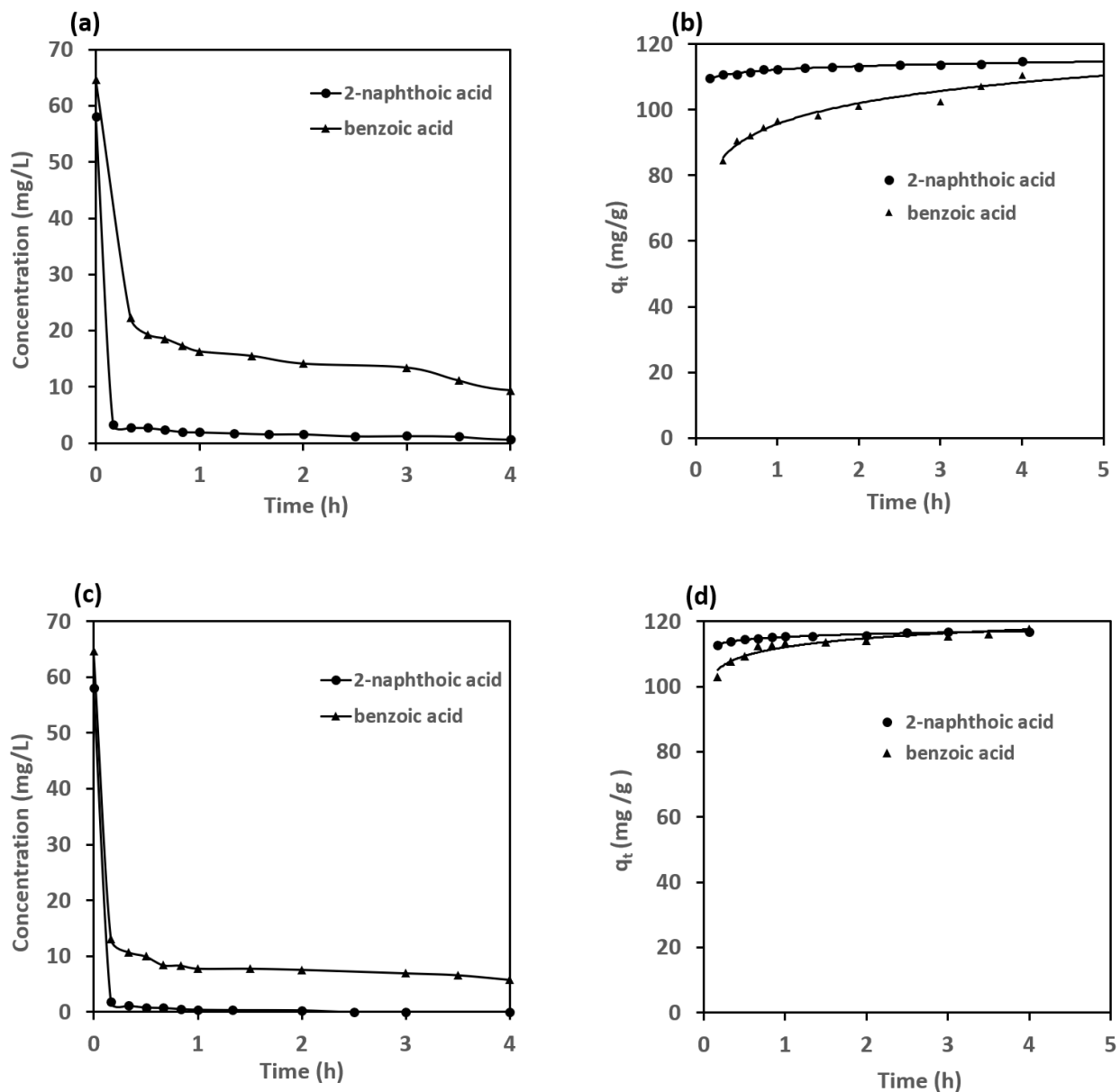


**Figure 4.4. Adsorption of 2-naphthoic acid and benzoic acid as a function of contact time on HFC (a and b) and N-HFC (c and d). Volume of test solution = 100 mL, weight of adsorbent = 50 mg, shaking speed = 200 rpm, temperature =  $25 \pm 2^\circ\text{C}$ , pH of model NA solutions = 4.4.**

The rates of adsorption of model NAs on both the carbon materials were analyzed in terms of the pseudo-first-order as well as pseudo-second-order kinetic models. The

Lagergren equations for pseudo-first-order and pseudo-second order equations are described as follows:

$$\log(q_e - q_t) = \log q_e - \frac{k_1}{2.303} t \dots\dots\dots [4.3a]$$

Or

$$\ln\left(1 - \frac{q_t}{q_e}\right) = -k_1 t \dots\dots\dots [4.3b] \text{ (for pseudo-first-order)}$$

And,

$$\frac{t}{q_t} = \frac{1}{q_e} t + \frac{1}{k_2 q_e^2} \dots\dots\dots [4.4] \text{ (for pseudo-second}$$

order)

In these equations,  $q_e$  and  $q_t$  are the amount of adsorbed model NAs at equilibrium and any time, respectively, and  $k_1$  ( $\text{h}^{-1}$ ) and  $k_2$  ( $\text{kg mol}^{-1}\text{h}^{-1}$ ) are the pseudo-first-order and pseudo-second-order rate constants.

According to the above equations, the fitting of these models can be checked by linear plot of  $\ln\{1 - (q_t/q_e)\}$  vs  $t$  for pseudo-first-order, and the plot of  $t/q_t$  vs  $t$  for pseudo-second-order reactions, respectively. Figures 4.5a and b show the plots fitted for the two kinetic models for adsorption of model NAs on HFC, and figures 4.6a and b show the plots fitted for the two kinetic models for adsorption of model NAs on N-HFC. The linearity of the plots and the correlation coefficient ( $R^2 = 1$ ) showed that the pseudo-second-order model, an indication of a chemisorption mechanism, fits better with the experimental data than the pseudo-first-order model (though the plots were linear,  $R^2$  was in the range of 0.86-0.95).

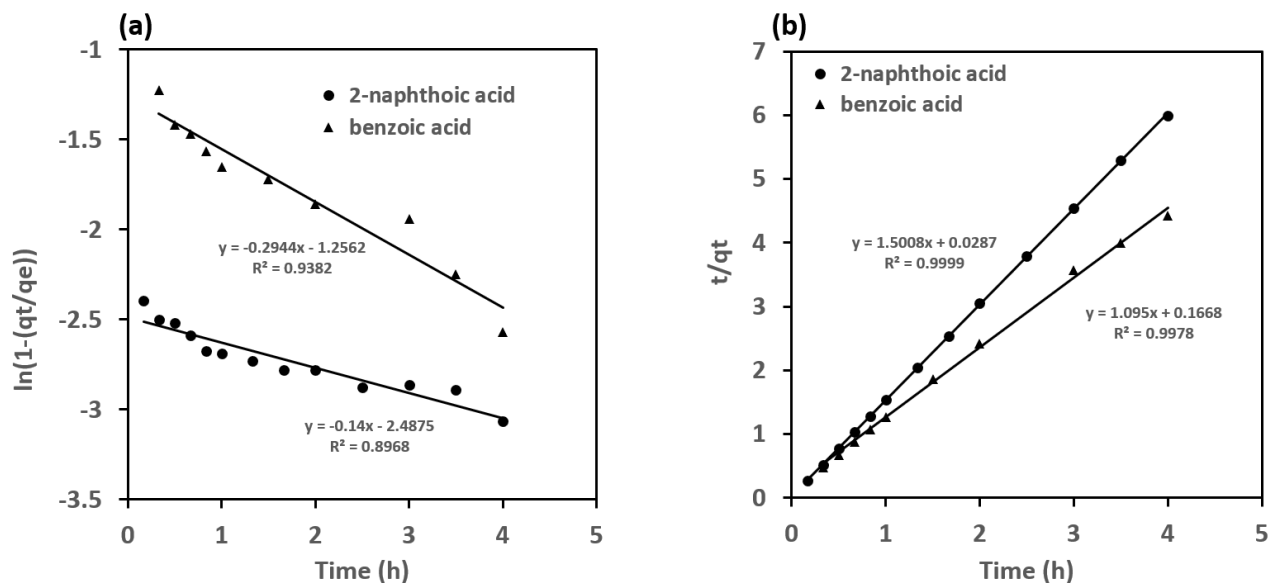


Figure 4.5. Fitting of kinetic data of adsorption of 2-naphthoic acid and benzoic acid on HFC according to (a) pseudo-first-order kinetic model and (b) pseudo-second-order kinetic model.

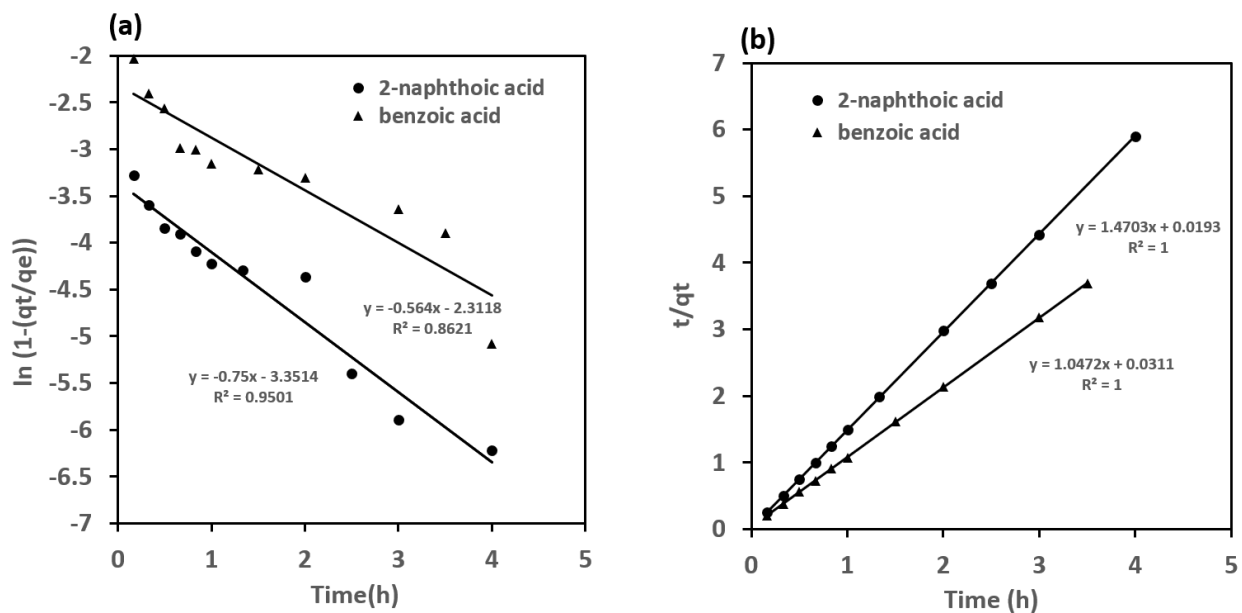


Figure 4.6. Fitting of kinetic data of adsorption of 2-naphthoic acid and benzoic acid on N-HFC according to (a) pseudo-first-order kinetic model and (b) pseudo-second-order kinetic model.

The pseudo-first-order rate constant ( $k_1$ ) for adsorption of model NAs on HFC and N-HFC were calculated from the values of slopes of straight lines of Figures 4.5a and 4.6a, and pseudo-second-order rate constant ( $k_2$ ) were evaluated from the values of intercepts of the straight lines in Figures 4.5b and 4.6b, respectively. The correlation coefficients and rate constants,  $k_1$  and  $k_2$ , evaluated according to these two models are listed in Tables 4.1 and 4.2.

**Table 4.1. Evaluated pseudo-first-order and pseudo-second-order rate constants and correlation coefficient for the adsorption of 2-naphthoic acid and benzoic acid on HFC.**

Model NAs	Pseudo-first-order		Pseudo-second-order	
	$k_1$ (h <sup>-1</sup> )	R <sup>2</sup>	$k_2$ (kg mol <sup>-1</sup> .h <sup>-1</sup> )	R <sup>2</sup>
2-naphthoic acid	0.32	0.89	78.5	0.99
Benzoic acid	0.68	0.93	7.19	0.99

**Table 4.2. Evaluated pseudo-first-order and pseudo-second-order rate constants and correlation coefficient for the adsorption of 2-naphthoic acid and benzoic acid on N-HFC.**

Model NAs	Pseudo-first-order		Pseudo-second-order	
	$k_1$ (h <sup>-1</sup> )	R <sup>2</sup>	$k_2$ (kg mol <sup>-1</sup> .h <sup>-1</sup> )	R <sup>2</sup>
2-naphthoic acid	1.72	0.95	112	1
Benzoic acid	1.30	0.86	35.3	1

Table 4.3 compares the adsorption kinetics and adsorption capacity of present hemp-derived carbon materials with various carbon-based adsorbents reported in the literature for adsorption of model NAs. From this table, it is evident that the carbon adsorbent

prepared from hemp fibers exhibit faster adsorption kinetics than other carbon-based adsorbents.

**Table 4:3 Comparative studies of hemp-derived materials with various kinds of other adsorbents for model NAs reported in the literatures.**

<b>Carbon precursors</b>	<b>Model NAs</b>	<b>Adsorption equilibrium (h)</b>	<b>Adsorption capacity (mg/g)</b>	<b>Ref.</b>
GAC	(2-napthoic acid, diphenylacetic acid, 1,4-cyclohexane dicarboxylic acid)	48	358, 318, 453	[24]
Sawdust AC	(Commercial, technical grade naphthenic acid)	-	20-30	[21]
PAC	(2-napthoic acid, diphenylacetic acid, 1,4-cyclohexane dicarboxylic acid)	48	776, 624, 566	[28]
PAC-NH <sub>2</sub>	(2-napthoic acid, diphenylacetic acid, 1,4-cyclohexane dicarboxylic acid)	48	545, 450, 390	[28]

PAC-NH <sub>3</sub>	(2-napthoic acid, diphenylacetic acid, 1,4-cyclohexane dicarboxylic acid)	48	693, 600, 601	[28]
CX	Heptanoic acid (HPA), 5-cyclohexane pentanoic acid (CHPA), 5-phenylvaleric acid (PVA)	24	65, 61, 87	[32]
<i>Umbaúba</i> - Wood	n-dodecanoic carboxylic acid			
Charcoal		6	1.1	[33]
B-CD	OSPW		0-75	[6]
Ion-exchange Resins	Technical grade naphthenic acid			
		-	0.3-0.9	[11]
<b>HFC</b>	(2-napthoic acid, benzoic acid)	1	70, 27	This work
<b>N-HFC</b>	(2-napthoic acid, benzoic acid)	0.5	71, 33	This work

---

#### 4.3.5. Effect of solution pH on adsorption of model NAs

The initial pH of the solution is expected to significantly affect the adsorption behavior as the solution pH affects properties such as surface charge of the adsorbents and extent of dissociation of model NAs. Since the pH of the OSPW is in the range of 8.0 to 8.5, the adsorption experiments were conducted using model NA solutions whose pH was adjusted to 8.5. The purpose of evaluating the adsorption performance of HFs derived carbon products with model solutions of pH 8.5 was to explore how these adsorbents will likely behave with the ionized acidic components of real time OSPW. The adsorption behavior of 2-naphthoic acid and benzoic acid on HFC and N-HFC towards at pH 8.5 are shown in Figures 4.7a and b, respectively. It is obvious from the results of Figure 4.7a that both the carbon materials have quantitative adsorption affinity towards 2-naphthoic acid from the solutions of varying concentrations in the range of 40 to 70 mg/L at pH 8.5. For adsorption of benzoic acid, N-HFC demonstrated remarkably higher efficiency than HFC. It is believed that the combination of hydrophobic and van der Waals interactions as well as ionic interactions are in place. As the model acids are negatively charged and the surface of HFC also becomes negatively charged at pH 8.5, electrostatic repulsion likely playing a substantial role in the case of adsorption of benzoic acid on HFC, thus resulting in moderate adsorption.

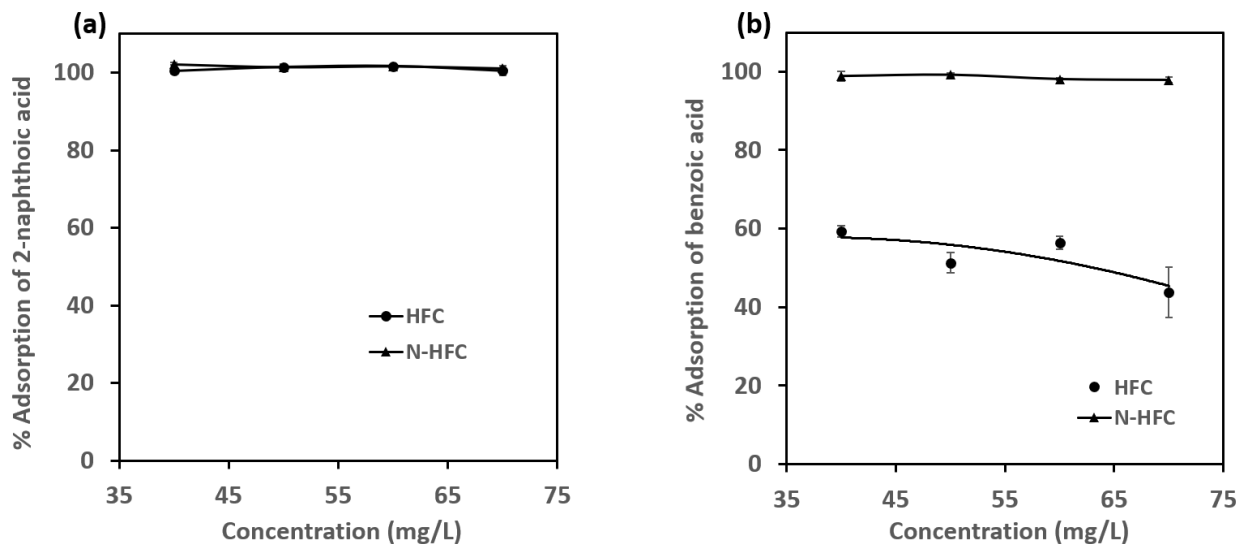


**Figure 4.7. Adsorption of model NAs at pH 8.5 on HF-derived carbon adsorbents.**

**Adsorption of (a) 2-naphthoic acid and (b) benzoic acid on HFC and N-HFC.**

**Weight of adsorbent = 10 mg (for adsorption 2-naphthoic acid) and 20 mg (for adsorption benzoic acid), volume of test solution = 10 mL, shaking time = 48 h, temperature =  $25 \pm 2$  °C, shaking speed = 200 rpm.**

#### 4.3.6. Comparison of adsorption performance

Figure 4.8 compares the adsorption efficiency of HFC, N-HFC, HFs without activation (HFC-0-500), and a commercial granular activated carbon towards the model NAs at weakly acidic and weakly basic conditions. Both HFC and N-HFC demonstrated significantly higher adsorption efficiency over HFs without activation, and N-HFC demonstrated superior performance over commercial activated carbon (Figure 4.8a and b).

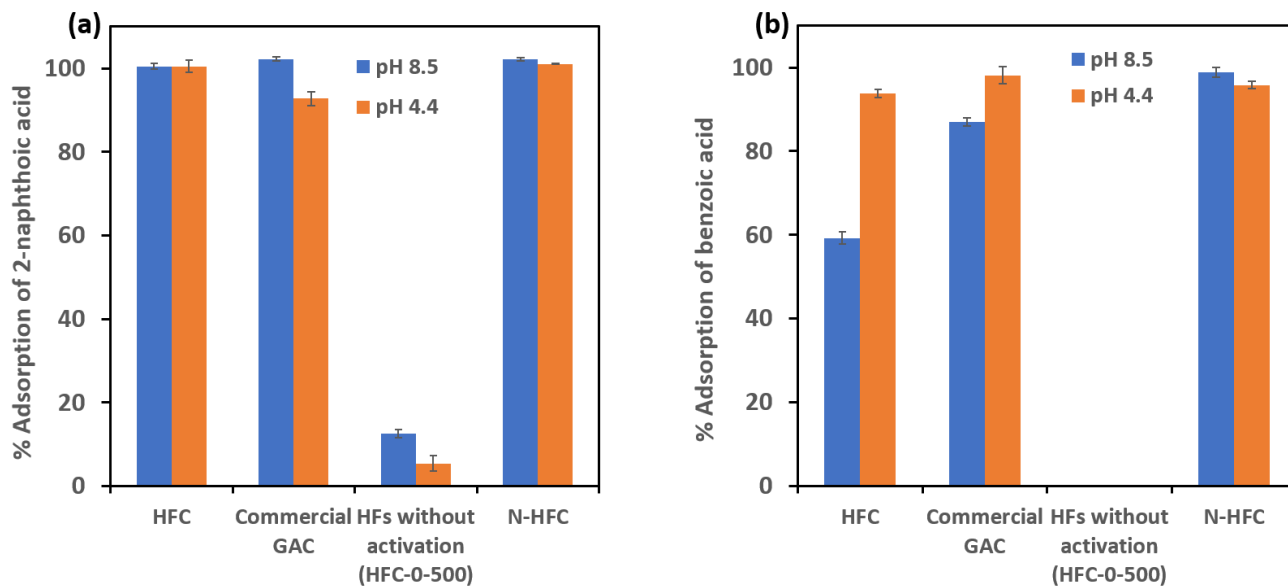


**Figure 4.8. Comparison of adsorption performance of hemp-derived carbon materials and commercial activated carbon for adsorption of (a) 2-naphthoic acid, and (b) benzoic acid. Weight of adsorbent = 10 (for 2-naphthoic acid adsorption experiments) and 20 mg (for benzoic acid adsorption experiments), volume of test solution = 10 mL, initial concentration of NAs = 40 mg/L, shaking time = 48 h, temperature =  $25 \pm 2^\circ\text{C}$ , shaking speed = 200 rpm, pH of the solution = 4.4 or 8.5.**

#### 4.3.7. Proposed adsorption mechanism

Usually several non-covalent interactions are involved in the adsorption of organic compounds on the surface of carbonaceous adsorbents. Some of the most important interactions are the interactions between the aromatic ring of organic molecules and the  $\pi$  electrons of graphenes (of carbon having certain extent of graphitic structure), electron donor-acceptor interactions between the aromatic ring and the non-acidic surface sites, electrostatic attractive or repulsive interactions between the charged carbon surface and the ions in the solution [25]. In cases where the adsorbent possesses charged centers, electrostatic interactions are likely the pre-dominant forces that control the adsorption phenomenon. For instance, the nitrogen atoms of N-HFC are converted to positively charged centers in a wide pH range (from acidic to weakly basic), and adsorption of

negatively charged species (such as the anionic species of model NAs) is very likely controlled by electrostatic interactions.

As evident from the results of adsorption kinetics, adsorption of the model NAs likely proceeded through pseudo-second-order phenomenon, suggesting that the adsorption process is very likely controlled by chemical adsorption involving sharing or exchanging electrons between adsorbent and adsorbate. At low pH, all model NAs would remain mostly un-dissociated, thus adsorption of NAs likely occurs mainly due to van der Waals forces, hydrophobic interactions, and hydrogen bonding [24,28]. The aromatic ring presents in NAs is also expected to enable these compounds to be adsorbed more easily onto carbon materials by van der Waals forces.

#### 4.4. Conclusions

The experiments conducted and the obtained results clearly demonstrated that hemp-derived mesoporous carbonaceous materials are highly effective to adsorb persistent and toxic organic contaminants from acidic as well as basic aquatic environments, and these adsorbents have comparable or superior efficiency when compared to the high cost commercially available granulated carbon (GAC). The salient features of HFC and N-HFC materials, like possessing hierarchical pore structure, large specific surface area, and abundant surface nitrogen-containing functional groups should be responsible for their excellent adsorption capacity. The adsorption reached equilibrium within 1 h under the experimental conditions, which is a notable efficacy of these materials for removal of naphthenic acids and naphthenic acid-like organic pollutants from contaminated aqueous streams. The kinetic analysis provided a cue that chemisorption was involved in the adsorption of model NAs, and adsorbents consisting of positively charged centers are highly suitable for targeted removal of NAs from slightly acidic to slightly basic environments. From the results, it is concluded that the HFs derived porous carbons, because of its high adsorption capacity, fast adsorption rate, as well as the nature of natural and low cost, can be expected to be used to preconcentrate and separate NAs from aqueous environment.

## 4.5. References

- [1] J. V. Headley, K. M. Peru, M. H. Mohamed, L. Wilson, D. W. McMartin, M. M. Mapolelo, V. V. Lobodin, R. P. Rodgers, and A. G. Marshall, Atmospheric pressure photoionization fourier transform ion cyclotron resonance mass spectrometry characterization of tunable carbohydrate-based materials for sorption of oil sands naphthenic acids. *Energy and Fuels* 2013(28)1611-1616.
- [2] J. V. Headley, K. M. Peru, B. Fahlman, A. Colodey, and D. W. McMartin, Selective solvent extraction and characterization of the acid extractable fraction of Athabasca oils sands process waters by orbitrap mass spectrometry. *Int. J. Mass Spectrom.* 2013(345)104-108.
- 3] E. W. Allen, Process water treatment in Canada's oil sands industry: I. Target pollutants and treatment objectives. *J. Environ. Eng. Sci.* 2008(7)123–138.
- 4] J. Brient, P. Wessnet, and M. Doyler, 1995. Naphthenic acids- Kirk-Othmer encyclopedia of chemical technology. John Wiley and Sons, New York: 1017-1029.
- 5] E. Allen, Process water treatment in Canada's oil sands industry: II. A review of emerging technologies. *J. Environ. Eng. Sci.* 2008b (7)499-524.
- 6] M. H. Mohamed, L. D. Wilson, J. V Headley, K. M. Peru, Sequestration of naphthenic acids from aqueous solution using  $\beta$ -cyclodextrin-based polyurethanes. *Phys. Chem. Chem. Phys.* 2011(13)1112–1122.
- 7] P. J. Quinlan, K. C. Tam, Water treatment technologies for the remediation of naphthenic acids in oil sands process-affected water. *Chem. Eng. J.* 2015(279)696–714.
- 8] A. C. Scott, W. Zubot, M. D. Mackinnon, D.W. Smith, and P.M. Fedorak, Ozonation of oil sands process water removes naphthenic acids and toxicity. *Chemosphere* 2008(71)156-160.

- 9] W. Zubot, M. D. MacKinnon, P. Chelme-Ayala, D. W. Smith, M. Gamal El-Din, Petroleum coke adsorption as a water management option for oil sands process affected water. *Sci. Total Environ.* 2012(427–428)364–72.
- 10] M. Gamal El-Din, H. Fu, N. Wang, P. Chelme-Ayala, L. Pérez-Estrada, P. Drzewicz, J. W. Martin, W. Zubot, D. W. Smith, Naphthenic acids speciation and removal during petroleum-coke adsorption and ozonation of oil sands process-affected water. *Sci. Total Environ.* 2011(409)5119–25.
- [11] V. G. Gaikar, D. Maiti, Adsorptive recovery of naphthenic acids using ion-exchange resins. *React. Function. Polym.* 1996(31)155-164.
- [12] B. Sarkar, Adsorption of single-ring model naphthenic acid from oil sands tailings pond water using petroleum coke-derived activated carbon, MSc. Thesis, University of Toronto, Ontario, Canada, 2013.
- [13] I. Md Shahinoor, N. M. Kerry, A. M. Selamawit, L. Yang, Isotherm and kinetic studies on adsorption of oil sands process-affected water organic compounds using granular activated carbon. *Chemosphere* 2018(202)715-725.
- 14] K. N. Aboua, Y. A. Yobeuet, K. B. Yao, D. L. Goné, A. Trokourey, Investigation of dye adsorption onto activated carbon from the shells of Macoré fruit. *J. Environ. Manag.* 2015(156)10–14.
- 15] B. Niu, F. Lu, H.-Y. Zhang, Y. Zhang, J. Zhao, Synthesis of nitriles from aerobic oxidation of amines catalyzed by ruthenium supported on activated carbon. *Bull. Chem. Soc. Jpn.* 2017(46)330–333.
- 16] E. H. Mohan, S. Anandan, B.V.A. Rao, T. N. Rao, Neem leaf-derived micro and mesoporous carbon as an efficient polysulfide inhibitor for sulfid cathode in a Li-S battery. *Bull. Chem. Soc. Jpn.* 2019(48)62–64.
- 17] B. Li, H. Zhang, D. Wang, H. Lv, C. Zhang, Agricultural waste-derived activated carbon for high performance lithium-ion capacitors. *RSC Adv.* 2017(7)37923–37928.

- 18] Y. Shu, A. Dobashi, C. Li, Y. Shen, H. Uyama, Hierarchical porous carbon from greening plant shell for electric double-layer capacitor application. *Bull. Chem. Soc. Jpn.* 2017(90)44–51.
- 19] Y. Shu, J. Maruyama, S. Iwasaki, Y. Shen, H. Uyama, Activated carbon monolith derived from *Amygdalus pedunculata* shell and polyacrylonitrile for supercapacitors. *Bull. Chem. Soc. Jpn.* 2017(90)1333–1336.
- 20] Z. Barnard, Conversion of petroleum coke to activated carbon and its application to naphthenic acid removal from tailings pond water. M.Sc. Thesis, University of Alberta, Edmonton, Alberta, Canada, 2011.
- 21] S. Iranmanesh, T. Harding, J. Abedi, F. S-Azad, D. B. Layzell, Adsorption of naphthenic acids on high surface area activated carbons. *J. Environ. Sci. Health, Part A* 2014(49)913-922.
- 22] C. Small, A. Ulrich, Z. Hashisho, Adsorption of acid extractable oil sands tailings organics onto raw and activated oil sands coke. *J. Environ. Eng.* 2012(138)833-840.
- [23] S. H. Wu, P. Pendleton, Adsorption of anionic surfactant by activated carbon: effect of surface chemistry, ionic strength, and hydrophobicity. *J. Colloid Interf. Sci.* 2001(243)306-315.
- [24] A. Martinez-Iglesias, H. S. Niasar, C. Xu, M. B. Ray, Adsorption of model naphthenic acids in water with granular activated carbon. *Adsorpt. Sci. Technol.* 2015(33)881-893.
- [25] R. C. Bansal, M. Goyal, *Activated Carbon Adsorption*. Taylor & Francis, 2005.
- [26] F. W. Shaarani, B. H. Hameed, Ammonia modified activated carbon for the adsorption of 2,4-dichlorophenol, *Chem. Eng. J.* 169(2011)180-185.
- [27] Z. Zhang, M. Xu, H. Wang, Z. Li, Enhancement of CO<sub>2</sub> adsorption on high surface area activated carbon modified by N<sub>2</sub>, H<sub>2</sub> and ammonia. *Chem. Eng. J.* 2010(160)571-577.

- [28] H. S. Niasar, H. Li, T. V. R. Kasanneni, M. B. Ray, C. Xu, Surface amination of activated carbon and petroleum coke for the removal of naphthenic acids and treatment of oil sands process-affected water (OSPW). *Chem. Eng. J.* 193(2016)189-199.
- [29] Z. A. Zakaria, M. Suratman, N. Mohammed, W.A. Ahmad, Chromium (VI) removal from aqueous solution by untreated rubber wood saw dust. *Desalination* 2009(244)109-121.
- [30] V. K. Garg, R. Gupta, A. B. Yadav, R. Kumar, Dye removal from aqueous solution by adsorption on treated sawdust. *Bioresour. Technol.* 2003(89)121-124.
- [32] Y. Rashed, S. A. Messele, H. Zeng, M. G. Ei-Din, Mesoporous carbon xerogel material for the adsorption of model naphthenic acids: structure effect and kinetics modelling. *Environ. Technol.* <https://doi.org/10.1080/09593330.2019.1615130>
- [33] N. F Campos, C. MBM Barbosa, J. M Rodríguez-Díaz, M. MMB Duarte, Removal of naphthenic acids using activated charcoal: Kinetic and equilibrium studies. *Adsorp Sci. Technol.* 2018(36)1405-1421.

## Chapter 5

# Collaboration with Industry Partner: Characterization of Supplied Hydrothermal Carbon (HTC) and Production of Activated Carbon from HTC

### Abstract

This chapter describes the methods/methodologies and results of characterization of hydrothermal carbon (HTC) provided by Sarnia-based industry partner. The supplied HTCs were humins derived from acid-catalyzed conversion of biomass residues. The provided materials were obtained from southern pine, blend of corn starch and southern pine, and coffee mill ground, and were named as S17, S97 and S2015, respectively. The as received HTC samples S17 and S97 were converted to calcined carbon by calcination at different carbonization temperatures (400, 450, 500, 550, and 1000°C) under N<sub>2</sub> atmosphere. The S17 and S97 HTC samples were also heated at 1000°C in presence of air to burn off the combustibles for ash analysis. The provided HTC samples as well as the calcined carbon samples prepared at 1000°C were characterized through the analysis of BET (Brunauer-Emmett-Teller) surface area, XRD (X-Ray Diffraction) and Raman scattering. The qualitative and quantitative analysis of amorphous silica, crystalline silica, and polymorphs of crystalline silica in the ash was carried out using SEM-EDX (low angle backscattered electrons imaging). The silica content of the ash was also analyzed with ICP-MS analysis. The organic solvent-soluble components of all three HTC samples were extracted by Soxhlet extraction with THF, acetone, and ethyl acetate at refluxing condition. Among the three solvents, THF extracted the larger amounts of soluble components. Molecular weight and dispersity ( $\mathcal{D}$ ) of the components soluble in THF fraction were analyzed using gel permeation chromatography (GPC).

### *Keywords*

HTC, Humins, Carbonization temperatures, Crystalline silica, Soxhlet extraction, Gel permeation chromatography

## 5.1. Introduction

Developing advanced carbonaceous materials from processed biomass is of interest for integration into a variety of high-performance applications including plastics, rubbers, and adsorbents. Due to their high theoretical surface area, excellent electrical conductivity, extraordinary mechanical flexibility, and good thermal conductivity, carbon nanomaterials have very promising applications in polymeric nanocomposites [1-3]. One of the most attractive characteristics of carbon nanoparticles is their high surface area as it creates a large interfacial surface area in the composite, and thereby results in strong interaction between the matrix and the reinforcement at a very low nanofiller loading [4, 5].

Carbon materials are used in many molded and extruded industrial rubber products, such as tires, belts, hoses, commercial roofing, footwear, roll flooring, gaskets, diaphragms, etc. In such composite materials, carbon acts as a filler and a strengthening or reinforcing agent. Reinforcement behavior of fillers and rubber–filler interaction has been the subject of much attention, and needs more investigations to better understand these phenomena and develop advanced composite products [6-9]. The demand for rubber composites with strong durability, and heat and chemical resistance is continuously increasing. The properties of carbon such as composition and surface characteristics play a significant role in determining its application as a filler in composite materials. Likewise, the properties of composites can be improved by tuning the structural properties of carbons and minimizing the presence of undesired inorganic materials (e.g. crystalline silica). Most of the carbon used in these applications comes either from graphite or from synthetic sources such as pyrolysis of polyacrylonitrile [10, 11]. Use of naturally available substances for preparation of reinforcement materials in composites is not only cost effective but also utilizes renewable resources, thus enabling conservation of non-renewable resources and helping in minimizing environmental problems [8, 9, 12].

The company partner of my studies is building a production site in Sarnia, Ontario for manufacturing bio-based plastics from biomass residues. For this purpose, they produce 2,5 furandicarboxylic acid from biomass residues, which is then utilized for making bio-based plastics bottles. Whilst increasing interest and legislation to utilize renewable

resources for reducing the global carbon footprint are supporting industrial transition to bio-based high-performance materials for advanced applications [13-15], growing interest also lies on developing circular economy wherein a side product of one process becomes the resource for another process. One of the side products produced by them from their bio-based plastic bottle manufacturing technology is humins, which is a by-product of production of 2,5 furandicarboxylic acid from lignocellulosic biomass. The industry's approach to utilize humins is to convert this by-product to valuable carbon materials by a two-step process – production of hydrothermal carbon (HTC) followed by inert-atmosphere carbonization of HTC.

Working in collaboration with company partner, this project investigated on characteristics of HTC, carbonization of HTC in an inert atmosphere to produce high quality carbon and characterization of the produced carbon, and analysis of crystalline silica content of provided HTC samples. Characterization involved analysis of chemical composition of provided HTC and morphological analysis of produced carbon.

### **5.1.1. Project goals and deliverables**

The goal and deliverables of the project were achieved by dividing the project in three different sub-projects and achieving the respective deliverables as,

#### **A. Structural characterization of HTC and prepared carbons**

The influence of feedstock on properties of HTC, and the effects of carbonization temperature on conversion/calcination of HTC to carbon were evaluated through the properties of HTC and prepared carbon studied by:

- (i) BET: analysis of porosity, pore volume, and surface area.
- (ii) XRD: study of crystallinity and graphitic spacing; determination of silica.
- (iii) Raman scattering: analysis of orderness/disorderness of carbon materials.

#### **B. Determination of crystalline silica in HTC**

Understanding the crystalline silica content in carbons is a major importance for composites applications. The qualitative and quantitative analysis of amorphous silica, crystalline silica, and polymorphs of crystalline silica was carried out using SEM-EDX

(low angle backscattered electrons imaging) and by ICP-MS analysis (InnoTech Alberta) by hydrofluoric acid digestion method.

## C. Extraction and determination of molecular weight of soluble components of HTC

Soxhlet extraction was carried out to extract organic soluble components from the provided HTC materials using different solvents. Gel permeation chromatography (GPC) of THF extract was carried out to determine the molecular weight distribution of soluble components.

### 5.2. Morphology and structural characterization

#### 5.2.1. Surface characterization of parent HTC materials

##### 5.2.1.1. N<sub>2</sub> adsorption-desorption isotherms and BET surface area

The specific surface area and pore characteristics of the HTC samples were determined from nitrogen adsorption-desorption isotherm data obtained at  $-196^{\circ}\text{C}$  in a constant-volume adsorption apparatus (Tristar II 3020, Micromeritics Instrument Corporation, Norcross, GA, USA) using 99.995% pure N<sub>2</sub> gas obtained from Praxair (Oakville, ON, Canada). The samples were degassed at  $150^{\circ}\text{C}$  for 12 h prior to measurement. The surface area of the sample was estimated by BET (Brunauer-Emmett-Teller) method. Table 5.1 shows the specific surface area, pore volume and pore size of the samples.

**Table 5.1. Summary of BET surface area, total pore volume and pore size of the sample. Duplicate runs were performed for each sample, and the results are presented as average  $\pm$  maximum deviation.**

<b>Sample (named as received)</b>	<b>Sample renamed as</b>	<b>BET surface area (m<sup>2</sup>/g)</b>	<b>Pore volume (cm<sup>3</sup>/g)</b>	<b>Average pore size (Å)</b>
17(1PR6)	S17	77.38 $\pm$ 5.71	0.2731 $\pm$ 0.034	142.2 $\pm$ 28.57
Aveka dried CSSP	S97	67.77 $\pm$ 3.025	0.2515 $\pm$ 0.010	148.9 $\pm$ 12.61
CS-HTC 2015	S2015	13.04 $\pm$ 1.287	0.024 $\pm$ 0.001	75.63 $\pm$ 10.89

The N<sub>2</sub> adsorption-desorption isotherms of HTC samples S17, S97, and S2015 are shown in Figure 5.1a-c. The adsorption isotherms for all the samples investigated were primarily of Type IV, a characteristic of mesoporous materials.

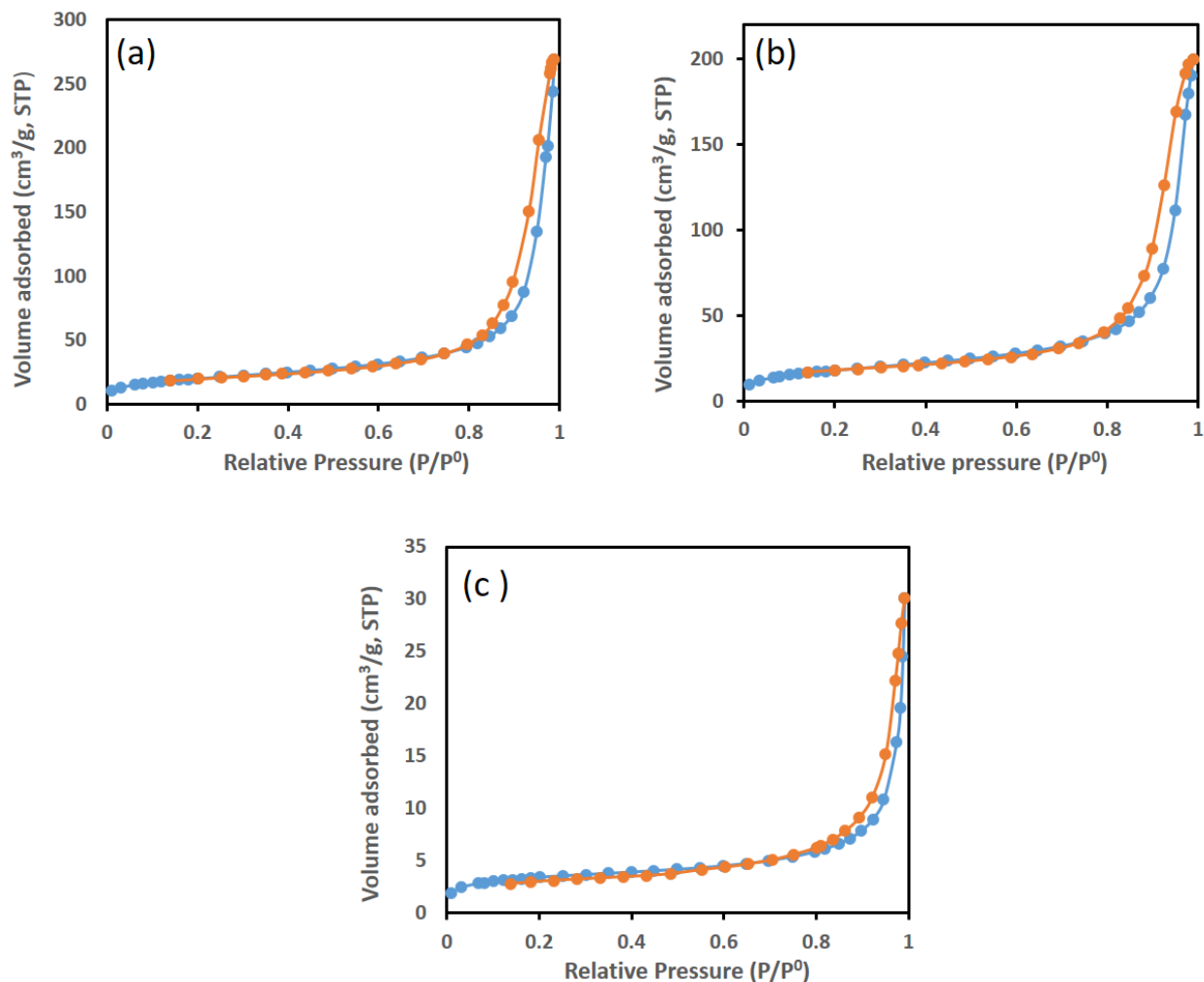


**Figure 5.1. Nitrogen adsorption-desorption isotherms of (a) S17, (b) S97, and (c) S2015.**

### 5.2.1.2. XRD Analysis

The X-ray diffraction analysis of the HTC samples did not exhibit any sharp peaks (Figure 5.2), which is an indicative of amorphous nature of the material, and also an indicative of the absence of crystalline silica in the sample. As seen in figure, XRD patterns of all the samples were identical.

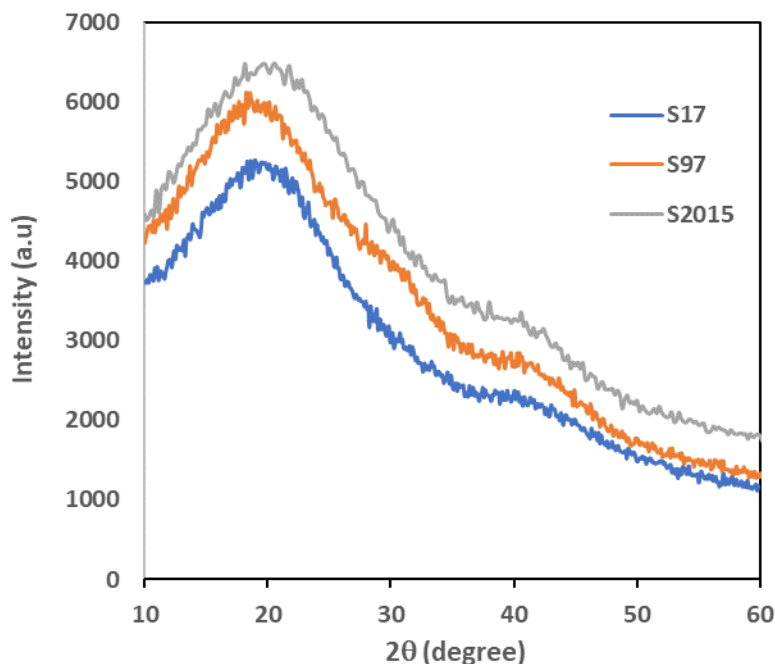


**Figure 5.2. XRD analysis of S17, S97 and S2015.**

### 5.3. Carbonization of HTC samples

#### 5.3.1. Method of carbonization

The provided parent HTC materials S17 and S97 were carbonized according to the procedure described in chapter 2 (section 2.2.2.1). In a typical run, known weight of HTC sample was carbonized at a temperature ( $^{\circ}\text{C}$ ) of 400, 450, 500, 550, or 1000 $^{\circ}\text{C}$  for a holding time of 2 h under  $\text{N}_2$  atmosphere in a tubular furnace. The heating rate was 5 $^{\circ}\text{C}/\text{min}$ . The produced carbon materials were stored in a borosilicate glass container until used for the characterization studies.

##### 5.3.1.1. Effect of carbonization temperature on carbon yield

The carbonization temperature plays an important role on the yield of carbon materials. As seen in Table 5.2, it is found that the yield of carbon materials decreased continuously

with increasing carbonization temperature. This is attributed to the removal of volatile compounds from the decomposition of lignocellulosic materials in the form of CO, CO<sub>2</sub> and CH<sub>4</sub> (details in chapter 2, section 2.2.2.3).

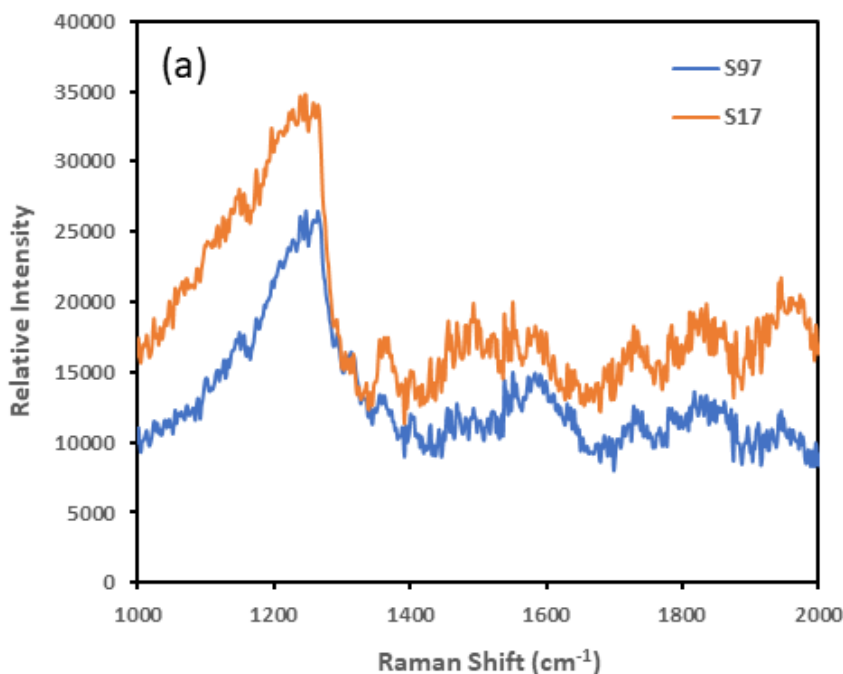
**Table 5.2. Yield (%) of carbon as a result of carbonization of HTC at different temperatures**

Sample	Temperature (°C)	Yield (%)
S17	400	68.8
	450	66.2
	500	59.8
	550	57.5
	1000	52.2
S97	400	66.5
	450	58.8
	500	56.4
	550	53.8
	1000	49.8

### 5.3.2. Raman spectra

Raman spectroscopy provides information on orderness/disorderness of carbon materials. In the Raman spectra of carbon samples, generally two bands are observed – a band at 1500 cm<sup>-1</sup> called G band, and the other band at 1300 cm<sup>-1</sup> called D band. The ratio of intensity of G and D band ( $I_D/I_G$ ) gives information about orderness/disorderness of the carbon (details in chapter 2, section 2.3.7). Raman spectra of HTC samples S17 and S97 and the carbons prepared as described in 5.3.1 were obtained with Renishaw InVia Reflex Raman Spectrometer with an excitation wavelength of 633 nm as the light source.

Figure 5.3a shows the Raman spectra of parent HTC samples S17 and S97. As can be seen in the figure, the parent HTC samples contain only D band, lacking G band, which is an indicative of low degree of orderness. Figure 5.3(b-e) compare the Raman spectra of carbons of S17 and S97 obtained at different carbonization temperatures (the Raman spectra of carbon prepared at 1000°C is significantly different from those of the samples prepared at lower temperatures, and are presented separately in Figure 5.3c and 5.3e). All samples exhibited a broad disorder D-band at  $\sim 1330\text{ cm}^{-1}$  and graphitic order G-band at  $\sim 1590\text{ cm}^{-1}$ . It can be seen in the figures that the height of D peak decreases and that of G peak increases with increasing carbonization temperature indicating the increase of disorderness or defects in the carbon materials with increasing temperature. This effect is much pronounced in the sample prepared by carbonization at 1000°C (compare the spectra of figure 5.3b vs 5.3c for sample S17 and figure 5.3d vs 5.3e for sample S97).



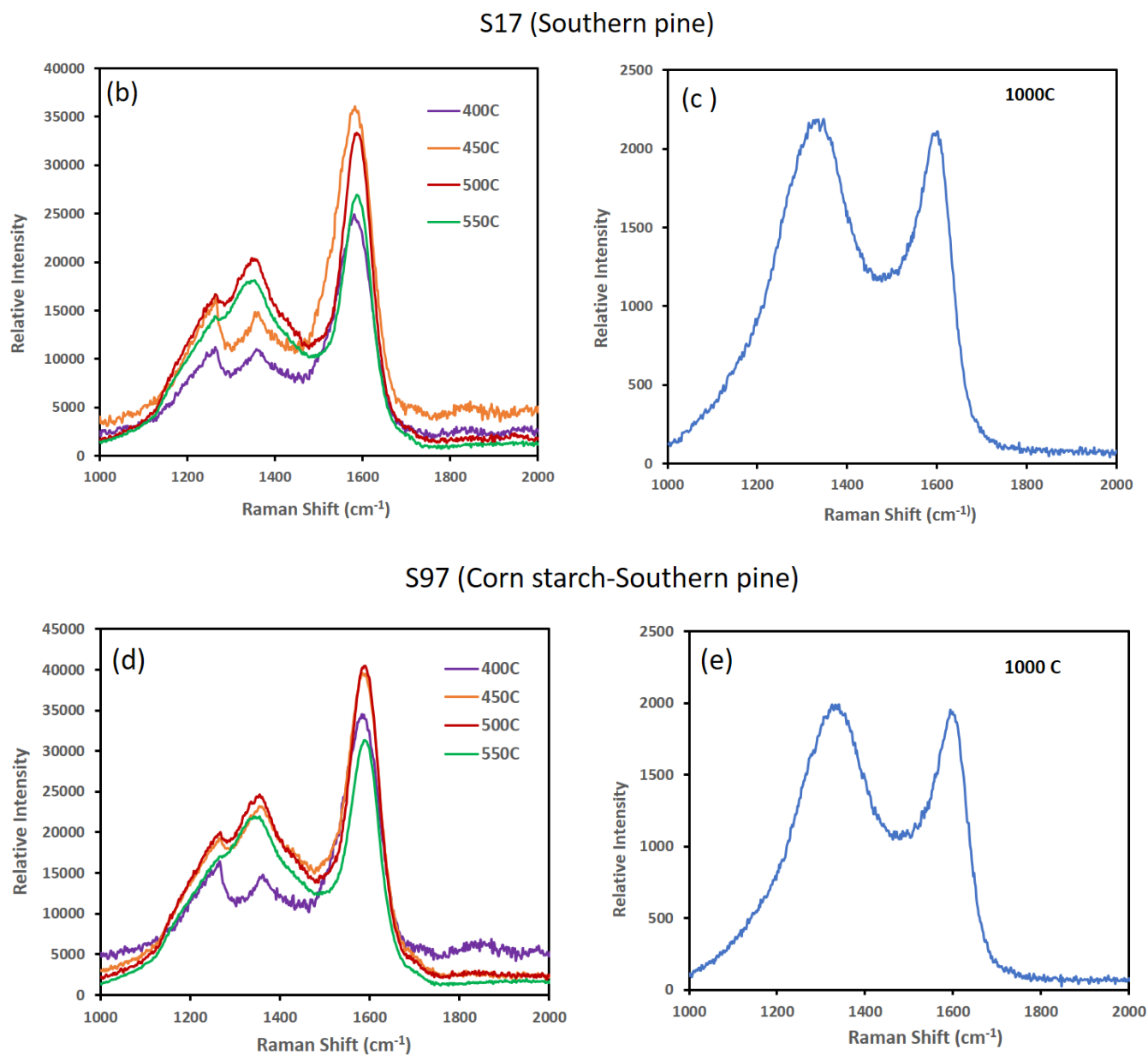


**Figure 5.3. Raman Spectra of HTC samples S17 and S97 (a), and the carbons prepared from the feed materials at different carbonization temperatures (5.3b to 5.3e).**

### 5.3.3. N<sub>2</sub> adsorption-desorption isotherms

Since the carbon prepared by carbonization of HTC samples at 1000°C demonstrated significantly different Raman scattering, only the samples prepared by carbonization at 1000°C were subjected to N<sub>2</sub> adsorption-desorption isotherm analysis. Figure 5.4 compares the BET surface area of HTC samples S17 and S79, and the carbonized materials of respective HTC samples. The raw data of N<sub>2</sub> adsorption-desorption isotherm were also treated with Rouquerol transform, and the results obtained after Rouquerol transform of N<sub>2</sub> adsorption-desorption isotherm are also presented in Figure 5.4. The specific surface area of both S17 and S97 increased notably after carbonization. The increase in the specific surface area is attributable to the removal of volatile substances at high temperature. The surface areas obtained from BET studies was 75 m<sup>2</sup>/g for S17 and 66 m<sup>2</sup>/g for S97. After activation at 1000°C, the surface area increased to 138 m<sup>2</sup>/g for S17 and 130 m<sup>2</sup>/g for S97, which is an increase by 84% for S17 and 97% for S97, respectively.

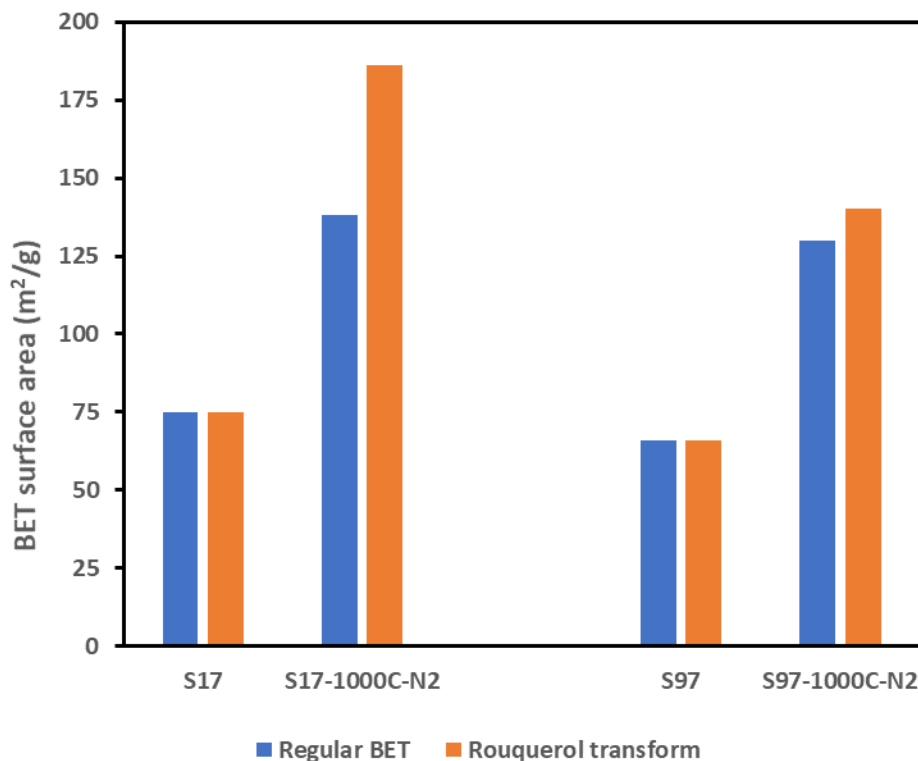


**Figure 5.4. Comparison of BET surface area of HTC samples and respective carbons prepared by carbonization at 1000°C. The data obtained by BET analysis were also treated with Rouquerol transform software.**

## 5.4. Analysis of crystalline silica

### 5.4.1. Ash preparation

For the analysis of crystalline silica in HTC samples, the provided samples were burnt in presence of air to burn off all the organic materials. In a typical experiment, known amount of parent HTC samples was taken in crucible and heated at 1000°C in a muffle furnace for 2 h or 20 h. The ash produced as a result of burning was analysed for crystalline silica content. Table 5.3 shows the % ash content of provided HTC samples, and Figure 5.5 shows the photographs of the ash obtained after 1000°C treatment of HTC samples for 2 and 20 h.

**Table 5.3. Summary of calcination results.**

Sample	Temperature (°C)	Duration (h)	Yield (%)
S17	1000	2	0.85
	1000	20	0.91
S97	1000	2	0.44
	1000	20	0.6

**Figure 5.5. Photographs of the residues of burnt HTC samples.**

## 5.4.2. Ash characterization

### 5.4.2.1. SEM-EDX of HTC ashes

The results of elemental analysis of ashes determined with SEM-EDX are given in Table 5.4. From the results it is observed that the ash obtained after burning of HTC samples is abundant in Ca and O, and possess trace amount of Si, Cl, Mo, and Mg. Both the samples also contained some unburnt carbon.

**Table 5.4. Elemental analysis by SEM-EDX**

<b>Sample</b>	<b>Element</b>	<b>Average wt%<sup>1</sup></b>	<b>Average Atomic%<sup>1</sup></b>
S17-2h	C	7.87	13.9
	O	43.3	58.4
	<b>Si</b>	<b>0.34</b>	<b>0.26</b>
	Ca	44.9	21.6
	Mg	1.13	1.03
	Mo	1.06	0.23
	Cl	0.48	0.33
S17-20h	C	3.4	6.5
	O	43.8	64.7
	<b>Si</b>	<b>0.25</b>	<b>0.21</b>
	Ca	43.2	25.6
	Mg	0.14	0.14
	Mo	8.25	2.12
	Cl	0.1	0.06
S97-2h	C	8.3	14.8
	O	43.6	58.3
	<b>Si</b>	<b>1.85</b>	<b>1.48</b>
	Ca	37.4	20.15
	Mg	3.9	3.43
	Mo	3.4	0.75
	Cl	0.26	0.16

S97-20h	C	6.8	12.4
	O	45.1	61.5
	<b>Si</b>	<b>0.1</b>	<b>0.1</b>
	Ca	41.1	22.7
	Mg	1.9	1.7
	Mo	4.3	1.0
	Cl	0	0

<sup>1</sup>Average of six scans per sample

#### 5.4.2.2. ICP-MS analysis

The silica and chlorine content of ash samples were also determined by ICP-MS analysis (InnoTech Alberta) by hydrofluoric acid digestion method of sample preparation, and the results are presented in Figure 5.6. The relative low contents of Si and Cl as seen in Figure 5.6 is consistent with the results of elemental analysis obtained from SEM-EDX analysis of ash.

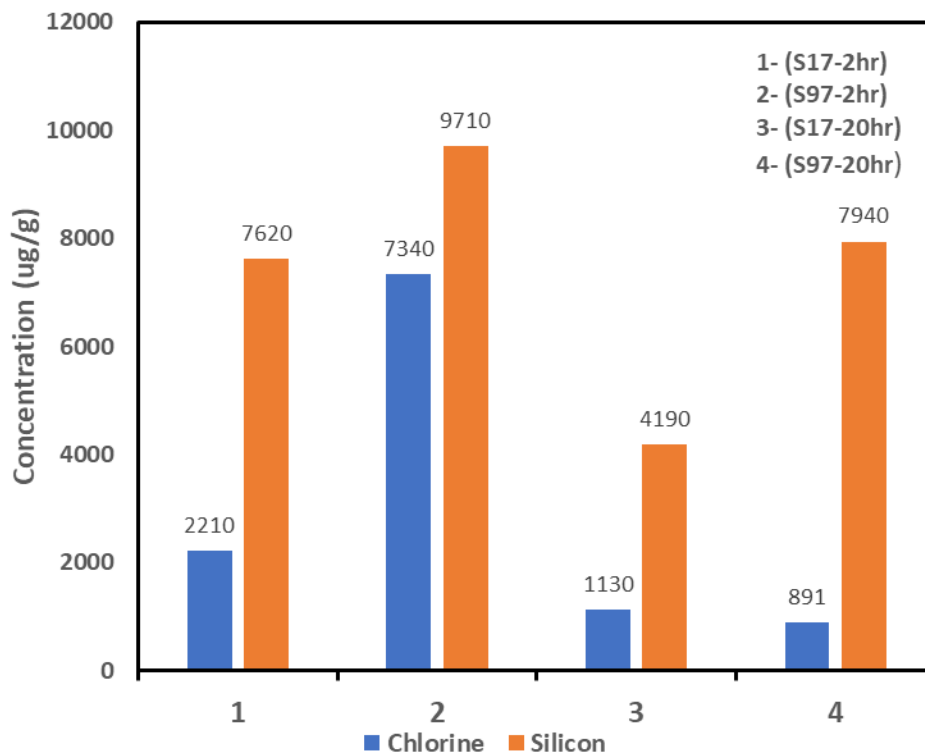


**Figure 5.6. ICP-MS analysis of ashes of S17 and S97.**

## 5.5. Extraction of soluble fractions from parent HTC samples

### 5.5.1. Extraction method

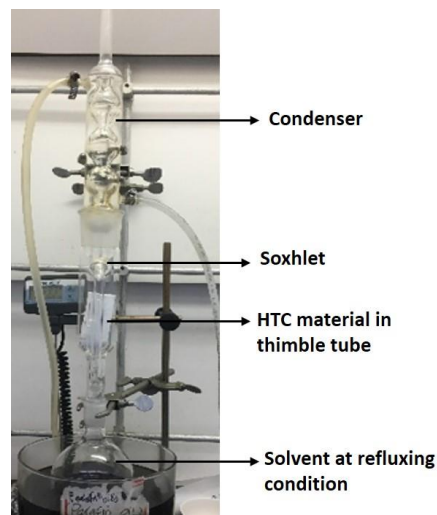
Extraction of the soluble fractions from parent feed materials, HTC samples S17, S97, and S2015, was performed using Soxhlet extraction method. In this study, four different solvents differing in boiling point and polarity were used for extraction of soluble components under refluxing condition. The solvents used were THF, acetone, dichloromethane (DCM), and ethyl acetate (EtOAc). The HTC samples were used as received without any further treatment. In preliminary investigations, THF demonstrated the highest efficiency to extract soluble components. For comparative studies to see if variability will be observed in sieved and non-sieved materials, Soxhlet extraction with THF was performed for non-sieved as well as sieved materials. In the case of sieved

sample, material consisting of particle size in the range of 150-212  $\mu\text{m}$  was employed for Soxhlet extraction.

### 5.5.2. Extraction procedure

In a typical experiment, known amount of feed material was transferred into the thimble tube of Soxhlet extractor, and the apparatus was assembled as seen in the figure on the right-hand side. Then, the extraction solvent was heated to refluxing condition for 24 (or 48) hours until the extract in the Soxhlet was colorless.

Afterwards, solvent was removed by rotary evaporation to dryness under vacuum maintaining the temperature of water bath at 40°C. The residue was collected, vacuum dried overnight at 50°C, and the percentage extraction yield (w/w) of soluble fractions was obtained using the formula,



$$\text{Percentage of extraction yield} = \frac{\text{Weight of extract obtained}}{\text{Weight of sample taken}} \times 100$$

### 5.5.3. Extraction of HTC sample S17

Solvents of different boiling points and polarity were used to determine which solvent gives the highest extract of soluble compounds. The extraction yield (%) obtained by using each solvent are presented in Table 5.5. Based on the obtained results, the highest extraction yield was found with THF extraction followed by extraction with acetone and ethyl acetate. Negligible extraction yield was obtained using dichloromethane (hence was not used for extraction of other samples).

**Table 5. 5. Extraction of S17 with different solvents**

Sample	Sample amount (g)	Extraction solvent <sup>1</sup>	Extraction time (h)	Amount of extraction solvent (mL)	Extraction yield (%)
Non-sieved	5.0171	THF	24	200	4.20
Non-sieved	5.0224	THF	24	200	4.61
Non-sieved	12.012	THF	48	200	4.78
Sieved	5.0177	THF	24	180	4.63
Non-sieved	2.0069	Acetone	24	200	3.77
Non-sieved	2.0048	EtOAc	24	200	3.17
Non-sieved	1.0547	DCM	24	100	0.00

<sup>1</sup>Boiling points of solvents: THF = 66°C, Acetone = 56°C, EtOAc = 77.1°C, DCM = 39.6°C.

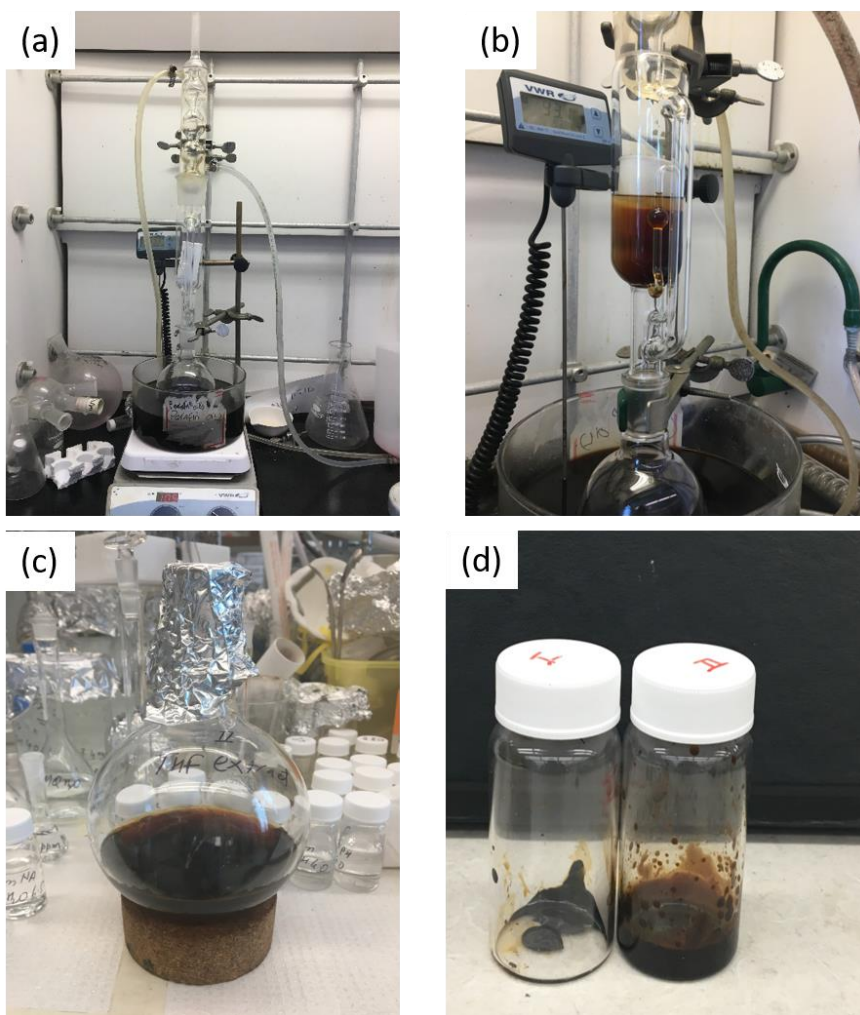


**Figure 5.7. Photographs of Soxhlet extraction of non-sieved S17 with THF. (a) Soxhlet extraction set up, (b) first fraction of soluble fraction collected in a thimble**

tube, (c) soluble fraction collected after Soxhlet extraction and, (d) dried residue after rotary-evaporator and after vacuum drying at 50°C overnight.

#### 5.5.4. Extraction of HTC sample S97

**Table 5. 6. Extraction of S97 with different solvents**

<b>Sample</b>	<b>Sample amount (g)</b>	<b>Extraction solvent<sup>1</sup></b>	<b>Extraction time (h)</b>	<b>Amount of extraction solvent (mL)</b>	<b>Extraction yield (%)</b>
Non-sieved	4.9536	THF	24	180	4.48
Sieved	5.0133	THF	24	200	3.98
Sieved	1.5236	Acetone	24	150	3.68
Sieved	2.0089	EtOAc	24	150	2.79

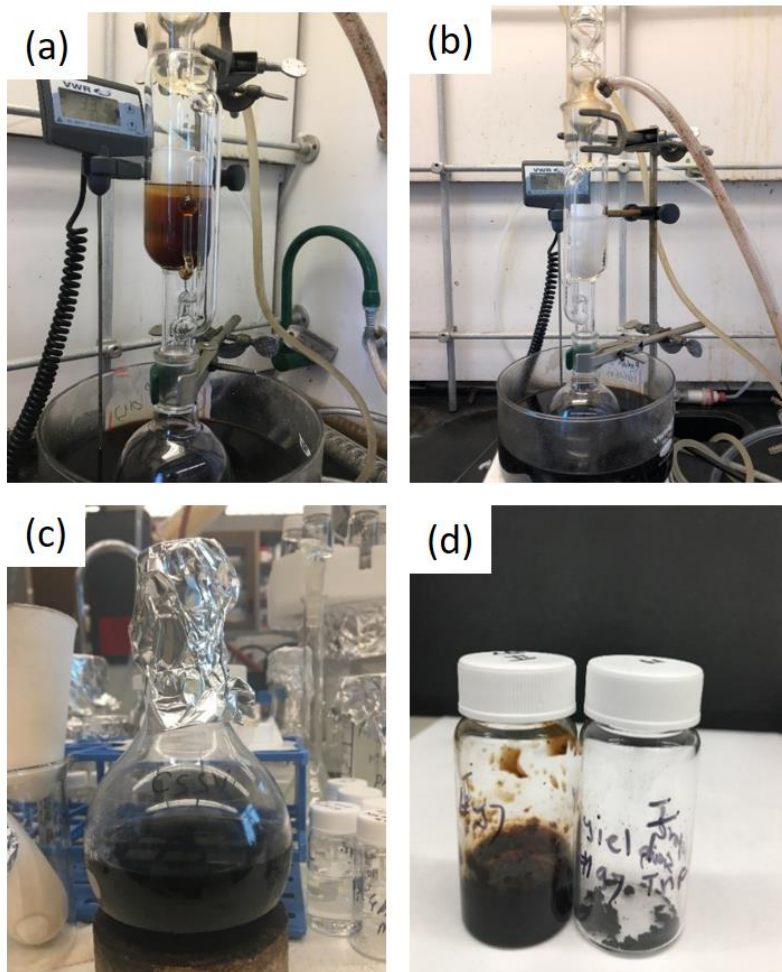


**Figure 5.8. Photographs of Soxhlet extraction of non-sieved S97 with THF. (a) first extract collected in a thimble tube, (b) after repeated extraction, the extract in the thimble tube is colorless, (c) soluble fraction collected after Soxhlet extraction in THF and, (d) residue after rotary-evaporation and vacuum drying at 50°C overnight.**

### 5.5.5. Extraction of HTC sample S2015

**Table 5.7: Extraction of S2015 with different solvents**

Sample	Sample amount (g)	Extraction solvent <sup>1</sup>	Extraction time (h)	Amount of extraction solvent (mL)	Extraction yield (%)
Non-sieved	5.0319	THF	24	180	7.60
Non-sieved	1.5052	Acetone	24	150	7.30
Non-sieved	1.4933	EtOAc	24	250	2.65

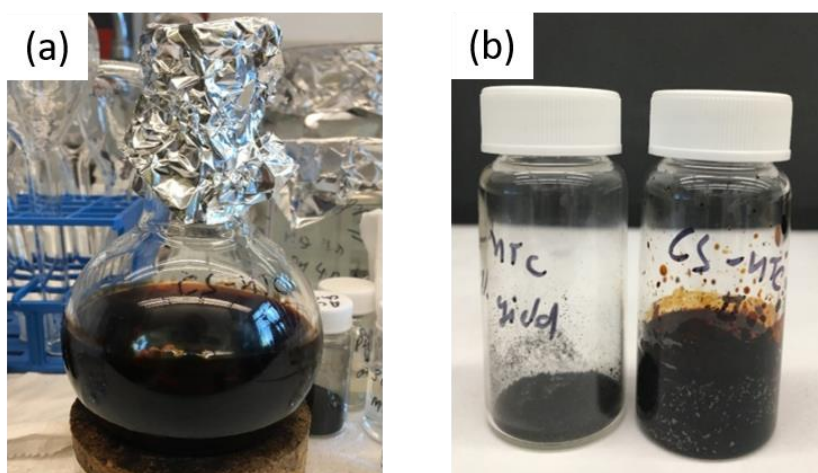


**Figure 5.9. Photographs of Soxhlet extraction of non-sieved S2015 with THF. (a) soluble fraction collected after Soxhlet extraction in THF and, (b) dried residue after rotary-evaporation and after vacuum drying at 50°C overnight.**

## 5.6. Summary of Soxhlet extraction

For all three samples, THF demonstrated better extraction efficiency than acetone and ethyl acetate for extraction of organic soluble components. Comparatively, S2015 contained relatively higher amount of organic soluble components than S17 and S97 in respective organic solvents as extractants. Since THF had better efficiency, the product obtained from the THF extract was subjected to gel permeation chromatography (GPC) studies for analysis of molecular weight distribution.

## 5.7. Gel permeation chromatography (GPC) of THF extract samples

### 5.7.1. Sample Preparation

For the analysis of molecular weight distribution of THF soluble components extracted from provided HTC samples, THF extract of HTC samples were subjected to GPC analysis. In a typical procedure, each HTC sample was subjected to Soxhlet extraction as described in the extraction procedure. Then, 10 mL THF extract of known concentration (mg/mL and w%) of soluble components was supplied to Dr. William Z. Xu (Research Engineer, Charpentier group) who kindly ran GPC for this analysis. The concentrations (mg/mL and w%) of the samples submitted for GPC analytical samples was determined as follows:

- i) 10 mL of THF extract (out of bulk extract) of each sample was transferred into a 20 mL glass vial.
- ii) THF was evaporated off using rotary evaporator followed by vacuum drying the sample overnight to ensure complete dryness.
- iii) Following weights were noted:
  - a) the weight of empty vial (W1),
  - b) the weight of vial and 10 ml THF extract (W2), and
  - c) the weight of vial and residue after vacuum drying (W3).
- iv) The concentration (C) and w% of the extract were then calculated using the formulas,

$$C \left( \frac{\text{mg}}{\text{mL}} \right) = \frac{W3-W1}{10}$$

and,

$$Wt\% = \frac{(W3-W1)}{W2-W1} * 100$$

Sample preparation for concentration determination was done in duplicate/triplicate to ensure that the particle/solute distribution was identical in the solution, and the results of concentration (mg/mL and w%) of samples submitted for GPC analysis are summarized in the following tables.

**Table 5.8. Average concentration (mg/mL) and wt% of THF extract of the samples subjected to GPC analysis**

Sample	Run	C (mg/mL)	w%	Average concentration (mg/mL)	Average w%
S17 Sieved (sieve size: 150-212 $\mu\text{m}$ )	1	3.19	0.355	3.23	0.363
	2	3.27	0.371		
S17 Non-sieved	1	1.74	0.197	1.72	0.195
	2	1.71	0.194		
	3	1.73	0.196		
S97 Sieved (sieve size: 150-212 $\mu\text{m}$ )	1	3.62	0.403	3.63	0.405
	2	3.65	0.408		
S97 Non-sieved	1	1.62	0.185	1.71	0.194
	2	1.73	0.197		
	3	1.79	0.202		
S2015 Non-sieved	1	3.21	0.365	3.25	0.369
	2	3.19	0.363		
	3	3.35	0.381		

*Note: The variability in concentration (mg/mL) of sieved and non-sieved samples as seen in table 10 is due to the variation in the amount of material taken, but not due to the nature (sieved vs non-sieved) of material.*

## 5.8. Molecular weight distribution analysis

Molecular weight and dispersity ( $\mathcal{D}$ ) of the polymers were analyzed by cirrus gel permeation chromatography (GPC) system (PL-GPC 220) using refractive index detector and PAS columns (PAS-101, PAS-103M-UL, PASC-105M-M, PolyAnalytik, Canada). THF eluent flow rate was 1 mL/min and the column temperature was 30°C. The system was calibrated using a series of polystyrene narrow standards [ $M_p$  (Da) = 570, 2340, 6300, 12100, 19900 (STD-6A, Scientific Polymer Products, Inc.), and 580, 1260, 3370, 8450, 19720, 60450, 184900, 483000, 915000, 3053000, and 6035000 (Polymer Laboratories) and 104 (styrene)].

Table 5.9 shows the molecular weight parameters and polydispersity of THF extract of different parent materials. From GPC analysis, the average molecular weight of the THF soluble fractions was lower than 3000 Daltons, indicating that relatively low molecular weight components were extracted. (Molecular weight distribution curves for parent feed materials obtained by GPC is shown in Appendix 5.1).

**Table 5.9. Molecular weight parameters and polydispersity of THF extract of different parent materials using PAS columns (PAS-101 + PAS-103M-UL + PASC-105M-M).**

Sample	Mn (Da)	Mw (Da)	Mp (Da)	$\mathcal{D}$	f <sub>Mw</sub>	f <sub>Mw</sub>	f <sub>Mw</sub>
					<500Da	=500-1000 Da	>1000 Da
<b>S17</b>	549	2773	351	5.1	0.39	0.31	0.30
<b>Sieved</b>	564	2885	351	5.1	0.37	0.31	0.32
<b>S17</b>	470	2541	192	5.4	0.43	0.28	0.29
<b>Non-sieved</b>	488	2650	188	5.4	0.41	0.29	0.30
<b>S97</b>	498	2188	509	4.4	0.45	0.34	0.21
<b>Sieved</b>	510	2296	509	4.5	0.44	0.33	0.23
<b>S97</b>	506	1065	509	2.1	0.43	0.34	0.23

<b>Non-sieved</b>	507	1168	509	2.3	0.43	0.34	0.23
<b>S1500</b>	522	1390	862	2.7	0.36	0.35	0.29
	627	1731	914	2.8	0.26	0.37	0.37

## 5.9. Conclusions

The hydrothermal carbon (HTC) samples supplied by the company partner as well as the carbon samples prepared by carbonization of HTC at different temperatures were characterized through the analysis of BET (Brunauer-Emmett-Teller) surface area, XRD (X-ray Diffraction) and Raman scattering. The results indicated amorphous nature of the material, and absence of crystalline silica in the HTC samples. Elemental analysis and ICP-MS determined the trace amount of Si present in the ash samples. In Soxhlet extraction, THF was found to extract the larger amounts of soluble components from all three HTC samples. Molecular weight distribution analysis by GPC studies of the THF soluble fractions indicated that the average molecular weight was lower than 3000 Daltons, indicating that relatively low molecular weight components were extracted.

## 6. References

- [1] M. Sevilla, C. Sanchís, T. Valdés-Solís, E. Morallón, A. B. Fuertes, Synthesis of graphitic carbon nanostructures from sawdust and their application as electrocatalyst supports. *J. Phys. Chem.* 2007(111)9749-9756.
- [2] L. Sun, C. Tian, M. Li, X. Meng, L. Wang, R. Wang, J. Yin, H. Fu, From coconut shell to porous graphene-like nanosheets for high-power supercapacitors. *J. Mater. Chem. A*, 2013(1)6462-6470.
- [3] L. Wang, G. Mu, C. Tian, L. Sun, W. Zhou, P. Yu, J. Yin, H. Fu, Porous graphitic carbon nanosheets derived from cornstalk biomass for advanced supercapacitors. *Sustain. Chem.* 2013(6)880-889.

- [4] H. Mahfuz, A. Adnan, V. R. Rangari, S. Jeelani, B. J. Jang, Carbon nanoparticles/whiskers reinforced composites and their tensile response. *Compos. Part A Appl. Sci. Manuf.* 2004 (35) 519-527.
- [5] J. Sandler, P. Werner, M. S. P. Shaffer, V. Demchuk, V. Altstadt, A. H. Windle, Carbon-nanofibre-reinforced poly (ether ether ketone) composites. *Compos. Part A Appl. Sci. Manuf.* 2002(33)1033-1039.
- [6] H. D. Chae, U. Basuli, J. H. Lee, C. I. Lim, R. H. Lee, S. C. Kim, N. D. Jeon, C. Nah, Mechanical and thermal properties of rubber composites reinforced by zinc methacrylate and carbon black. *Polym. Compos.* 2012(33)1141-1153.
- [7] S. N. Tripath, G. S. S. Rao and A. B. Mathur, R. Jasra, Polyolefin/graphene nanocomposites: a review. *RSC Adv.* 2017(7)23615-23632.
- [8] H. D. Rozman, G. S. Tay, A. Abubakar, R. N. Kumar, Tensile properties of oil palm empty fruit bunch-polyurethane composites. *Eur. Polym. J.* 2001(37)1759-1765.
- [9] M. Jawaid, H. P.S. A. Khalil, A. A. Bakar, Mechanical performance of oil palm empty fruit bunches/jute fibers reinforced epoxy hybrid composites. *Mater. Sci. Eng. A* 2010(527)7944-7949.
- [10] J. J. Mack, L. M. Viculis, A. Ali, R. Luoh, G. Yang, H. T. Hahn, F. K. Ko, R. B. Kaner, Graphite nanoplatelet reinforcement of electrospun polyacrylonitrile nanofibers. *Adv. Mater.* 2005(17)77-80.
- [11] K. Zhang, L. L. Zhang, X. S. Zhao, J. Wu, Graphene/polyaniline nanofiber composites as supercapacitor electrodes. *Chem. Mater.* 2010(22)1392-1401.
- [12] A. Nourbakhsh, A. Ashori, Wood plastic composites from agro-waste materials: analysis of mechanical properties. *Bioresour. Technol.* 2010(7)2525–2528.
- [13] A. K. Mohanty, M. Mishra, L. T. Drzal, Sustainable bio-composites from renewable resources: opportunities and challenges in the green materials world. *J. Polym. Environ.* 2002(10)19-26.

[14] V. K. Thakur, A. S. Singha, M. K. Thakur, Green composites from natural fibers: mechanical and chemical aging properties. *Int. J. Polym. Anal. Ch.* 2012(17)401-407.

[15] V. K. Thakur, A. S. Singha, M. K. Thakur, Surface modification of natural polymers to impart low water absorbency. *Int. J. Polym. Anal. Ch.* 2012(17)133-143.

## Chapter 6

### Overall conclusions and future directives

#### 6.1. Overall conclusions

A holistic approach is required for development of sustainable environment and conservation of energy and resources. Utilization of renewable resources for sustainable production of fuel/energy and materials is at the forefront of research in this direction. The waste stream of oil sand industry is one of the pressing issues requiring immediate attention for the development of sustainable environment. Consequently, removal of organic pollutants from oil sands process-affected water (OSPW) is one area of research that is gaining escalating attention. Although there are some techniques in practice to achieve selective removal of such organic compounds, they are tough tasks in real time application due to incomplete/insufficient removal of target species, costly operation, production of secondary waste materials/sludge and soon. Among conventional techniques, adsorption technology offers several advantages, and is considered one of the most effective methods. In consequence, there are a wide variety of commercial adsorbents available for removal of organic pollutants from aqueous environment. However, challenges facing implementation of commercial adsorbents available so far for removal of organic compounds include, but not limited to, low binding capacity/affinity, broad selectivity of targeted compounds, generation of sludge and so on. Consequently, selectivity of adsorbent is crucial for effective and efficient removal a of the desired compound.

In addition, utilization of renewable resource-derived environmentally benign materials for separation and purification operations is the recent interest connected with resource recycling and reservation. From this prospective, our focus on this research work was for the development of low cost, biomass-based porous carbon

using agro-waste such as hemp fibers as renewable resource of carbonaceous material.

In this work, I prepared a number of porous carbons from hemp fibers either by single-step carbonization at different carbonization temperature using  $\text{ZnCl}_2$  as activators or by introduction of nitrogen-containing functional groups on surface of hemp fibers followed by simultaneous activation and carbonization. These carbons were named as HFCs and N-HFCs, respectively. The prepared carbons were characterized with the methods/techniques used for characterization of carbon materials, and the properties of the prepared carbons were compared with those of commercial activated carbon products. Potentiality of the hemp fiber derived carbons as adsorbents for the removal of model naphthenic acids (NAs) from contaminated aqueous environment was studied, and the removal efficacy of the prepared carbons was evaluated against that of commercial granular activated carbon.

The following conclusions have been drawn from this research:

- Zinc chloride ( $\text{ZnCl}_2$ ) is a highly effective activator for preparation of high surface area porous carbons (HFCs) from hemp fiber by simple, single-step carbonization method. A systematic evaluation of effects carbonization temp in the range of 400 to 700°C and effects of  $\text{ZnCl}_2$  mass ratio of activator: substrate on the surface properties of the porous carbons indicated that a carbonization temperature of 500°C and mass ratio of activator: substrate of 2:1 (w/w;  $\text{ZnCl}_2$ : hemp fibers) were ideal for preparation of high surface area activated carbon.
- Introduction of nitrogen-containing functional group (eg, N-aminoguanidine) on the surface of hemp fiber followed by carbonization and activation is a highly effective method of preparation of N-containing porous activated carbon resulting in carbon with much higher nitrogen content than the nitrogen-doped carbons reported in literature prepared by the carbonization of mixture of carbon precursor, nitrogen precursor, and activator.

- The hemp-derived mesoporous carbonaceous materials are highly effective to adsorb model naphthenic acids from slightly acidic as well as basic aquatic environments, and these adsorbents have comparable or superior efficiency when compared to the high cost commercially available granulated carbon (GAC). The adsorption reached equilibrium within 1 hr under the experimental conditions, which is a notable efficacy of these materials for removal of naphthenic acids and naphthenic acid-like organic pollutants from contaminated aqueous streams. Analysis of adsorption kinetics provided a cue that chemisorption was involved in the adsorption of model naphthenic acids, and adsorbents consisting of positively charged centers are highly suitable for targeted removal of naphthenic acids from slightly acidic to slightly basic environments.
- From the overall results, it is concluded that the hemp fibers derived porous carbons have remarkable potential to be used to preconcentrate and separate naphthenic acids from aqueous environment due to their high adsorption capacity, fast adsorption rate, as well as the nature of natural and low cost.

## 6.2. Future directives

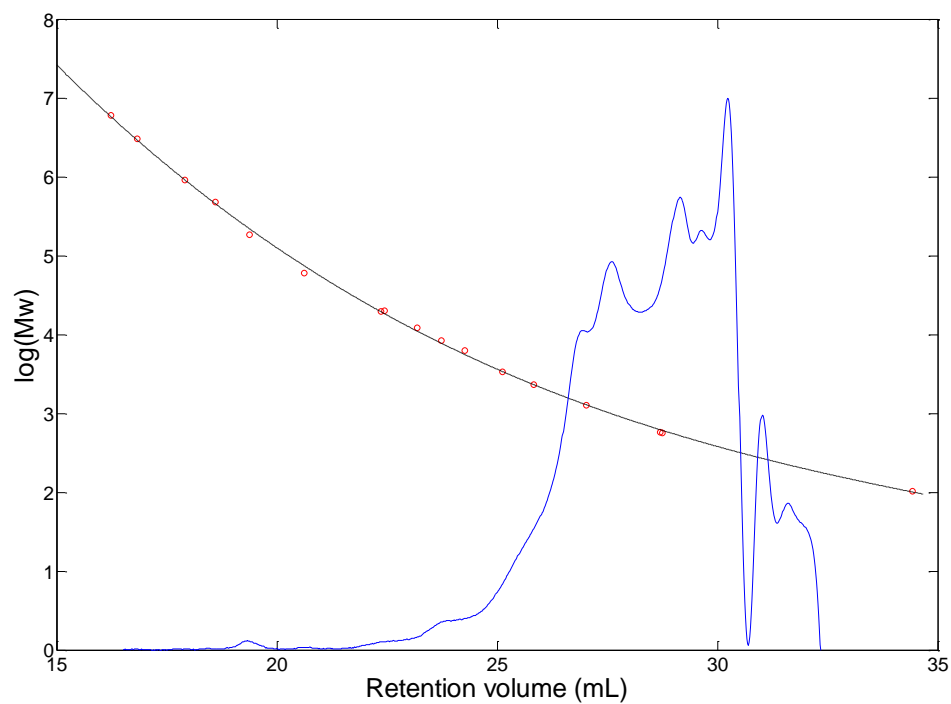
- Relatively low carbon yield was obtained with  $\text{ZnCl}_2$  activation of hemp fibers. As discussed, the low yield is most likely due to the low carbon content of hemp fibers. Therefore, using a precursor biomass with higher carbon content will potentially improve the carbon yield.
- The effects of various process parameters on the characteristics of the nitrogen functionalized porous carbon can be further investigated. The residence time (length of activation) is crucial to final activated carbon characteristics and can be evaluated further with additional tests. XPS can be very useful for investigation of the functional groups/nitrogen content of N-HFCs.
- Other surface modification techniques might be helpful in increasing the surface area of carbon materials. For instance, surface amination at low temperature, in a way that does not cause collapse of micro and meso pore structure, could be an effective method.

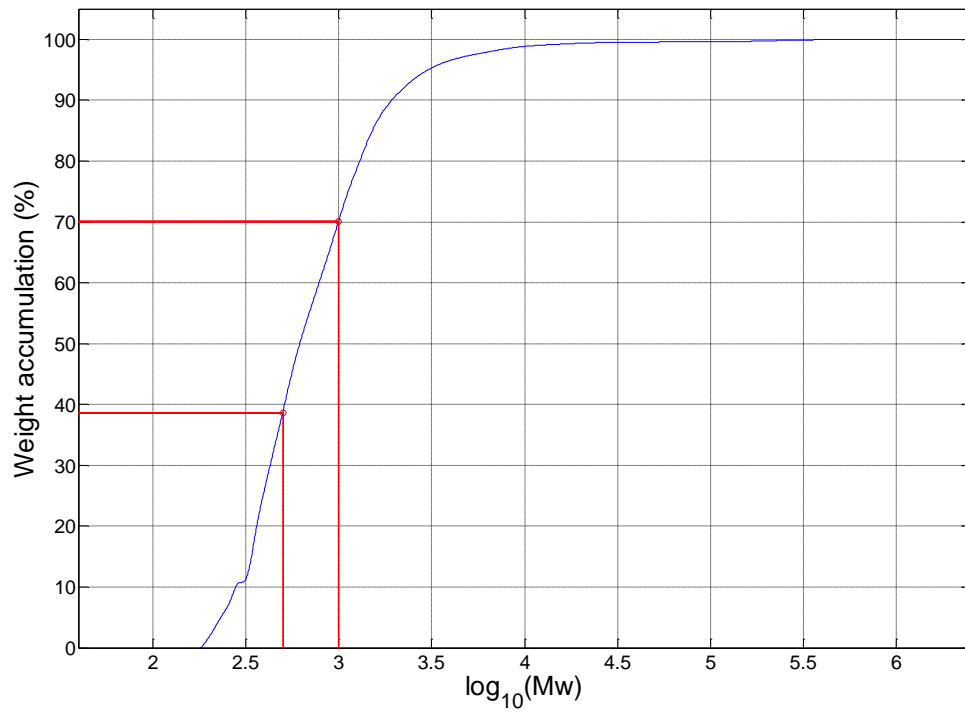
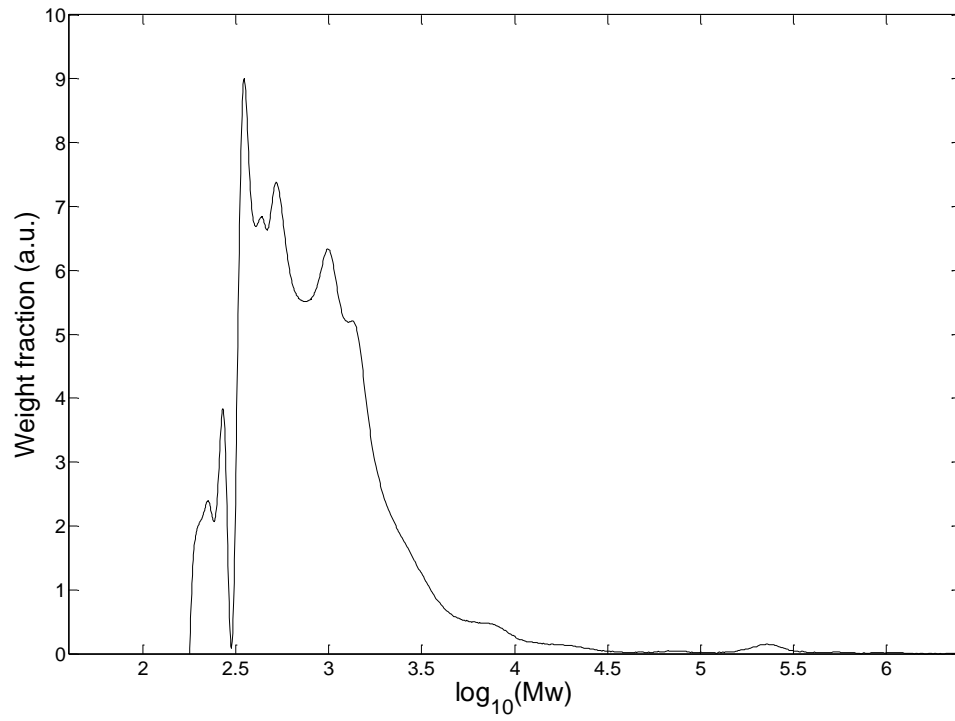
- A potential solution for real time application in removal of organic contaminants in tailings ponds can be the use of continuous column adsorption units. It is expected that the performance of activated carbon in packed columns will be different than the performance in batch operations. Column tests are recommended for further study of the performance of produced activated carbons and evaluation of bed volume (the volume that can be safely passed through the packed bed of the column ensuring the target removal efficiency).
- Given the complexity of the problem of removal of naphthenic acids from tailing ponds, commercial grade model naphthenic acids in deionized solutions were used this study. For more representative results, use of actual tailings pond water samples is recommended for future studies.
- An optimization study is needed at batch-wise method for regeneration of exhausted carbons with different solvents at various operating conditions.
- The produced carbon is in the form of powder which creates a considerable pressure drop in a continuous column. For this reason, produced activated carbon needs to be pelletized for its applications in larger scales.

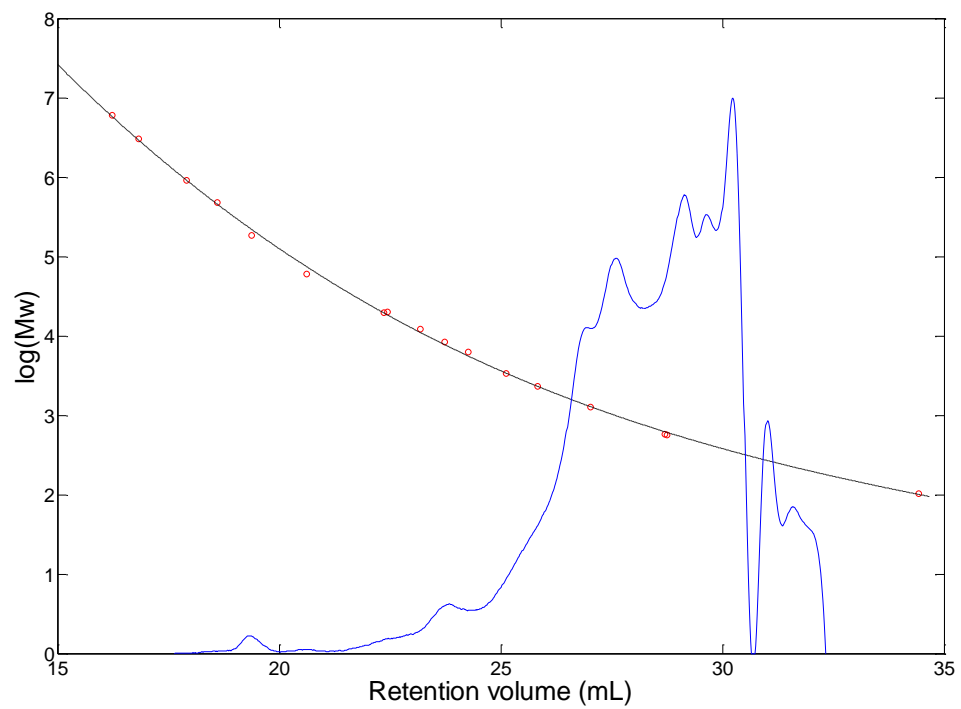
## Appendices

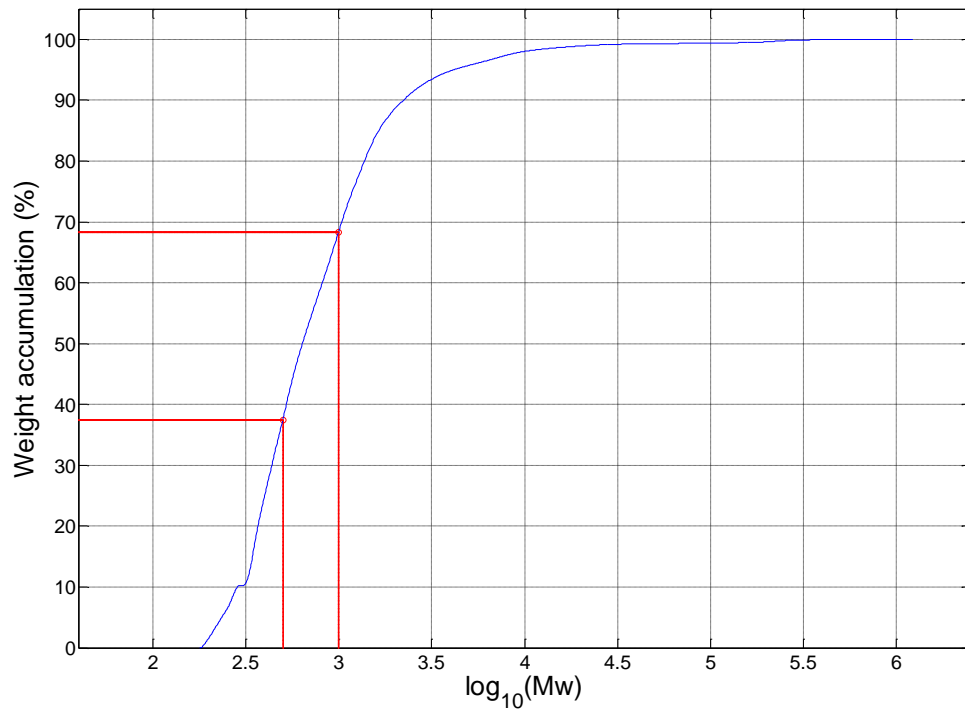
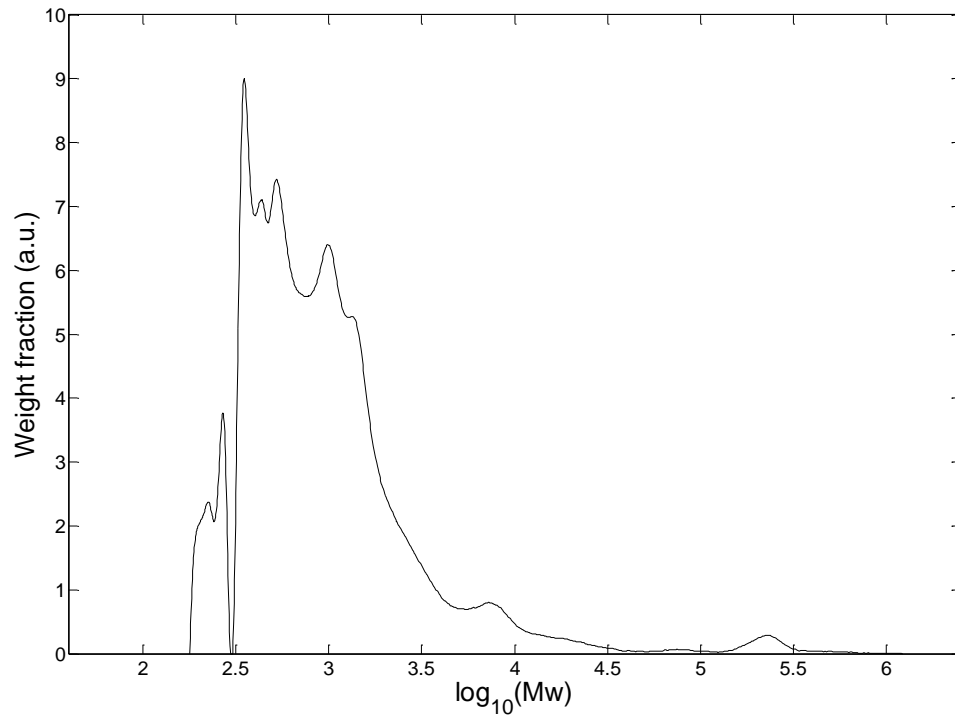
Appendix 5.1. Molecular weight distribution curves for parent feed materials obtained by GPC.

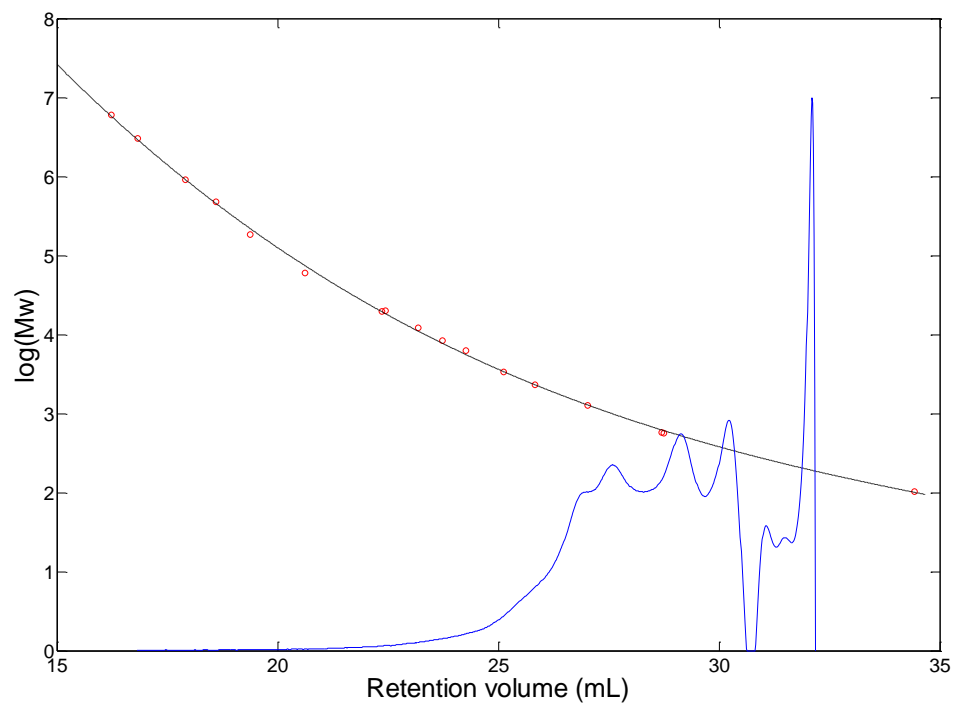
### Sample 17 Sieved 1<sup>st</sup> run

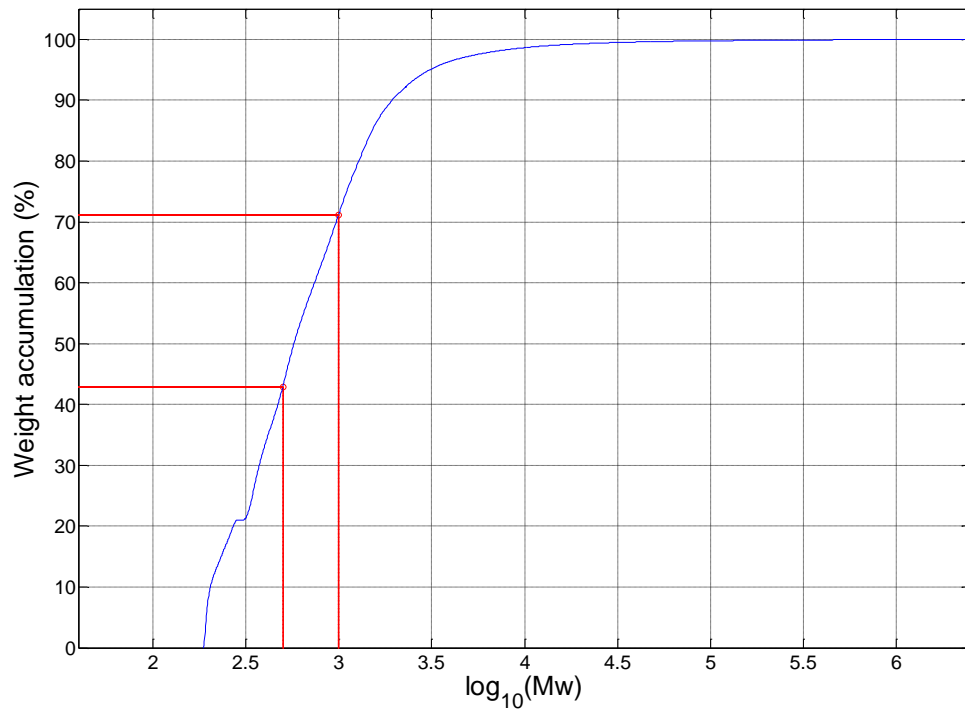
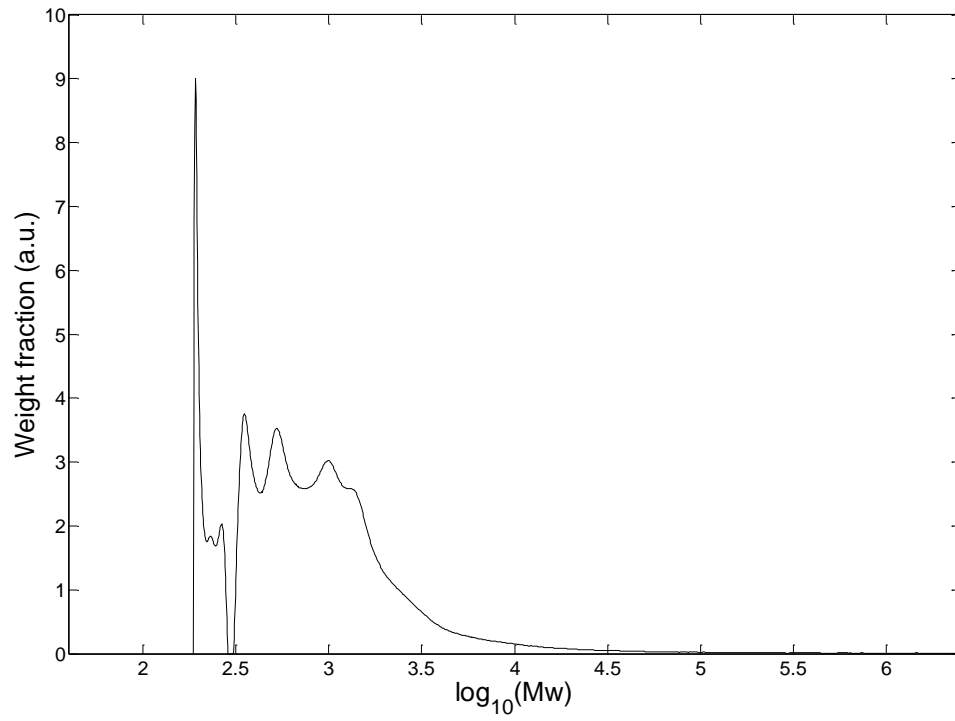


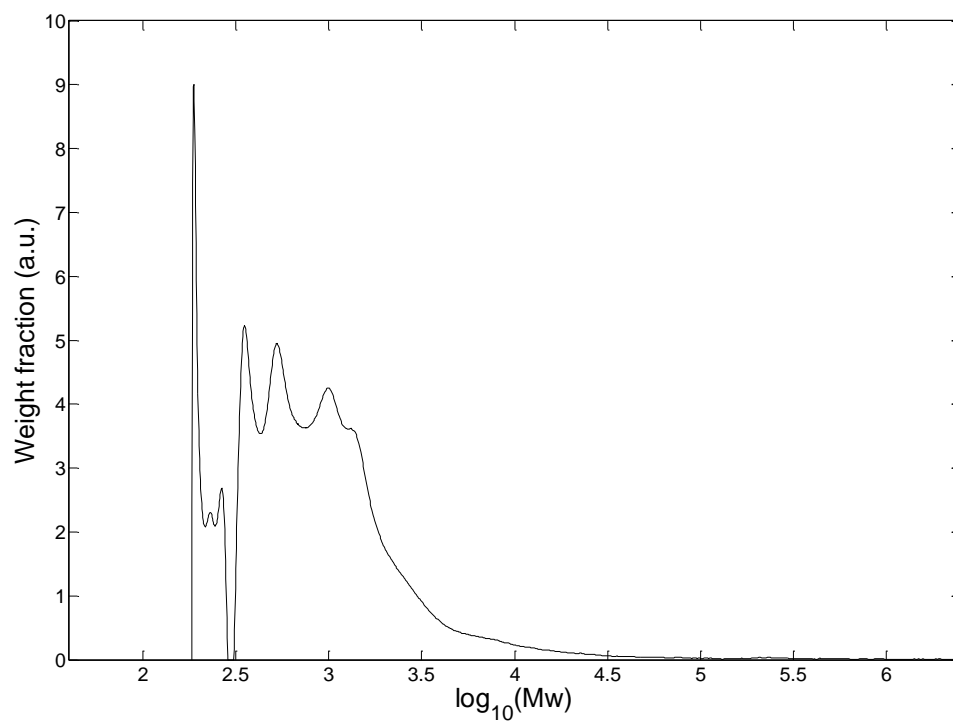
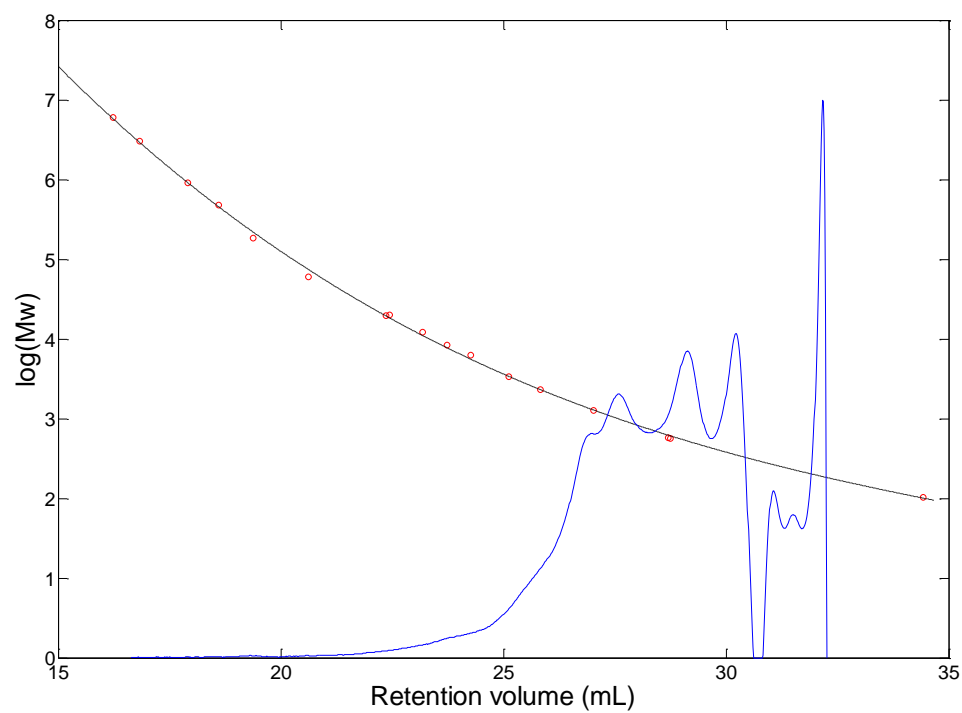


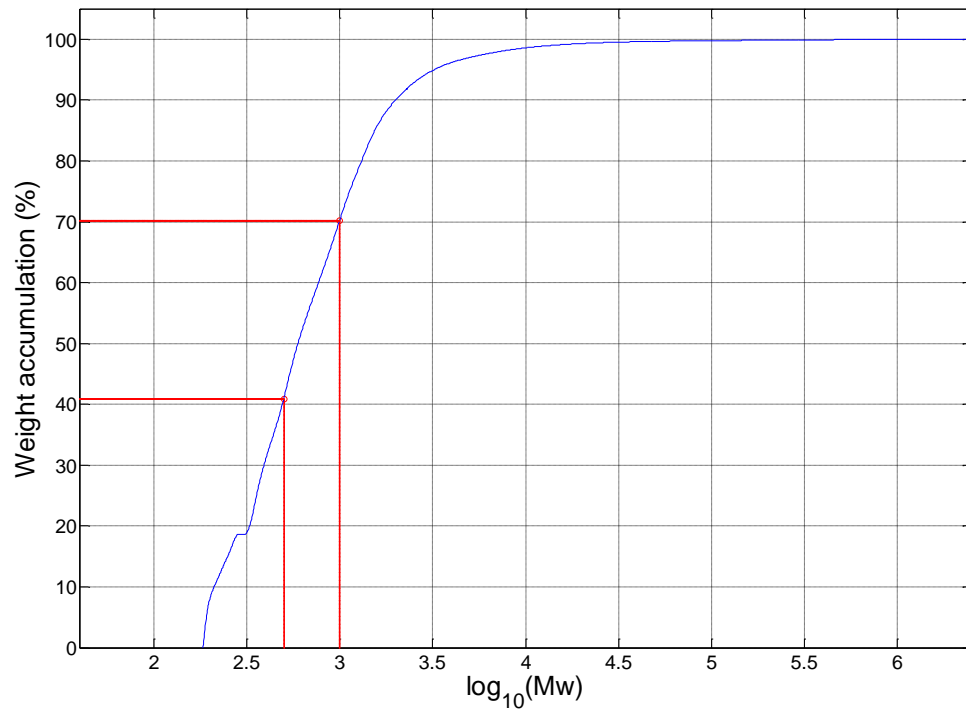
**Sample 17 Sieved 2<sup>nd</sup> run**

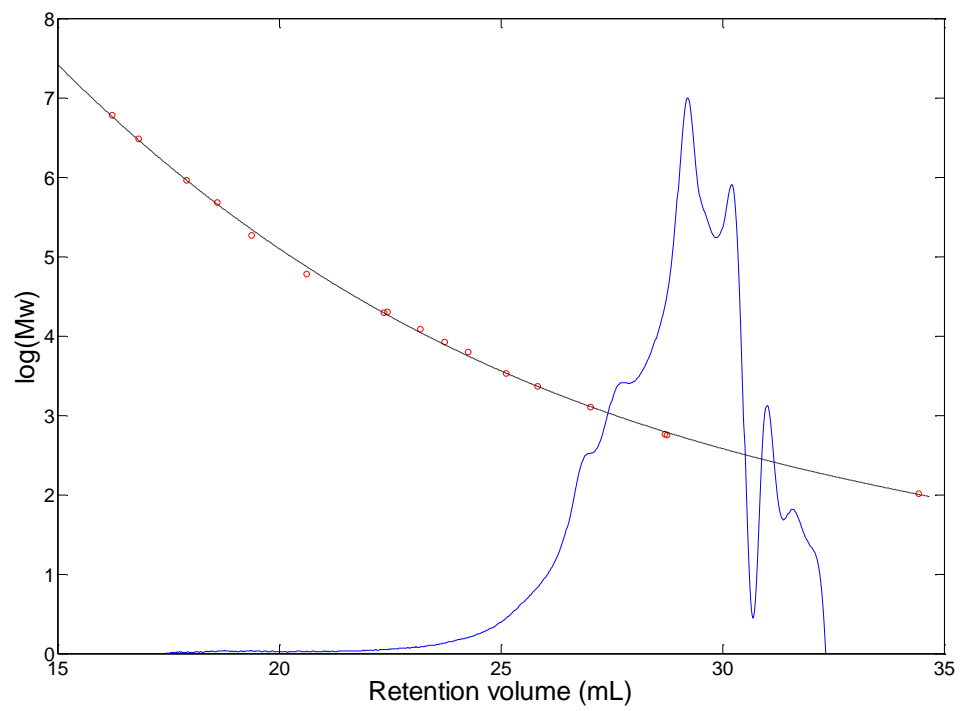


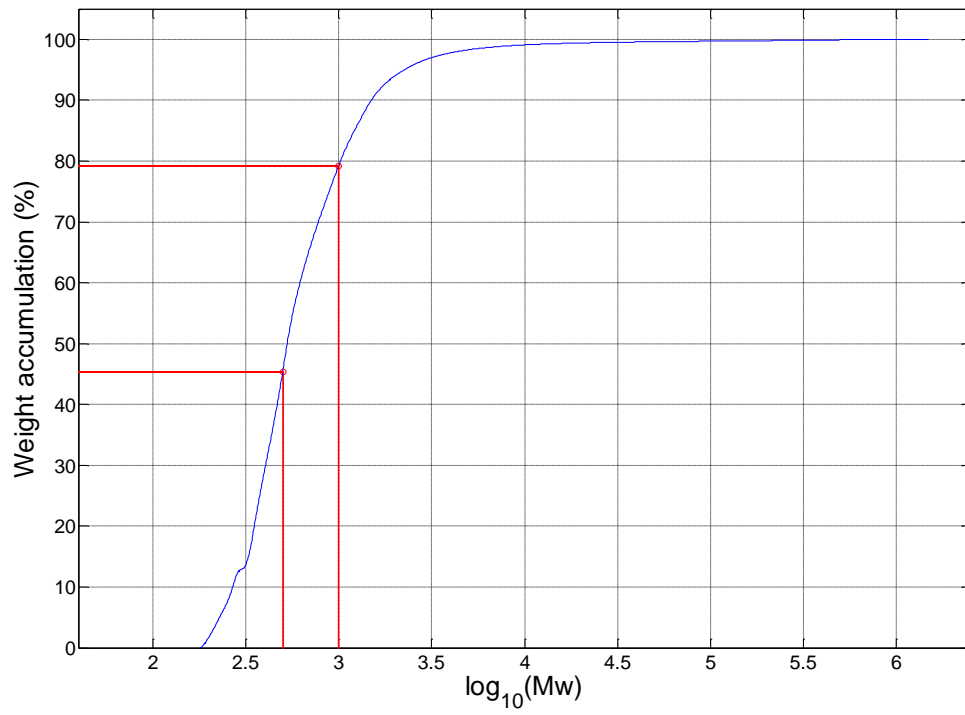
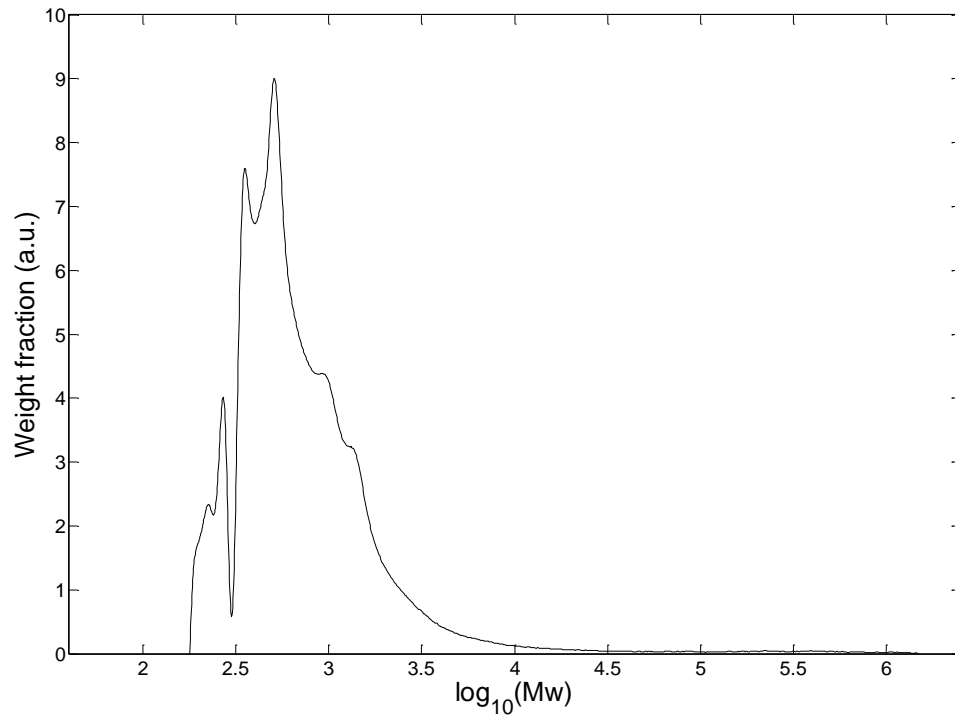
**Sample 17 Non-Sieved 1<sup>st</sup> run**

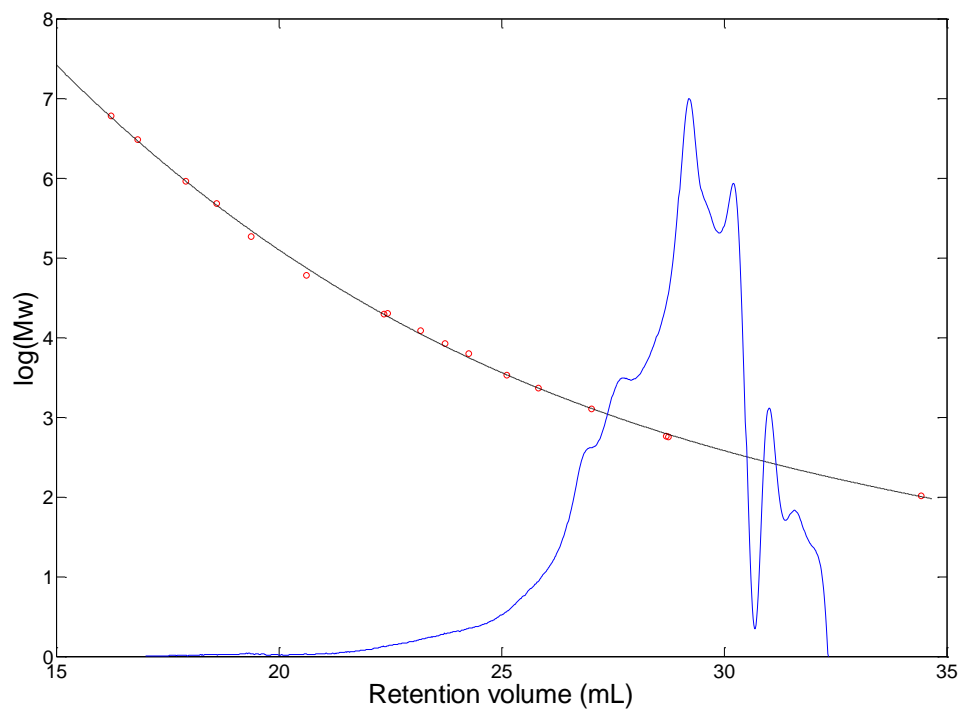


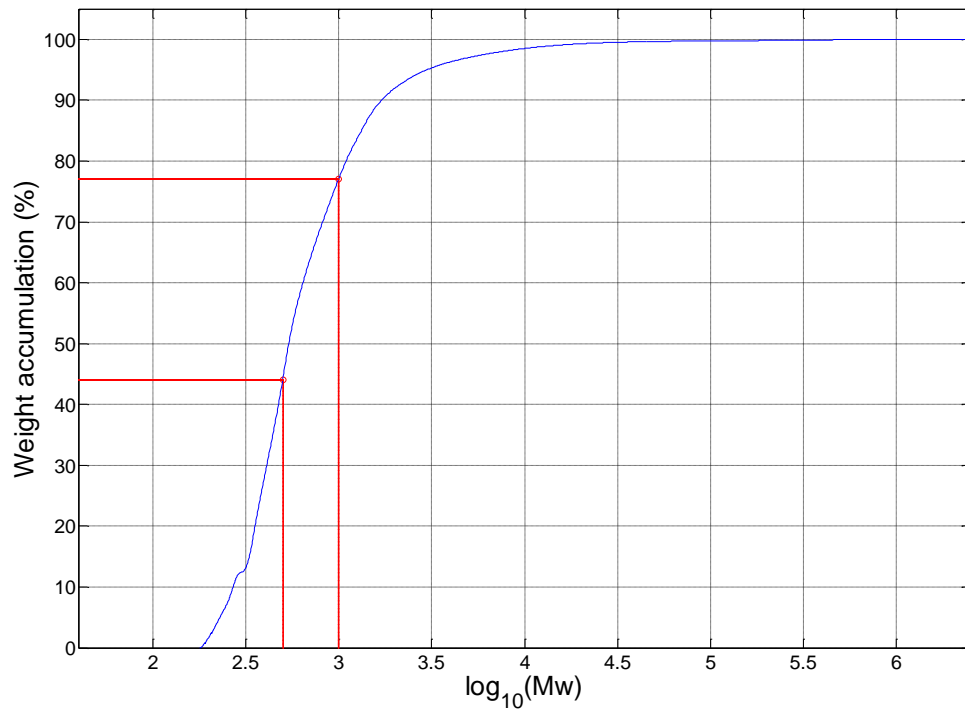
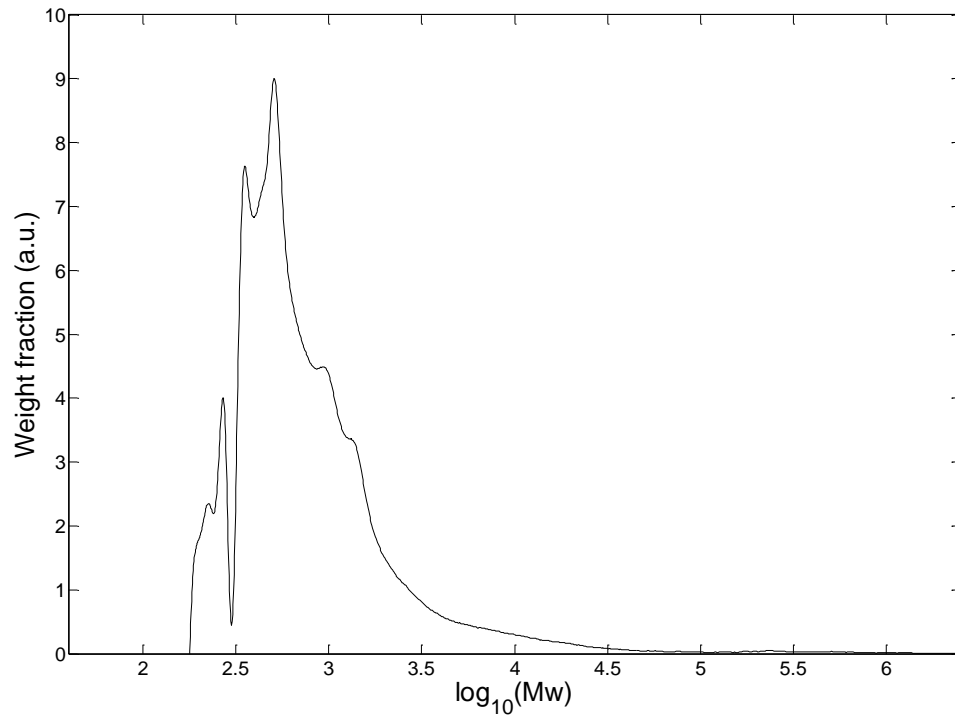
**Sample 17 Non-Sieved 2<sup>nd</sup> run**

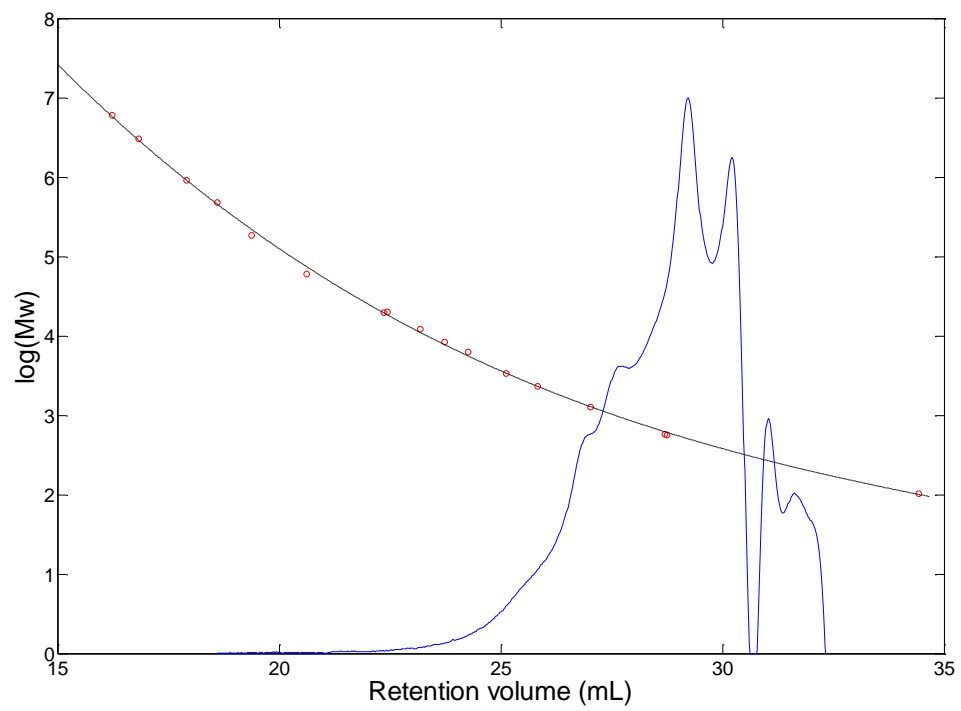


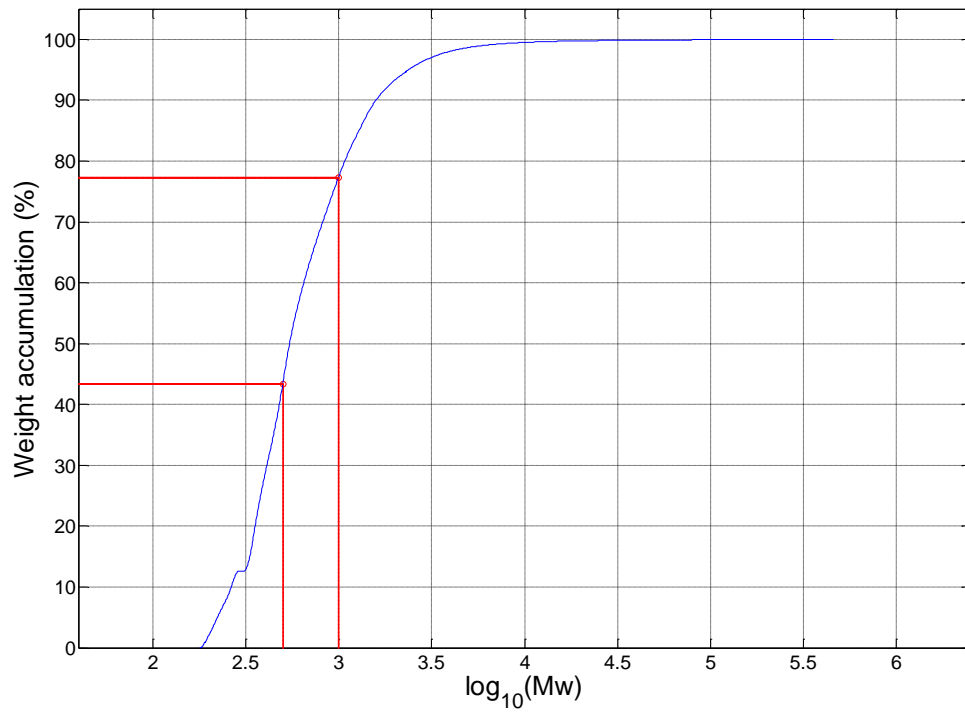
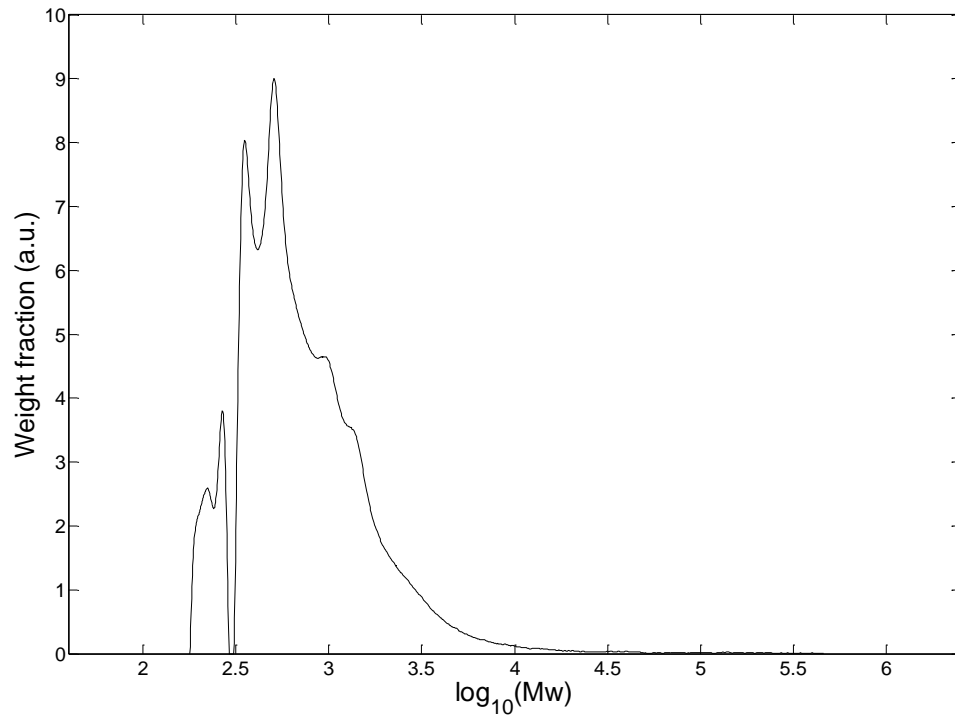
**Sample 97 Sieved 1<sup>st</sup> run**

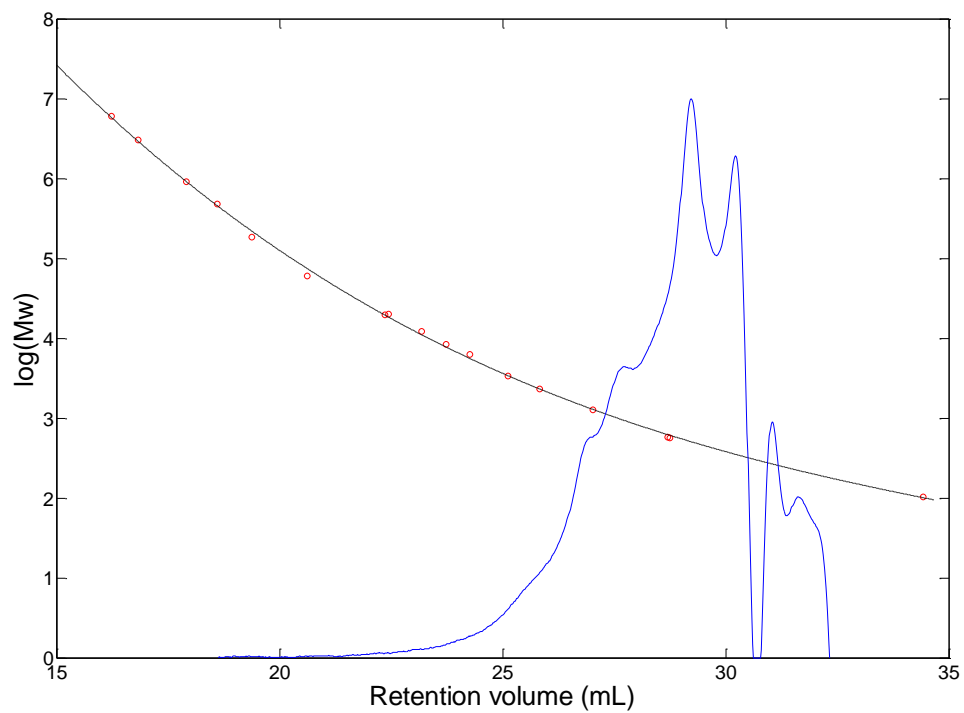


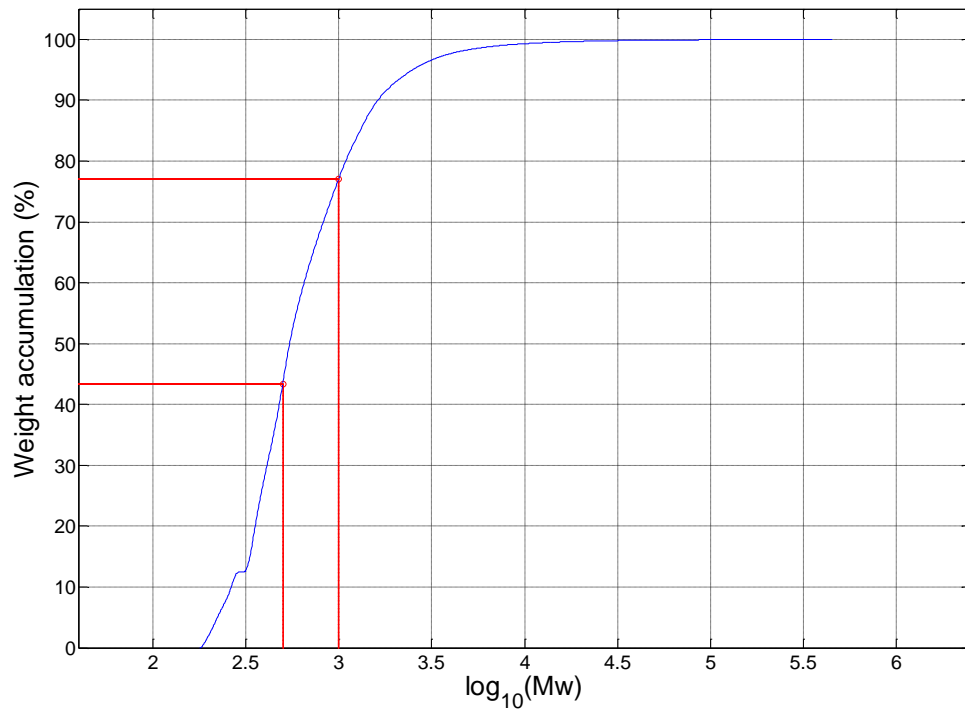
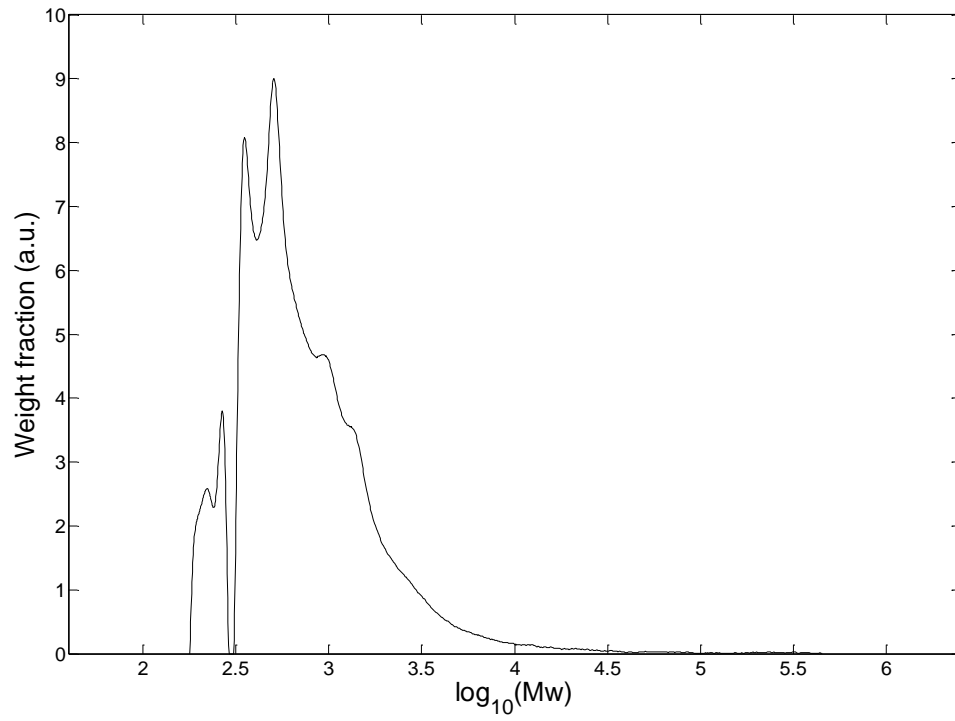
**Sample 97 Sieved 2<sup>nd</sup> run**

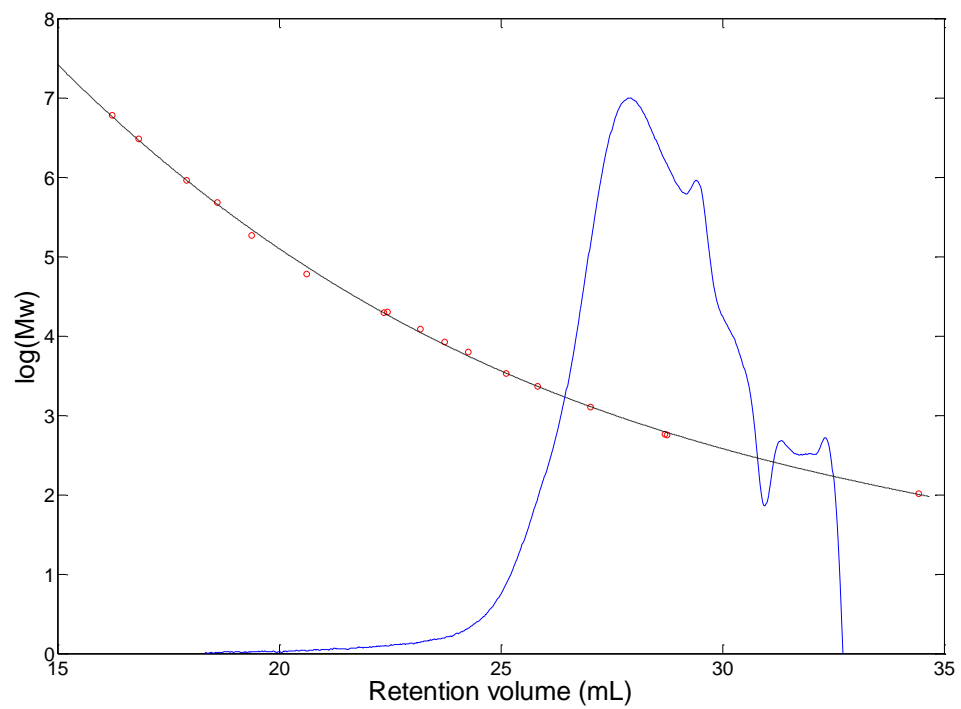


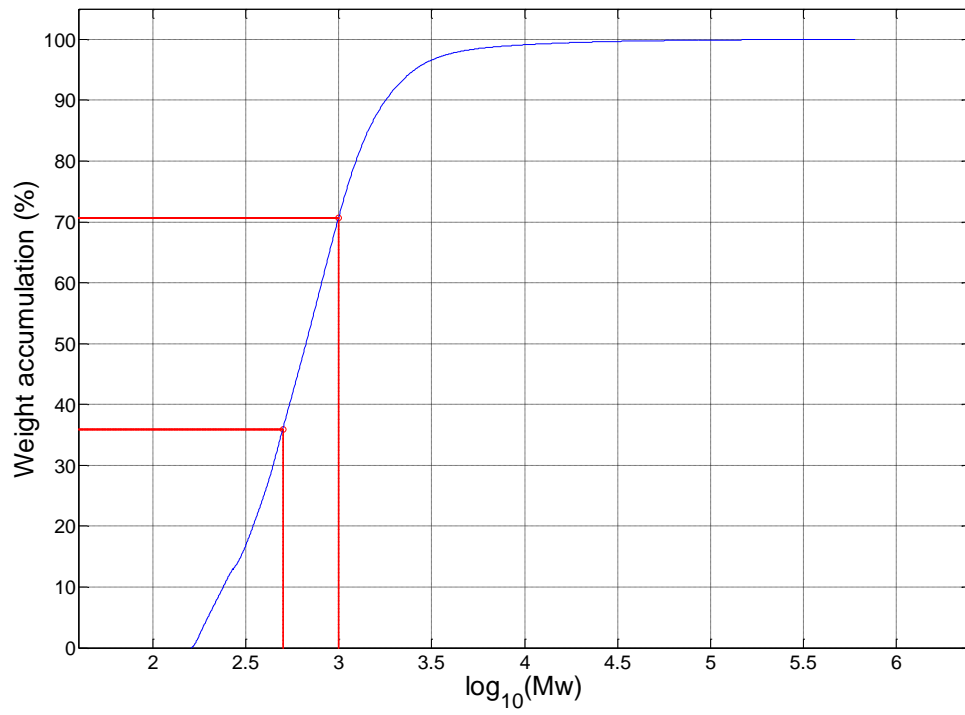
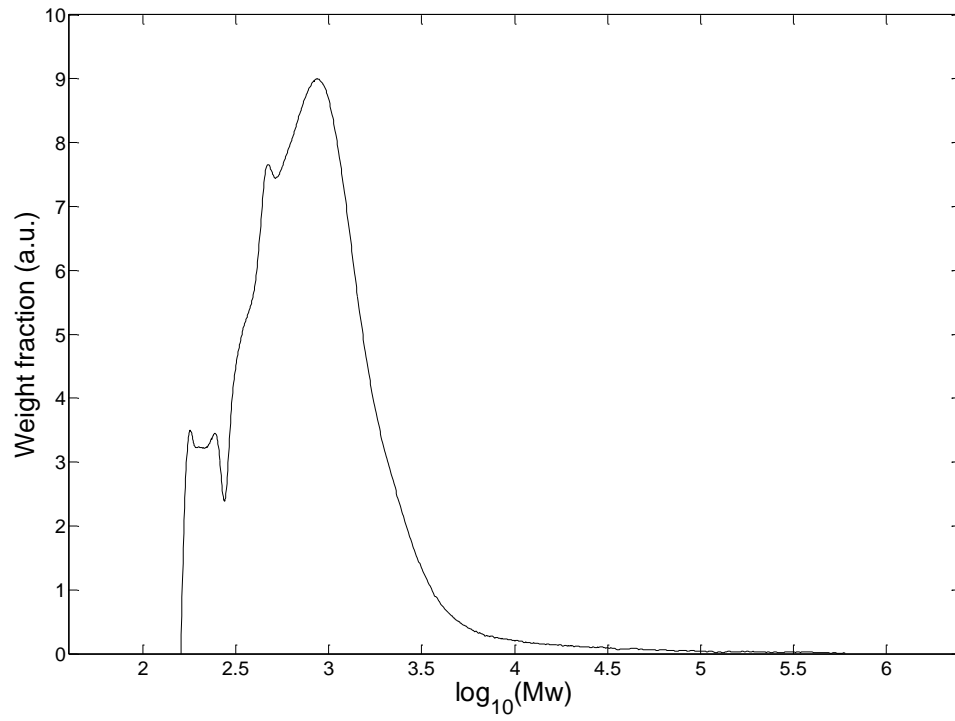
**Sample 97 Non-Sieved 1<sup>st</sup> run**



**Sample 97 Non-Sieved 2<sup>nd</sup> run**



**Sample CS-HTC Non-sieved 1<sup>st</sup> run**



**Sample CS-HTC Non-sieved 2<sup>nd</sup> run**